Role of corticostriatal projections in auditory discrimination

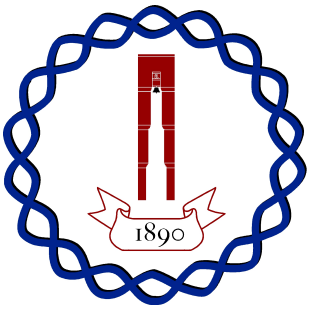

Petr Znamenskiy

Watson School of Biological Science

A thesis submitted for the degree of

PhilosophiæDoctor (PhD)

March 2013

Acknowledgements

I would like to thank the members of my thesis committee, Adam Kepecs, Pavel Osten, Anne Churchland and Terri Grodzicker for their comments and suggestions. In particular, the many 2am discussions with Adam have done more to help me grow as a neuroscientist than all neuroscience courses I had ever taken. Barry Burbach's input into the setup of *in vivo* light delivery was invaluable. Tomáš Hromádka had taught me most of what I know about surgery. I thank him for sharing his experience and his infectious cheer. With the help of Santiago Jaramillo I got my start with animal behavioral training; he has been a great colleague and sparring partner in scientific discussions. Gonzalo Otazu has provided numerous suggestions, especially the design of the Arch-inactivation experiments, and has tought me the perils of double-dipping. Balázs Hangya has provided the code for calculating neuronal cross-correlograms. Qiaojie Xiong collaborrated on corticostriatal plasticity experiments. I thank Hassana Oyibo for her support and patience, especially during the preparation of this thesis. A special thanks to Audible.com and the creators of public radio programs, whose voices kept me company during tedious experiments. I also owe a debt of gratitude to David and Fanny Luke and the Watson School of Biological Sciences for providing me with an opportunity to learn to do science and be part of a graduate program truly unlike any other. Finally, I would like to thank my scientific supervisor, Tony Zador, for his scientific vision, continuous encouragement and support. I could not have wished for a better mentor.

Contents

List of Figures

List of Abbreviations

AAV	Adeno-associated virus
ACx	Auditory cortex
Arch	archaerhodopsin 3
BAC	Bacterial artifical chromosome
ChR2	Channelrhodopsin-2
CMV	Cytomegalovirus
CNS	Central nervous system
EIAV	Equine infectious anemia virus
GFP	Green Fluorescent Protein
GPe	External globus pallidus
GPi	Internal globus pallidus
HSV	Herpes simplex virus
IC	Inferior colliculus
ITR	Inverted terminal repeat
LTD	Long-term depression
LTP	Long-term potentiation
MGB	Medial geniculate body
mPFC	Medial prefrontal cortex
MSN	Medium spiny neuron
pfu	Plaque-forming unit
PRV	Pseudorabies virus
PSTH	Peristimulus time histogram
RVG	Rabies virus glycoprotein
scAAV	Self-complementary AAV
SNr	Substantia nigra pars reticulata
STDP	Spike-timing dependent plasticity
trs	Terminal resolution site
TU	Transducing unit
VSV	Vesicular stomatitis virus
VSV-G	Vesicular stomatitis virus glycoprotein

1

Introduction

Selection of appropriate actions in response to the changing sensory environment is one of the key functions of the nervous system. Research on this topic historically has fallen into two camps. The first camp has applied the insights from the field of *reinforcement learning* in computer science to understand how the brain learns to predict future rewards and select actions to maximize them. In the current view, the neurobiological basis of this process lies in the network of forebrain nuclei known as the basal ganglia and their connections. The second camp has focused on understanding how signals from the sensory world are perceived and used by the brain to make decisions but has viewed this transformation as static, neglecting the fact that the links between perception and action are established through prior experience. This work has been primarily corticocentrist, focusing on the interaction of sensory and motor or premotor cortical areas.

The goal of this thesis was to attempt to understand the neural pathways, through which the auditory cortex mediates selection of actions. We were particularly interested in behaviors involving arbitrary, acquired associations between auditory stimuli and behavioral responses. We focused our attention on connections of the auditory cortex with the striatum, a structure implicated not only in selection and execution of actions but also in learning the stimulus-response contingencies leading to rewards. The experiments described in this thesis focused on testing the role of corticostriatal neurons in the auditory cortex on learning and performing auditory discrimination tasks. This chapter will briefly review the current understanding of cirtuit mechanisms of perceptual decisions, focusing in particular on the experiments on the

role of macaque area MT in perception of motion, from which we adapted many elements of our experimental approach. This chapter will also examine the role of auditory cortex in discrimination of sounds and the function of the striatum in acquisition and execution of motor responses.

The dissection of the function of specific populations of cortical neurons has become possible with the advent of optogenetics, a technique exploiting light to manipulate neuronal activity. A summary of this approach is also provided below.

1.1 Motion discrimination as a model of perceptual decisions

In the search for neuronal substrates of perception, the role of macaque area MT in perception of visual motion is perhaps the best studied example. MT stands out among visual cortical areas in that the majority of its neurons are sensitive the direction of visual motion (Albright, 1984). No other visual area appears as specialized for a particular feature of visual stimuli (Felleman and Van Essen, 1987). Lesions of area MT impair macaques' judgments of motion direction but strikingly have little or no effect on their judgments of orientation of static grating stimuli (Newsome and Pare, 1988).

Stimulation experiments further supported the hypothesis that MT neurons carry the signals used by subjects to make decisions on the direction of visual motion. Direction selectivity in area MT is organized in a columnar fashion, such that nearby neurons have similar preferences for motion direction (Albright et al., 1984). Electrical stimulation of clusters of MT neurons biases macaques to report that a the motion of a visual stimulus is toward the their preferred direction (Salzman et al., 1990).

Further support for this hypothesis is provided by correlations between activity of single MT neurons and monkeys' behavioral choices, refered to as *choice probability* (Britten et al., 1996). Trial-to-trial variation in responses on MT cells can predict the animal's choices even when the sensory stimulus is kept constant. The monkey is more likely to report motion in the preferred direction of the neurons on trials when the neuron's firing rate is above average. The interpretation of these results has been controversial. Of course the spiking of a single neuron among millions cannot itself bias behavioral choices. Instead, it has been proposed that sensory

"noise" in the shared inputs of MT neurons introduce correlations to their responses and it is the correlated firing of many MT neurons that biases subjects' decisions (Shadlen et al., 1996; Zohary et al., 1994). In this view, the shared variability of MT neurons in the causal in subjects' behavioral choices.

An alternative view is that the inputs that give rise to the observed correlations between MT responses and choices arise not from the sensory periphery but from top-down feedback from higher order areas. In this view variability in responses of sensory neurons merely reflects the evolving decisions but does not influence them. Evidence for this interpretation has come from experiments in area V2 (Nienborg and Cumming, 2009), which related the timecourse of neuronal choice correlations to subjects' behavioral sensitivity to the stimulus. Monkeys appeared to largely base their decisions on sensory evidence presented at the start of the trial. In the causal view of choice probability, neuronal choice correlations should be highest during this time. Instead, they rise gradually during the course of the trial, suggesting that at least in part choice probabilities reflect top-down influences.

How does the activity of MT neurons give rise to subjects' behavioral responses? Since saccades are widely used as a behavioral readout in primate psychophysics, the efforts to answer this question have focused on areas involved in the planning of eye movements. The lateral intraparietal area (LIP) contains neurons, which encode the location of planned saccades (Gnadt and Andersen, 1988). LIP receives inputs from visual areas including MT (Felleman and Van Essen, 1991) and sends projections to regions involved in the control and execution of eye movements (Andersen et al., 1990). A subset of LIP neurons were found to signal the direction of an impending choice during discrimination of a motion stimulus (Shadlen, 1996). The activity of these neurons during the trial appears to reflect accumulation of sensory evidence for a particular choice (Shadlen, 1996; Shadlen and Newsome, 2001).

However, it unclear whether LIP performs the computations which generate subjects' responses or merely represents the results of these computation as a kind of efference copy. Another function commonly ascribed to LIP is of controling selective spatial attention (Bisley and Goldberg, 2010). Attention, intention and action are tightly coupled in the oculomotor system (Rizzolatti et al., 1987). LIP neurons may be using top-down signals about the current

saccade plan to direct attention to the target of the imminent eye movement. While stimulation of LIP during motion discrimination does bias subjects' choices, its effects are far smaller than those of MT stimulation (Hanks et al., 2006).

The difficulty in identifying the circuits that actually perform the computations leading to decisions has largely come from a lack of methods to specifically manipulate elements of the circuit. Electrical microstimulation demonstrated the causal role of MT neurons in motion perception. But since MT projects to many cortical and subcortical targets and microstimulation cannot discriminate between neurons participating in different projections, these experiments could not determine which downstream pathways were responsible for integrating motion signals. The development of optogenetics has opened the door for specific manipulation of connections between brain areas. The experiments described in this thesis combine the psychophysical approach summarized in this section with optogenetic techniques to study the pathways through which activity in the auditory cortex gives rise to decisions driven by sounds.

1.2 The auditory cortex in perception of sounds

While the role of the auditory cortex in audition is undisputed, it's precise role in the perception of sounds is not known. In humans, lesions of the auditory cortex have inconsistent effects on perception of sounds (Mendez and Geehan, 1988). They may initially manifest cortical deafness, complete loss of awareness of sounds or auditory agnosia, loss of ability to understand or categorize sounds. Patients often recover some ability to hear but the degree of recovery varies.

Macaques, following surgical removal of the auditory cortex, were initally unable to detect pure tones or vocalizations (Heffner and Heffner, 1986; 1990). Hearing returned gradually, but never recovered fully. Monkeys' auditory thresholds remained 30-50 dB above normal over a year after the lesion.

In rats, the requirement of the auditory cortex in perception of sounds seems less absolute. Following lesions of the auditory cortex, rats were still able to make fine judgments of sound location in a psychophysical task, although their sensitivity thresholds were increased (Kelly, 1980). Similarly, auditory cortex was not required for discrimination of sound duration

(Pai et al., 2011). On the other hand, auditory cortex appears important for perception of sound frequency. Talwar *et al.* (Talwar et al., 2001) trained rats to detect detect a deviant target tone at 9,600 or 8,420 Hz in a series of standard tones at 8 kHz. Transient reversible inactivation of the auditory cortex by the $GABA_A$ agonist muscimol reduced rats' performance to chance levels. Other studies, which required rats to discriminate whether a single presented pure tone is higher or lower in frequency than a learned midpoint, found that inactivation(Tai, 2008) or lesions(Pai et al., 2011) of the auditory cortex substantially reduced but did not abolish psychophysical performance. Beyond possible differences in methodology, the apparent discrepancy between these results may stem from differences in the behavioral tasks tested. First, the task employed by Talwar *et al.* required much finer judgments of frequency, since the target tones differed from the standard by at most 1/4 of an octave, while the later studies required rats to discriminate tone frequencies that differed by 1 and as much as 4 octaves. Second, as the deviant detection task requires the rats to compare the frequency of the target tone to a previously presented standard rather than an over-trained frequency threshold, it may require the standard tone to be entered into working memory or the "phonological store", in which the auditory cortex may play a key role.

1.3 Striatum in perception and action

Striatum[1] is the input nucleus of the basal ganglia and receives inputs from throughout the cortex (McGeorge and Faull, 1989). Basal ganglia together play a key role of in control of movement and their dysfunction is associated with movement disorders (DeLong, 1990).

1.3.1 Striatal cirtcuitry and connectivity

Majority of the neurons in the striatum are the GABAergic medium spiny neurons (MSNs), which project outside the striatum. Striatal output procedes through two distinct pathways, direct and indirect pathway, which are composed of distinct populations of MSNs. Direct pathway neurons project to the output nuclei of the basal ganglia, substantia nigra pars reticulata

[1]The striatum is usually subdivided into dorsal and ventral striatum. In primates, the dorsal striatum is further separated by the internal capsule into the caudate nucleus and the putamen but this distinction is absent in rodents. Here we will refer to the striatum meaning the dorsal striatum in general.

(SNr) and the internal globus pallidus (GPi, also refered to as the entopeduncular nucleus in rodents). These nuclei send inhibitory projections to the motor thalamus and midbrain motor nuclei. Activity of direct pathway neurons suppresses the firing of GPi and SNr cells and disinhibits motor output (Chevalier and Deniau, 1990). Indirect pathway MSNs project to the external globus pallidus (GPe), which in turn provides tonic inhibition to the subthalamic nucleus. Subthalamic nucleus is the only glutamatergic component of the basal ganglia and sends excitatory projections to SNr and GPi. By disinhibiting the subthalamic nucleus, activity in the indirect pathway excites SNr and GPi and suppresses motor output. Thus, direct and indirect pathway neurons play antagonistic roles in regulating movements. Direct and indirect pathway MSNs are distinguished by their expression of dopamine receptors. Direct pathway MSNs express dopamine receptor D1, while indirect pathway cells express D2.

The striatum also contains cholinergic and several classes of GABAergic interneurons (Kawaguchi et al., 1995). These interneurons reveive long-range excitatory inputs from cortex and thalamus and modulate the firing of striatal MSNs. The striatum also receives dopaminergic input from substantia nigra pars compacta (SNc). Dopamine regulates activity and plasticity of striatal MSNs (Gerfen and Surmeier, 2011).

In addition to the distinction between direct and indirect pathways, the striatum can also be subdivided histochemically into acetylcholinesterase (AChE) rich and poor compartments (Graybiel and Ragsdale, 1978). Most striatal tissue is AChE-rich and is referred to as the striatal matrix. Embedded within the matrix are AChE-poor zones called striosomes or patches. Striosomes and matrix compartments receive inputs from distinct cortical areas (Eblen and Graybiel, 1995). While both compartments projects to SNr, only striosome neurons send projections to SNc, the source of dopaminergic enervation of the striatum (Fujiyama et al., 2011).

1.3.2 Striatal plasticity

Activity-dependent plasticity is a hallmark of glutamatergic inputs of striatal MSNs (Kreitzer and Malenka, 2008). Some confusion arises from the fact that earlier studies did not attempt to

distinguish between cortical and thalamic inputs. More recent work has attempted to specifically examine plasticity of cortical afferents. Both long-term depression (LTD) and potentiation (LTP) of these connections have been described. Plasticity rules vary between direct and indirect pathway MSNs and depend on the pattern of synaptic stimulation and the activity of NMDA and dopamine receptors.

Striatal LTD is mediated by retrograde endocannabinoid signaling (Gerdeman et al., 2002) and requires activation of dopamine but not NMDA receptors (Calabresi et al., 1992a). LTP, on the other hand, depends on NMDA receptors and can be evoked in the absence of extracellular magnesium (Calabresi et al., 1992b). The switch between LTP and LTD appears to be controlled by both the relative timing of pre- and post-synaptic activity, as in cortical spike-timing dependent plasticity (STDP) (Markram, 1997), and dopamine signaling. In both D1 and D2 MSNs LTP is induced when presynaptic stimulation precedes a postsynaptic spike (Shen et al., 2008) and is abolished by blockers of NMDA receptors. In D1 MSNs in the presence of antagonists of D1 dopamine receptors this pairing instead results in depression. On the other hand, postsynaptic spiking preceding presynaptic stimulation induces LTD in D2 MSNs, which depends on the activity of D2 dopamine receptors. In contrast in D1 MSNs, this protocol only produces LTD when D1 receptors are blocked. In summary, dopamine plays antagonistic roles in plasticity of connections of D1 and D2 neurons, encouraging potentiation in D1 MSNs and depression in D2 MSNs.

1.3.3 Striatum in reinforcement learning

Owing to their architechture, the basal ganglia have attracted a lot of attention in the study of reinforcement learning. The modulation of striatal plasticity by dopaminergic neurons, which encode reward-related signals, make it a prime candidate as the substrate of sensorimotor association learning. Most models of the reinforcement learning place the basal ganglia in the context of the Actor-Critic architechture (Barto, 1995). In this framework both the Actor and the Critic receive signals about the current state whenever an action is performed. Both of these components are plastic and their responses to changes of state are modified by learning. The Actor selects reponses on the basis of state-related signals. The Critic evaluates the outcomes

of actions and generates feedback, which is used to train the Actor, modifying the weights between different sensory states and actions.

The signals sent by the Critic take the form of the Temporal Difference (TD) error function (Sutton, 1988). TD learning attempts to estimate value or the total future reward associated with a particular state. The TD error δ at time t is

$$\delta(t) = r(t) + \gamma\hat{V}(t+1) - \hat{V}(t)$$

where $\hat{V}$ is the estimate of the value of a given state and r is the reward received. The discounting factor γ allows distant rewards to be valued less than immediate ones. This error signal is used to update the Critic to improve future value estimates and the Actor to maximize selection of actions leading to high value states.

Signals that resemble δ are carried by midbrain dopamine neurons, which provide dopaminergic input to the striatum (Schultz, 1997). A subset of these neurons in macaques responds specifically to unexpected rewards. When the monkeys were taught that a sensory cue predicted reward, dopaminergic neurons responded instead to the cue rather than the reward itself (Schultz et al., 1993).

The striatum has been proposed to play the role of both the roles of the Actor and the Critic. Action selection is carried out by striatal neurons in the matrix compartment, whose outputs target SNr and GPi. Evaluation is carried out by striosome neurons, which project to dopaminergic SNc. Learning is proposed to take place through modification of corticostriatal synaptic weights gated by dopaminergic feedback.

Earlier models of the reinforcement learning and the basal ganglia did not consider the role of perception and sensory noise in value estimation and action selection. They can be modeled by "belief state", the posterior probability distribution of external states given past sensory inputs and actions (Rao, 2010). The model can not only reproduce monkeys' behavior in the random dot motion discrimination task, but the TD error signal in the model resembles the activity of dopamine neurons in SNc as the quality of sensory evidence is varied (Nomoto et al., 2010; Rao, 2010).

1.3.4 Striatum in perceptual decisions

Surprisingly few experiments have explored the role of the striatum in perceptual decisions. Merchant *et al.* examined the responses of striatal (putamen) neurons in monkeys performing a somesthetic discrimination task (Merchant et al., 1997). The task required the animal to discriminate whether the speed of movement of a stimulus probe on its left hand was faster or slower than a trained midpoint and to report its choice by touching a switch with the right hand. A subset of putamen neurons showed categorical responses to stimulus movement. In addition, some putamen cells were active while the monkey moved its right hand to the target switch.

Ding and Gold (Ding and Gold, 2012) measured the effects of striatal microstimulation on monkeys' choices in the random dot motion discrimination task. Stimulation biased monkeys' choices but surprisingly the direction of choice bias was opposite of the preferred direction of the neurons near the stimulation electrode. This result may be explained if stimulation preferentially recruits indirect pathway MSNs.

1.4 Optogenetics

Targeted manipulation of subpopulations of neurons has become feasible with the development optogenetics, a set of techniques using ectopically expressed light-gated ion channels to control the firing of neurons. Channelrhodopsin-1 and -2 are seven-transmembrane domain proteins originally found in the green algae *Chlamydomonas reinhardtii* and required for their phototaxis(Sineshchekov et al., 2002). Unlike most seven-transmembrane domain proteins, which function through second messengers, Channelrhodopsins are themselves are ion channels (Nagel et al., 2003), non-selectively permeable to cations. When expressed in neurons, ChR2 renders them light-sensitive, eliciting action potentials in response to brief flashes of blue light with millisecond precision (Boyden et al., 2005).

Through targeted expression ChR2, it can be used to specifically excite subpopulations of neurons. It was immediately realized that ChR2 expression could be controlled by cell-type specific promoters. This method has been applied widely to activate specific neuronal

populations, such as genetically defined populations of hypothalamic neurons (Adamantidis et al., 2007), subtypes of cortical interneurons (Cardin et al., 2009; Lee et al., 2012; Lima et al., 2009; Sohal et al., 2009) and direct and indirect pathway striatal MSNs (Kravitz et al., 2010; Tai et al., 2012).

An alternative approach, which makes possible specific manipulation of subpopulations of projection neurons, is anatomical targeting. Viruses, which undergo retrograde neuronal transport, can be used to direct ChR2 expression to neurons based on the location of their long-range projections (Lima et al., 2009). In contrast to promoter based targeting, which relies on production of transgenic animals and is therefore can by and large only be applied in mice, this approach can used in model organisms where transgenics are not feasible, including non-human primates and, as in this thesis, rats.

Following the discovery of ChR2, microbial opsins enabling inactivation of neural activity have been identified. A light-driven chloride pump from the archaebacterium *Natronomas pharaonis* Halorhodopsin was shown to hyperpolarize and supress firing of neurons (Han and Boyden, 2007). It is sensitive to longer wavelengths of light than ChR2, which allows them to be used simultaneously for bidirectional manipulation of neural activity. Archaerhodopsin-3 (Arch), a proton pump from the archaean *Halorubrum sodomense*, was also shown to silence neurons in response to light (Chow et al., 2010). The large currents produced by Arch even at low light powers make it particularly suitable for silencing neuronal activity *in vivo*.

1.5 Thesis outline

This thesis is divided into nine chapters following this introduction. They are largely self-contained, although chapters 5-7 reporting the behavioral effects of manipulation of auditory cortical neurons are best read in order.

Chapter 2 describes our efforts to develop new tools for genetic tagging of neurons on the basis of their anatomical connections.

The "cloud-of-tones" behavioral task we developed to study the function of projections of the auditory cortex in auditory decisions is described in Chapter 3. We summarize rats' per-

formance of this task attempting to characterize the relationship between the auditory stimulus and rats' behavior in the task.

The responses of neurons in the auditory cortex and striatum during performance of the task are described in Chapter 4.

Our experiments non-specifically stimulating auditory cortex are described in Chapter 5. We find that stimulation biases choices but surprisingly sound selectivity of the stimulated neurons has no bearing on the behavioral effects of stimulations.

Chapters 6 and 7 describe the effects of specific stimulation and inactivation of corticostriatal neurons in the auditory cortex. We show that subjects' responses in the task are driven by the activity of these neurons.

Plasticity of connections between corticostriatal neurons and their striatal targets is explored in Chapter 8. We find that training in the task specifically potentiates cortical inputs from neurons responding to sounds associated with contralateral choices in the task.

We describe the key details of our experiments within the narrative of the experiments in Chapters 2-8. More technical details of our methodology and data analysis are relegated to Chapter 9.

Finally, Chapter 10 places our findings on the role corticostriatal projections in the context of the larger brain circuit and discusses further questions on the function of this pathway in the transformation of perception in action.

1.6 Disclosures

The experiments described here were carried out under the supervision and guidance of Anthony Zador. Hassana Oyibo contributed to the development of IE180-null PRV (Sec. 2.3.2), generated the variants of the virus expressing Cre-recombinase and tested them *in vivo*. Qiaojie Xiong did the tracer injections depicted in Fig. 6.8a. Qiaojie Xiong and I carried out the experiments monitoring corticostriatal plasticity during behavioral training summarized in Section 8.3.

2

Development of viral tools for retrograde neuronal labeling

Most brain regions are composed of heterogeneous mixtures of neurons projecting to different target areas. Nearby neurons with different long-range targets may exhibit different physiological properties and play different roles in circuit function and behavior.

The development of optogenetics has made possible the specific manipulation of genetically defined populations of neurons. However, promoters that can direct expression to specific populations of projections neurons are not generally known. An alternative to promoter-based targeting is offered by viruses, which can infect neurons through their axons and undergo retrograde transport to the soma. A recombinant Herpes Silmplex Virus-1 (HSV-1) expressing ChR2 has been shown to undergo retrograde spread and drive ChR2 expression in specific populations of projection neurons (Lilley et al., 2001; Lima et al., 2009). This virus is used in Chapters 6 and 7 to target ChR2 expression to corticostriatal neurons. However, this HSV-1 based system was developed commercially and is not openly available for academic use. Therefore, we sought to develop alternative methods for retrograde tagging of neurons.

Although adeno-associated viruses (AAV) and lentiviruses widely used in neuroscience research show some capacity for retrograde spread, their efficiency is insufficient for most applications. Modifications to these viruses purported to enhance retrograde spread have been reported in the literature (Hollis et al., 2008; Mazarakis et al., 2001). Our attempts to verify the ability of these reagents to retrogradely infect projection neurons in the auditory cortex are

described in Sections 2.1-2.2. The rest of the chapter describes our efforts to adapt Pseudorabies virus (PRV) for long-term labeling of neurons.

2.1 Rabies glycoprotein pseudotyped lentivirus

Pseudotyping refers to the substitution of the endogenous envelope protein of a lentivirus by a heterologous one. Typically, the vesicular stomatitis virus (VSV) glycoprotein (VSV-G) is used. Lentiviruses pseudotyped with VSV-G efficiently infect neurons at the site of injection but do not undergo retrograde axonal transport.

Rabies virus undergoes retrograde axonal transport as a part of its infection cycle (Finke and Conzelmann, 2005). Viral attachment and entry into the cell is mediated by the rabies virus glycoprotein (RVG) (Mebatsion et al., 1996). Mazarakis and colleagues tested the ability of lentivirus (equine infectious anemia virus, EIAV) pseudotyped with RVG to undergo axonal uptake and retrograde spread in the mammalian CNS (Mazarakis et al., 2001). Upon injection into the rat striatum, infected neurons were found in many distal structures projecting to the site of injection. In contrast, injection of EIAV pseudotyped with VSV-G transduced neurons restricted to the striatum.

We tested whether RVG-pseudotyped EIAV carrying a GFP transgene would undergo retrograde transport to ACx when injected into brain regions that receive input from ACx. We first targeted the auditory cortex itself, which receive extensive projections from the contralateral ACx (Fig. 2.1a). The virus labeled small numbers of neurons and glia at the injection site (Fig. 2.1b). No infected neurons were found in the contralateral ACx (Fig. 2.1a). Surprisingly, highly expressing neurons were found in caudal globus pallidus (Fig. 2.1c). The pallidocortical neurons in this region are the source of basal forebrain cholinergic input to the auditory cortex (Moriizumi and Hattori, 1992).

We next injected RVG-pseudotyped EIAV into the region of the striatum that receives direct input from ACx. This injection resulted in efficient labeling in the striatum, as well as retrograde transport of the virus to globus pallidus (Fig. 2.1d) as has previously been reported (Mazarakis et al., 2001). However, very few retrogradely labelled neurons were found in the auditory cortex (Fig. 2.1d).

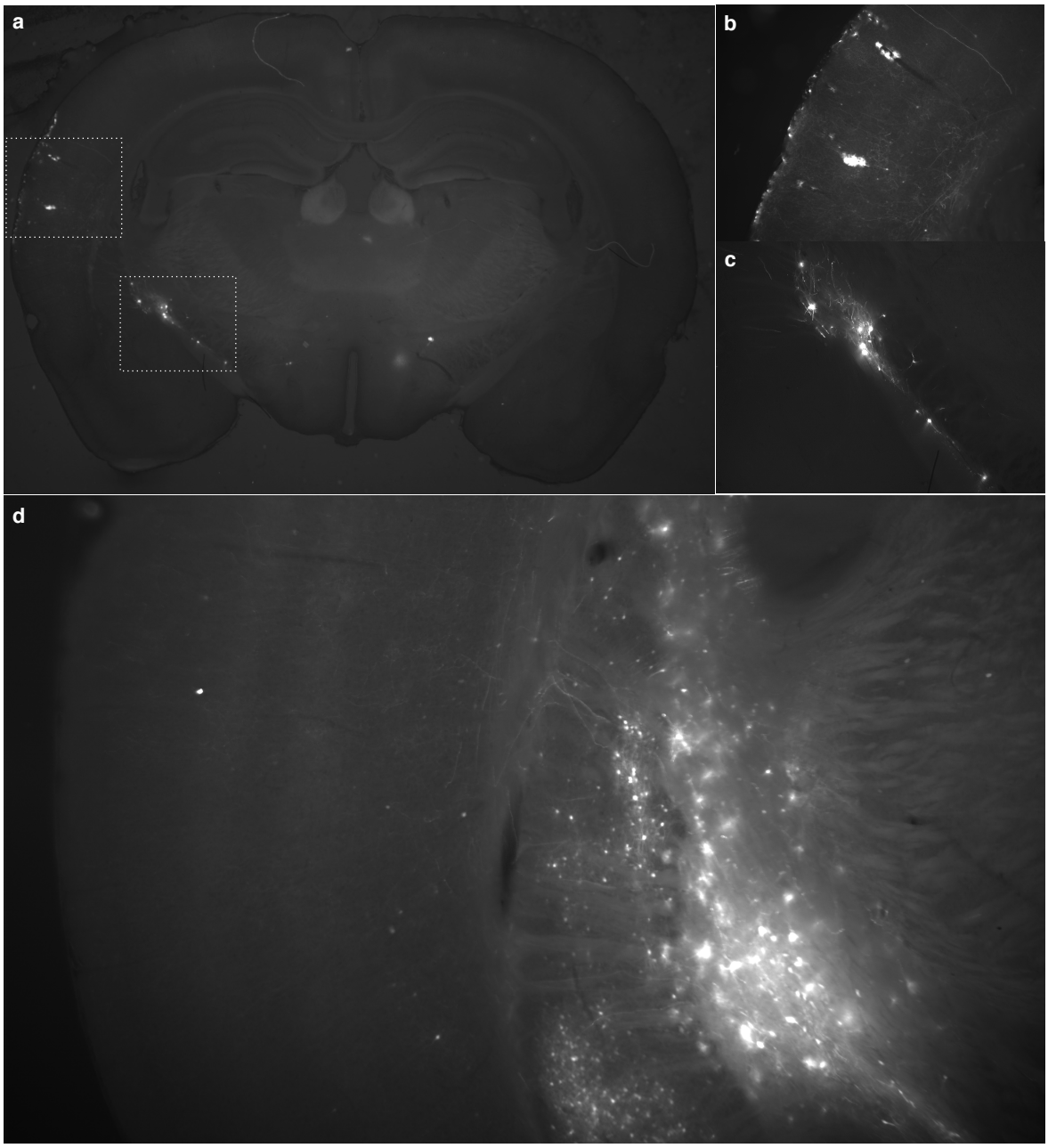

Figure 2.1: **Infection by RVG-pseudotyped EIAV a,** Section through a rat brain injected with RVG-pseudotyped EIAV GFP in the left primary ACx. **b,** Close-up of GFP expression near the injection site. **c,** Retrograde transport of EIAV to putative cholinergic neurons in globus pallidus. **d,** Section through a rat brain injected with RVG-pseudotyped EIAV GFP in the left auditory striatum.

Together, our observations suggest that while RVG-pseudotyped EIAV may be a useful tool for retrograde labeling in some pathways, it is unsuitable for the targeting cortical projection neurons.

2.2 Self-complementary AAV

Adeno-associated virus (AAV) is a single-stranded DNA virus. The sythesis of the second DNA strand is a rate-limiting step during AAV infection (Miao et al., 2000). However, concatamers of viral genomes containing alternating + and - strands form during viral DNA replication (Straus et al., 1976). If the AAV vector size is less than half of the packaging capacity of AAV, the virus can package two copies of the genome in inverted repeat configuration (Dong et al., 1996; Straus et al., 1976). These repeats are complementary to each other and can refold into double-stranded DNA upon entering the target cell (McCarty et al., 2001), thus bypassing the inefficient DNA synthesis step. Such self-complementary AAV (scAAV) vectors have been shown to result in retrograde infection in the spinal cord following intramuscular or intranerve injection (Hollis et al., 2008). We set out to test the ability of scAAV to retrogradely transduce neurons in the neocortex.

When AAV is packaged from a small vector, the resulting prep contains a mixture of virions carrying monomers and self-complementary dimers of the genome. Dimer particles can be enriched by fractionations using CsCl centrifugation (McCarty et al., 2001). A more efficient strategy for scAAV production employs a vector backbone carrying a deletion of the terminal resolution site (*trs*). During AAV replication *trs* is the target of cleavage by an endonuclease that results in production of viral genome monomers (Fife et al., 1977; Snyder et al., 1990). Vectors lacking the *trs* in one of the ITRs only generate viral particles carrying self-complementary genome dimers (McCarty et al., 2003).

To test the ability of scAAV to retrogradely transduce neurons in the neocortex, we subcloned the gene encoding Cre recombinase downstream of the CMV promoter in the *trs*-deleted vector pHpa-trsSK (McCarty et al., 2003) to generate PZ11 (Fig. 2.2a). AAV virions packaged from PZ11 carried dimeric genomes (Fig. 2.2b).

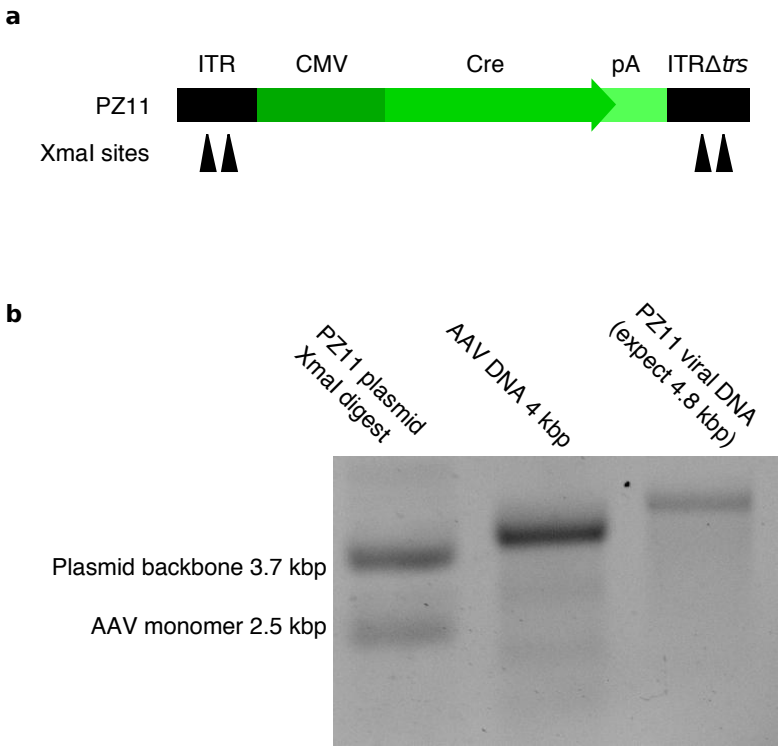

Figure 2.2: **Construction of scAAV Cre a,** Diagram of PZ11 scAAV Cre construct **b,** DNA was extracted from PZ11 virions and analyzed by alkaline agarose gel electrophoresis. PZ11 virions (lane 3) contain DNA molecules of the size expected for genome dimers.

We injected scAAV Cre into the auditory cortex of Ai9 mice, carrying a Cre-dependent tdTomato expression cassette (Madisen et al., 2010). As expected, tdTomato was expressed in cells near the injection site in the auditory cortex (Fig. 2.3a). Although AAV typically respects structural boundaries in the brain, scAAV also spread to the hippocampus (Fig. 2.3a). tdTomato was also expressed in brain regions connected to the auditory cortex, including auditory striatum, parietal cortex and contralateral auditory cortex (Fig. 2.3a) but was found in glial cells as well as neurons. As glia do not have long range projections, glial expression cannot be explained purely by retrograde spread. Similarly, expression in the auditory striatum cannot result from retrograde spread since auditory striatal neurons receive auditory input but do not project back to the cortex.

Similar results were obtained following injection into the inferior colliculus (IC), one of the targets of ACx projections (Fig. 2.3bc). tdTomato expression in the auditory cortex was found in glia as well as neurons.

2.3 Pseudorabies virus

Pseudorabies virus (PRV) is a herpesvirus of the *Alphaherpesvirinae* subfamily. It has been used to study the organization of neural circuits owing to its ability to spread between synaptically connected neurons (Pomeranz et al., 2005).

PRV is cytotoxic and rapidly alters physiological properties of infected neurons (McCarthy et al., 2009), which limits its utility for physiological and behavioral experiments. We explored two strategies for eliminating cytotoxicity of PRV while maintaining its capacity for retrograde axonal transport. First, we engineered PRV amplicons, virions packaged by PRV machinery but carrying no viral genes. Although PRV amplicons show promise as vehicles for retrograde gene delivery in the brain, we have to date not been able to produce them at sufficiently high titers required for most experimental applications. Second, we manipulated the PRV to prevent transcription of viral genes *in vivo*. The resulting virus can be readily grown at high titers and produces efficient long-term labeling of neurons when injected into the brain.

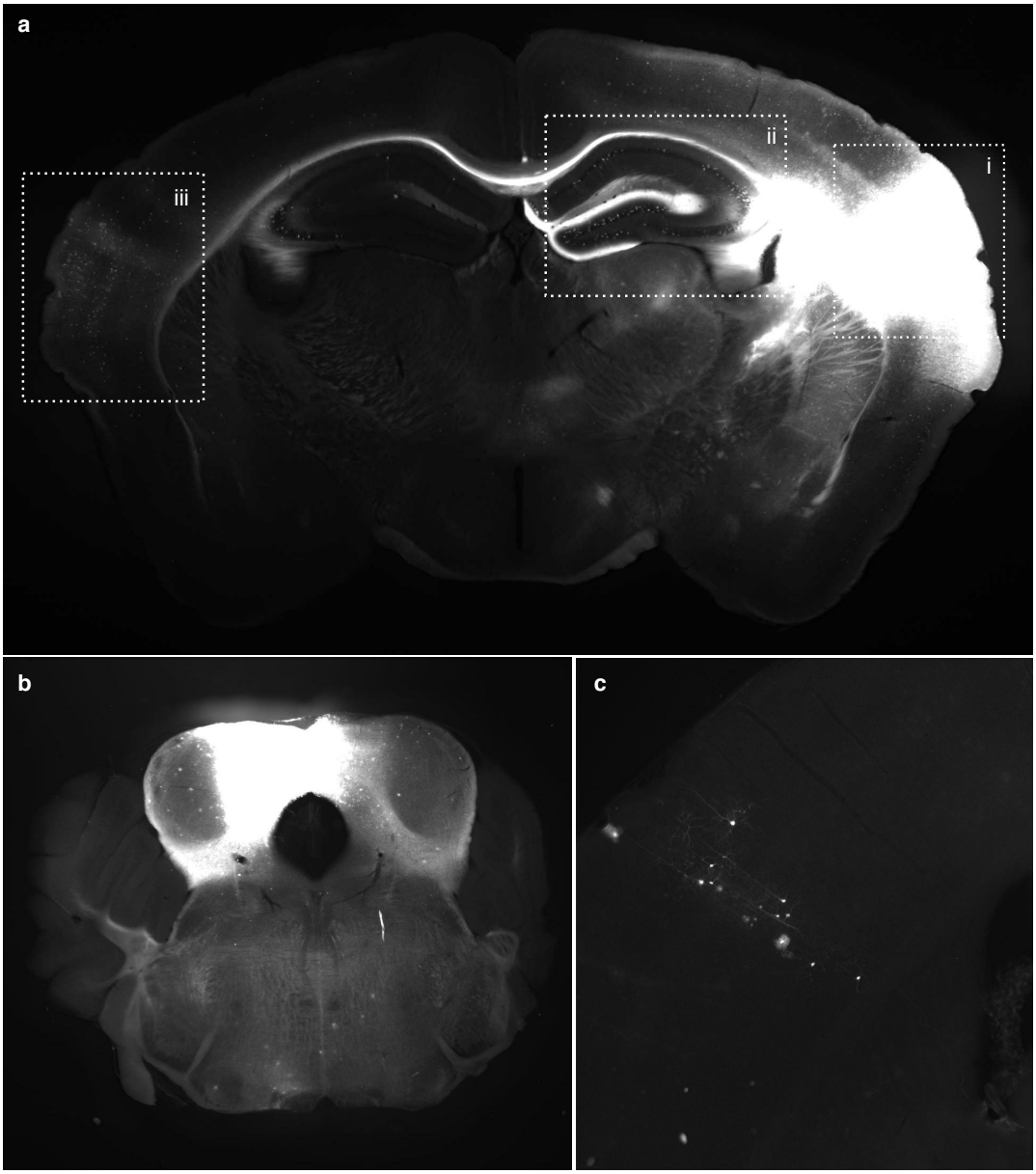

Figure 2.3: **scAAV Cre infection in the brain. a,** tdTomato fluorescence in Ai9(Madisen et al., 2010) mouse injected with PZ11 scAAV Cre in the right auditory cortex. The injection site (i), hippocampus (ii) and contralateral auditory cortex (iii) are highlighted. **b,** tdTomato fluorescence in Ai9 mouse injected in the inferior colliculus. **c,** scAAV-induced expression in the auditory cortex following inferior colliculus injection.

2.3.1 PRV amplicons

One approach that has been successful in adapting Herpes Simplex Virus type 1 (HSV-1), a related herpesvirus, for long-term gene delivery in the brain is the production of viral amplicons(Geller and Breakefield, 1988). Amplicons are packaged by viral machinery but carry none of the viral genes and consequently have a minimal impact on the cells they infect. During amplicon production, viral proteins are provided *in trans* by a helper virus. This approach can also applied to generate PRV amplicons (Prieto et al., 2002).

However, the helper virus used during amplicon production can contaminate amplicon stocks. Removal of the viral packaging signals from the helper genome can eliminate helper virus from HSV-1 amplicon stocks (Fraefel et al., 1996). We set out to test whether a similar strategy could be applied to generate helper-free PRV amplicons.

We used PRV HF22A as a helper virus. HF22A lacks the gene encoding glycoprotein B (gB), an essential component of the viral membrane fusion machinery (Curanovic and Enquist, 2009). PRV virions lacking gB on their surface are unable to infect target cells. Infectious virions can be generated by growing HF22A in gB-expressing cell line LP64e3 (Feierbach et al., 2007). When these functionally complemented virions are injected into the brain, they will not be able to spread from the primarily infected neurons. This provides an additional safety barrier if amplicon stocks are contaminated by helper virus.

Packaging of PRV is directed by a pair of conserved sequence elements, *pac1* and *pac2*. To prevent helper virus production, we used recombineering to delete these elements in the Bacterial Artificial Chromosome (BAC) carrying the HF22A genome. We used BAC recombineering to replace *pac* elements with a copy of the Zeocin antibiotic resistance gene (Fig. 2.4a). We generated two BACs carrying different size deletions of the *pac* domains: PZ5 carried a 200 bp deletion spanning just the conserved elements of *pac1* and *pac2*(McVoy et al., 1998); PZ6 carried a 1162 bp deletion, containing the entire fragment shown to be sufficient to direct packaging of PRV amplicons (Prieto et al., 2002). We tested the ability of these BACs to direct amplicon packaging by co-transfecting them with the pORI-PAC-GFP amplicon plasmid in cells expressing gB. To quantify the levels of helper virus contamination, we measured the

number of plaque-forming units in amplicon stocks on gB-expressing cells. To measure amplicon titers, we counted the number of GFP-positive cells after infection of PK15 cells not expressing gB. Deletion of *pac* domains in PZ5 and PZ6 reduced helper virus titers by 2 and 4 orders of magnitude respectively without affecting amplicon titers (Fig. 2.4c). Residual helper production is likely the result of homologous recombination between the helper BAC and the amplicon plasmid. Consistent with this interpretation, no helper virus was produced when PZ6 was transfected alone (data not shown).

Large scale amplicon preps (see methods) generated amplicon titers up to 4×10^7 TU/ml and helper titers up to 7×10^4 pfu. To test the ability of PRV amplicons to transduce neurons in the cortex and undergo retrograde transport we injected PRV amplicons in the rat auditory cortex. Sparsely labelled neurons were found near the injection site (Fig. 2.5a) as well as in regions projecting to the injection site, such as the contralateral auditory cortex (Fig. 2.5b).

Although this demonstrates the capacity of PRV amplicons for retrograde neuronal labeling, their possible applications are limited by the low efficiency of viral infection. Efficiency might be improved with higher viral titers, either by scaling up transfection or improving transfection efficiency.

2.3.2 IE180-deficient PRV

In contrast to most herpesviruses, PRV has a single immediate-early gene, IE180, which acts as a master switch of the viral transcriptional cascade (Pomeranz et al., 2005). PRV lacking the gene encoding IE180 is unable to replicate but can be rescued when IE180 is provided *in trans* (Yamada and Shimizu, 1994). These properties make IE180-deficient PRV a potential vehicle for safe delivery of genetic material in the brain. In addition, trans-synaptic spread of PRV together with IE180 expression targeted to neurons of a specific cell type could be used to specifically label synaptic partners of these neurons.

IE180 is present in two copies in the PRV genome, located in the inverted repeat regions. We took the following approach to delete IE180 from pBecker2, a BAC carrying the genome of PRV-Becker, a virulent isolate of PRV (Smith and Enquist, 2000). We first used BAC recombineering to replace the copy of IE180 located in the terminal repeat region of PRV

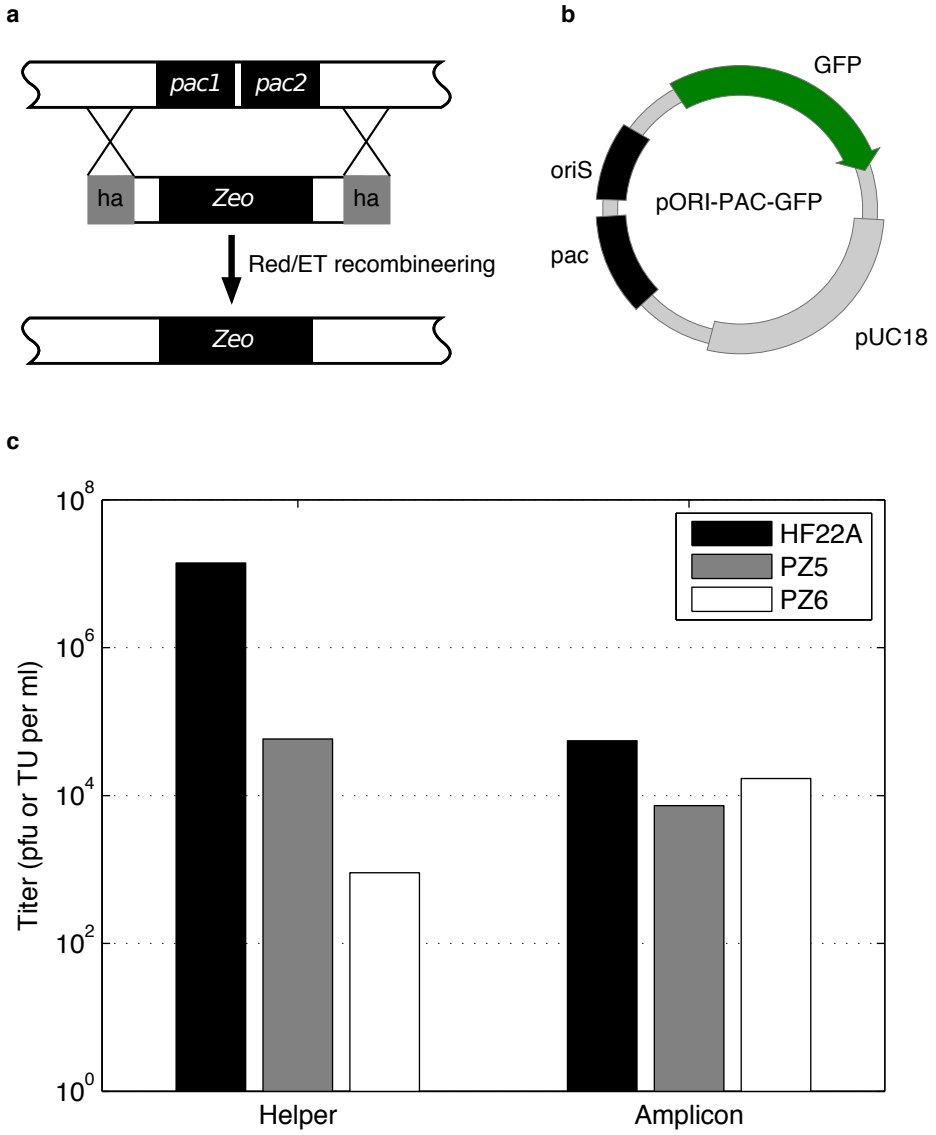

Figure 2.4: **Generation of helper-free PRV amplicons a,** Deletion of *pac* signals in the BAC carrying PRV genome. **b,** Amplicon vector pORI-PAC-GFP from (Prieto et al., 2002) used for testing helper-free amplicon production system. **c,** Helper and amplicon titers produced after co-transfections of pORI-PAC-GFP with helper BACs HF22A, PZ5 and PZ6.

(Fig. 2.6a) with a *rpsL-Neo* cassette flanked by FRT sequences, the target sites of Flp recombinase. *Neo* confers resistance to Kanamycin and is used to select recombinant clones. We then transiently expressed Flp-recombinase and used Streptomycin selection, sensitivity to which is conferred by *rpsL*, to isolate clones which successfully excized the selection cassette (Fig. 2.6b). We then repeated the same procedure to remove the internal repeat copy of IE180 (Fig. 2.6cd), generating PZ42, a BAC lacking both copies of IE180.

Transfection of PZ42 into PK15 cells produced no PRV virions detectable by plaque assay. Costitutive expression of IE180 may be to toxic to cells (Taharaguchi et al., 2003). Therefore, we generated a cell line PK15-IE180, which expresses IE180 under the control of the Tet-inducible promoter pTRE. We first infected PK15 cells with a MSCV-rtTA-hygro retrovirus and selected transduced cells with hygromycin. We then used BAC recombineering to subclone IE180 into the pUC19 cloning vector. IE180 was then excized from this vector and subcloned into the retroviral vector TTiGP. PK15-rtTA cells were then infected with TTiGP-IE180 retrovirus and plated at clonal density in the presence of puromycin to select positive clones.

To test the ability of PK15-IE180 cells to support replication of IE180-deficient PZ42, the cells were transfected with PZ42 in the presence of Doxicycline to induce IE180 expression. PZ42 transfection produced cytopathic effects indicative of PRV replication (Fig. 2.7b) and viral titers of 5×10^7 pfu/ml as measured by plaque assay on PK15-IE180 cells. One possibility was that PZ42 might recombine with the IE180 gene carried by the cell line generating fully infectious virus. However, PRV PZ42 did not generate plaques on PK15 cells lacking IE180 even when the multiplicity of infection exceded one. PK15-IE180 cells transfected by PZ42 in the absence of Doxicycline produced a viral titer of 5×10^3 pfu/ml, likely as the result of low levels of leak IE180 expression. PRV PZ42 could be amplified by passaging through PK15-IE180 cells to titers of 10^8-10^9 pfu/ml.

To examine the infection and spread of IE180-null PRV in the brain, we used BAC recombineering to insert a cassette driving expression of Cre recombinase under the neuron-specific Synapsin promoter into PZ42. The resulting BAC was transfected into PK15-IE180 cells in the presence of Doxicycline to generate virus. The viral supernatant was injected

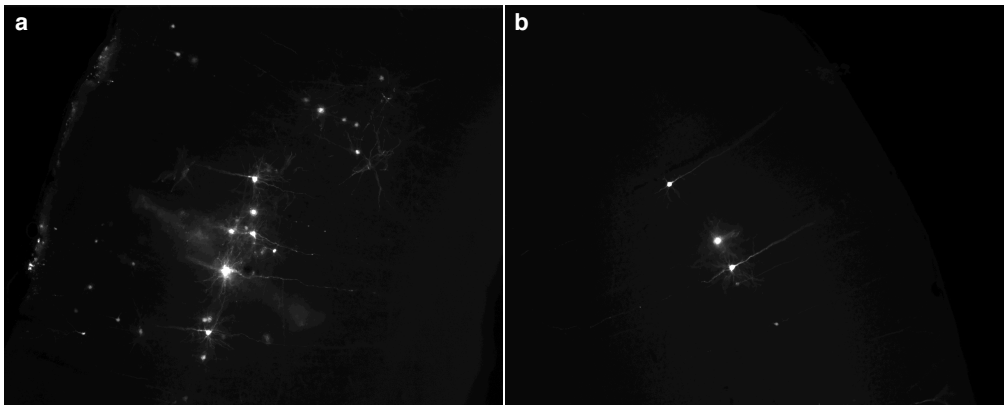

Figure 2.5: **Infection of auditory cortex neurons by PRV amplicons. a,** GFP fluorescence in the auditory cortex of a rat injected with PRV amplicons 7 days post injection. **b,** GFP fluorescence in the contralateral auditory cortex.

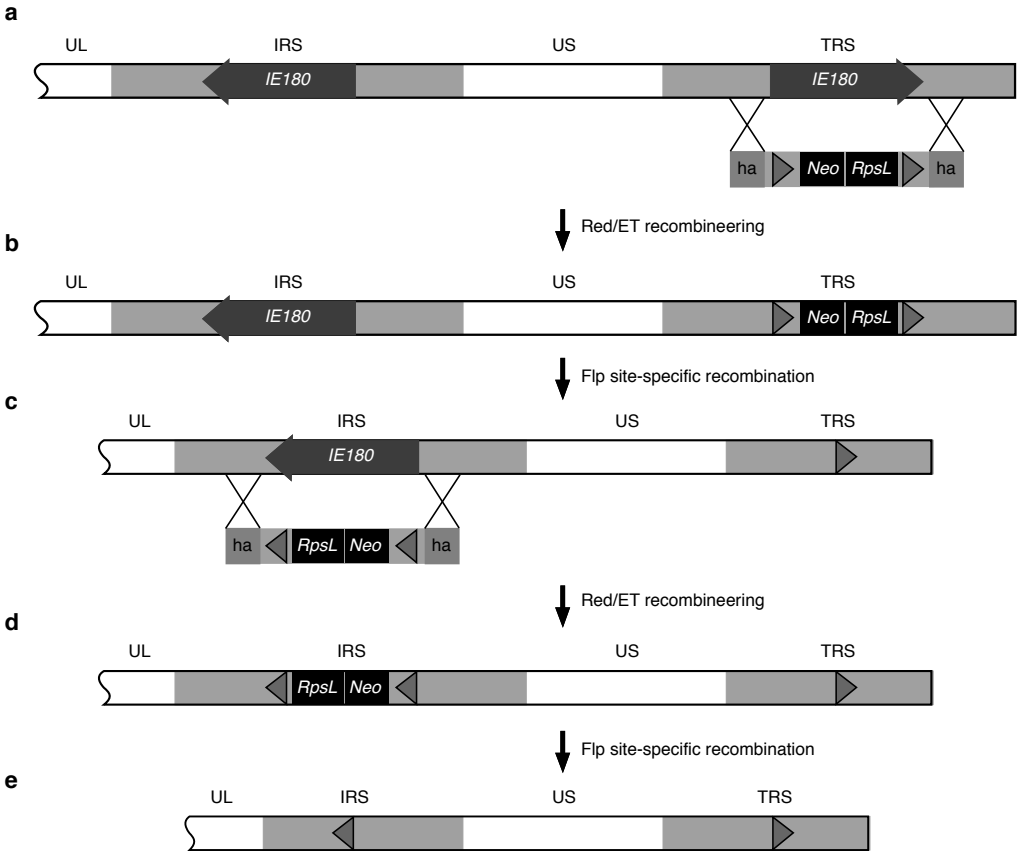

Figure 2.6: **Deleting IE180 from the PRV genome**

into the auditory cortex of Cre-reporter Ai14 mice, carrying a Cre-inducible cassette encoding tdTomato fluorescent protein. tdTomato expression was observed at the site of injection as well as in brain regions, which send projections to the auditory cortex (Fig. 2.8).

IE180-null PRV shows a lot of promise as a tool for long-term labeling of neurons based on their connectivity. It can be easily produced at a high titer using PK15-IE180 complementing cells skipping the inefficient step of BAC transfection. Retrograde labeling by PRV is efficient and does not appear to show tropism for any particular projection pathway. Furthermore, using *in vivo* complementation of IE180, PRV could be induced to spread transsynaptically between connected neurons. If IE180 expression is targeted to neurons of a specific cell type, this approach could be used to identify monosynaptic inputs to this population of cells. A caveat of this strategy is that it will likely result in toxicity in cells that express IE180. However, the cells infected by PRV transsynaptically and lacking IE180 should not be affected.

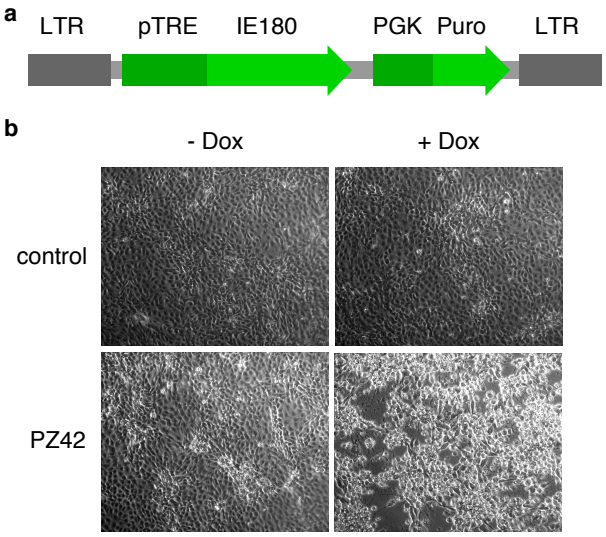

Figure 2.7: **IE180 complementation. a,** TTiGP-IE180, Tet-inducible retroviral vector for IE180 expression. **b,** Cytopathic effects indicative of PRV replication observed following transfection for PZ42 BAC when IE180 expression is induced by doxicycline.

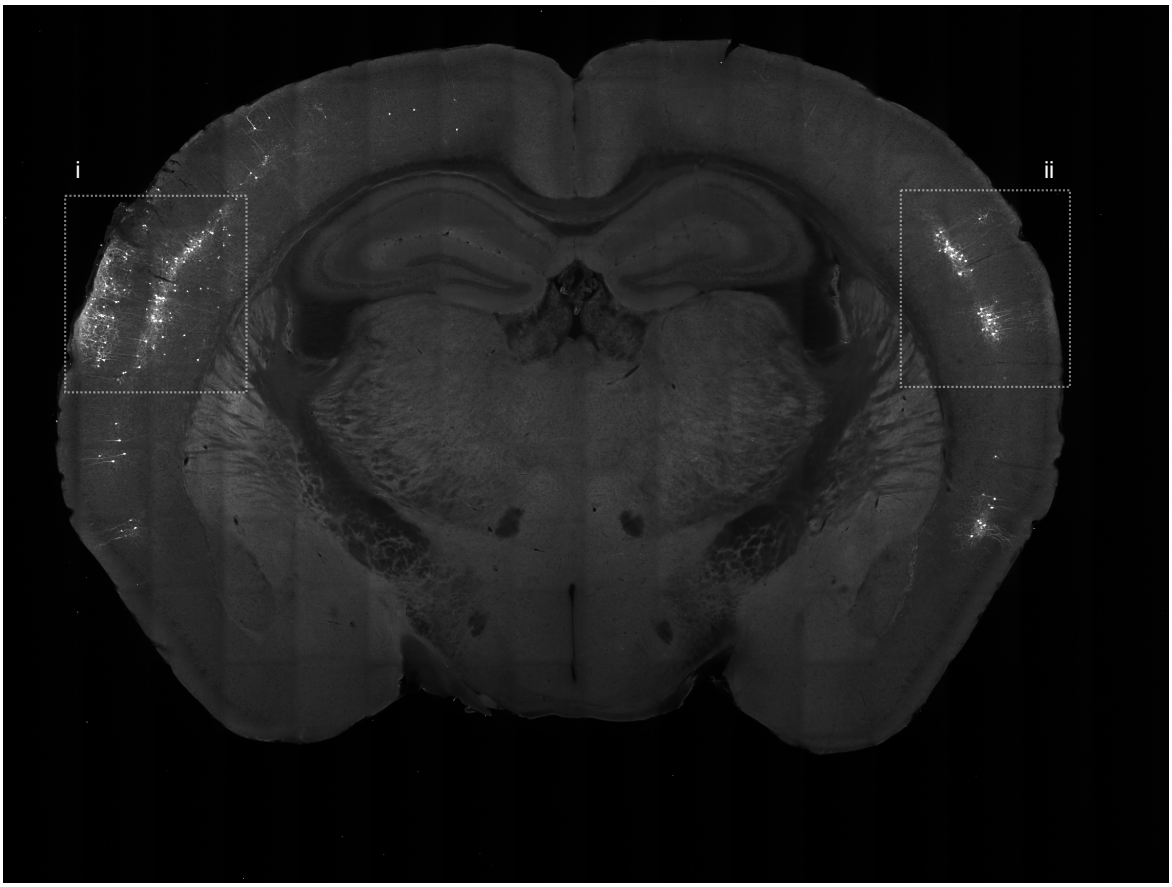

Figure 2.8: **Retrograde transport of IE180-null PRV in the mouse brain.** tdTomato fluorescence in the brain of an Ai14 mouse injected with IE180-null PRV carrying a Syn-Cre cassette. tdTomato expression was found at the injection site (i) as well as in brain regions, which send projections to the injection site, such as the contralateral auditory cortex (ii).

3

"Cloud of tones" behavioral task

The auditory cortex is organized tonotopically, with nearby neurons responding to similar sound frequencies. To investigate the function of the subpopulations of auditory cortex neurons in decisions driven by auditory stimuli, we set out to develop a frequency discrimination task that would allow us to exploit this organization to specifically manipulate neurons with similar frequency preference. With each millimeter of cortex, frequency tuning advances by $\sim$2 octaves (Doron et al., 2002). Therefore, the frequency judgments the rats would be required to perform would have to be relatively course to exploit the tonotopy. At the same time, we wanted to vary the difficulty of the task to include trials when the presented sensory evidence is ambiguous and subjects' might be more sensitive to manipulations of neuronal activity.

To satisfy these requirements, we trained rats to discriminate low and high frequency "cloud-of-tones" stimuli in a two-alternative choice task (Fig. 3.1a). On each trial the stimulus consisted of a train of short overlapping pure tones distributed over a three octave range (5-40 kHz) (Fig. 3.1b), where rats' audiogram is relatively flat (Heffner et al., 1994; Kelly and Masterton, 1977). The rate of tone presentation was constant at 100 tones/s but the frequency distribution varied from trial to trial. Subjects were required to choose between a left and a right reward port depending on whether most tones in the stimulus were drawn from the low (5-10 kHz) or high (20-40 kHz) octave. Rats were free to withdraw from the center port and report their choice at any time after the onset of the stimulus. The association between low/high frequency and left/right reward port was chosen arbitrarily for each rat.

This chapter summarizes the details of rats' behavior in the "cloud-of-tones" task. We first describe how their choices and response times vary with the frequency distribution of the stimulus. Next, we exploit the stochastic nature of the stimulus to characterize how individual tones contribute to subjects' choices. The goal of these analyses is to provide a phenomenological description of the behavior to inform the manipulation experiments described in subsequent chapters.

3.1 Psychophysical performance

To characterize the rats' performance in the task, we quantified their psychometric choices as we varied the difference in the rate of low and high frequency tones in the stimulus. Their performance varied smoothly with the number of low and high frequency tones in the stimulus and approached 100% for the easiest stimuli (Fig. 3.1c).

We fit the probability p of chosing the port associated with the high octave using logistic regression:

$$\ln \frac{p}{1-p} = \beta_0 + \beta_1(r_{high} - r_{low}) \tag{3.1}$$

r_{high} and r_{low} are the rates of high and low octave tones in the stimulus, respectively. Regression coefficients β_0 and β_1 quantify the rats choice bias and accuracy respectively. We use the slope of the psychometric curve β_1 as a measure of rats' performance in the task.

Rats learned the basic discrimination within 1000 trials but performance continued to improve during the course of 10s of thousands of trials (Fig. 3.2a). Figure 3.2b shows rats' psychometric curves at their peak performance levels.

3.2 Speed-accuracy trade-off

In addition to quantifying rats' choices, we measured their response time - time from onset of the stimulus to the rat's withdrawal from the center port. We quantified the change in response times as a function of stimulus strength $|r_{high} - r_{low}|$, referred to as the chronometric function. Drift-diffusion models of decision-making predict that subjects will respond more slowly on trials

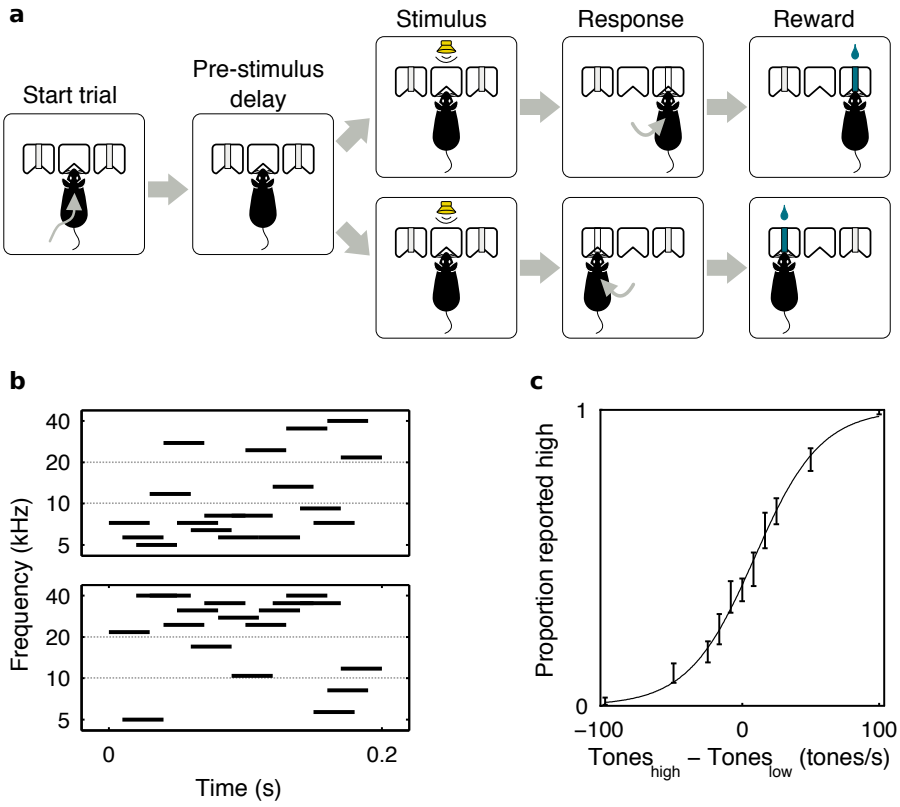

Figure 3.1: **"Cloud-of-tones" behavioral task.** **a,** Two-alternative choice task structure. **b,** Example spectrograms of stimuli at -50 and +50 tones/s (see methods). **c,** Psychometric curve for an example rat (N = 6731 trials).

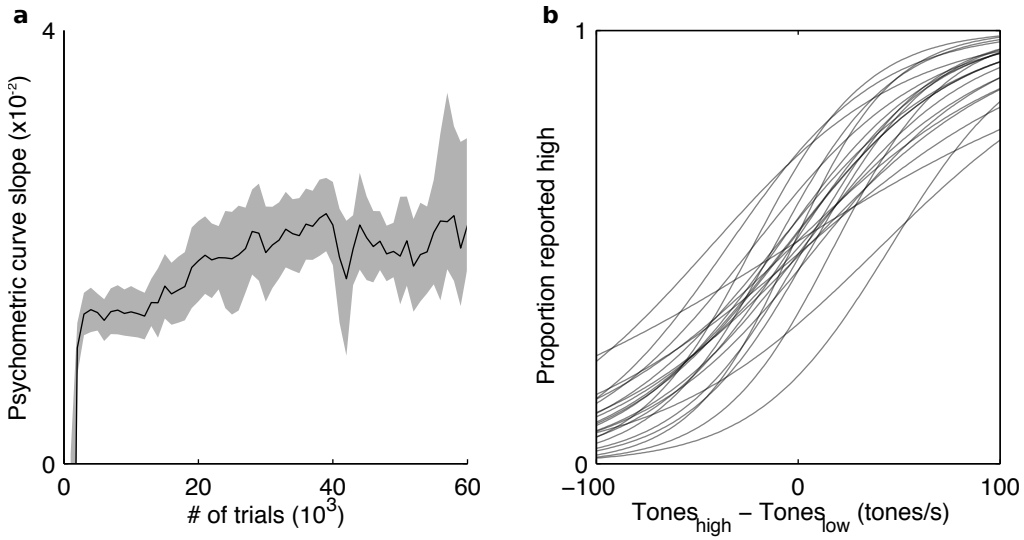

Figure 3.2: **Summary of psychometric performance. a,** Mean learning curve for N=23 rats. Gray shading is 95% confidence interval. **b,** Psychometric curves for these rats at peak performance.

with low stimulus strength, since it takes longer for accumulated sensory evidence to reach the decision threshold (Palmer et al., 2005). For many rats' response times were modulated by stimulus strength (Fig. 3.3ab). However, the direction of this modulation was inconsistent across subjects (Fig. 3.4a). For 15 of 33 rats, response times decreased significantly with stimulus strength, consistent with drift diffusion models of perceptual decisions. Paradoxically, 8 of 33 rats showed the opposite trend, responding faster on difficult trials. It is even more surprising, since reward delivery was delayed by at least 1.4 s following stimulus onset and withdrawing faster on difficult trials could not increase rats' rate of reward.

Strikingly, subjects that responded more slowly on difficult trials performed better at the task, as quantified by the slope of the psychometric curve (Fig. 3.4bc). One interpretation is that their performance benefited from longer integration times when sensory evidence was scant. The alternative explanation is that a third variable, such animals' motivation levels, influences both their accuracy and response times, speeding up reaction times on easy trials when reward expectation is high. In constrast, rats' mean response time had no impact on their response accuracy (Fig. 3.4d).

Together, these data suggest that individual rats adopt different strategies in the task. While some emphasize accuracy over speed, others respond as fast as possible at the expense

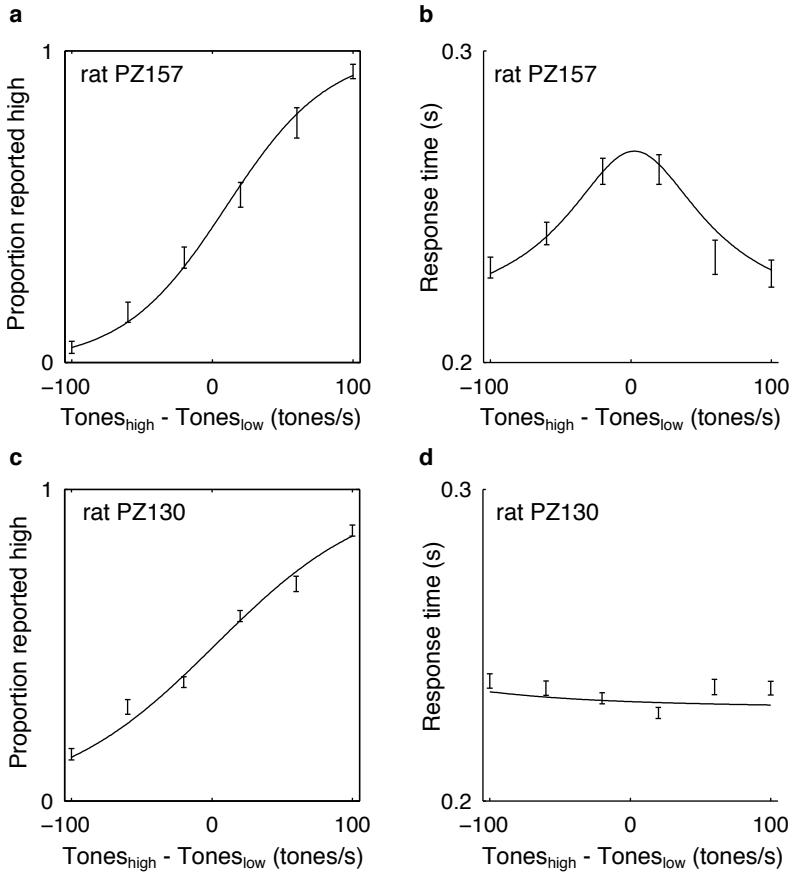

Figure 3.3: **Modulation of rats' response times by stimulus strength. a-b,** Psychometric and chronometric functions for an example rat that responds slower on difficult trials. Error bars - 95% confidence interval. **c-d,** Psychometric and chronometric functions for an example rat that shows no effect of stimulus strength on response times.

of accuracy. We found no obvious trend that influenced, which strategy the rats assumed. Littermates trained alongside each other often adopted opposite strategies, which persisted independent of the duration of training.

3.3 Psychophysical kernels

A subject aiming to perform the task optimally would compare the rate of high and low octave tones during the entire duration of the trial and select the reward port associated with the more prevalent octave. To quantitatively evaluate the strategy adopted by the rats, we computed psychophysical kernels measuring how rats' weigh tones presented at different time points during the trial.

Psychophysical kernels are often estimated using reverse correlation. Stimuli preceeding different choices are compared to the elements of the stimulus that have the greatest impact on behavior (Nienborg and Cumming, 2007). We took a different approach, analogous instead to the method used by Huk and Shadlen to measure the behavioral effects of transient perturbations of momentary motion evidence in a motion discrimination task (Huk and Shadlen, 2005).

To measure the behavioral impact of tones presented at a particular point during the trial, we computed the rates of high and low tones, r_{high} and r_{low}, excluding the tone presented at that point in time.

$$r_{high}(t) = \frac{\sum_{i \neq t}^{N} I_{high}(t)}{N}; \quad r_{low}(t) = \frac{\sum_{i \neq t}^{N} I_{low}(t)}{N} \tag{3.2}$$

$I_{high}(t)$ and $I_{low}(t)$ indicate the presence of a high or low frequency tone in the stimulus at time t; N is the total number of tones presented during the trial. We then fit subjects' choices with logistic regression by modifying equation (3.1):

$$\ln \frac{p}{1-p} = \beta_0 + \beta_1 (r_{high}(t) - r_{low}(t)) + \beta_2 \frac{I_{high}(t) - I_{low}(t)}{N} \tag{3.3}$$

$I_{high}(t)$ and $I_{low}(t)$ is normalized by total number of tones N, so that $\frac{I_{high} - I_{low}}{N}$ carries the same units as $r_{high} - r_{low}$. Coefficient β_2 measures the impact of tones presented at this

position in the stimulus on subjects' choices. Dividing β_2 by β_1 converts it to units the stimulus, measuring the change to the overall stimulus that would produce the same behavioral effect as adding a tone at time t.

An alternative approach is to simply directly model subjects choices by explicitly assigning weights to each position in the stimulus:

$$\ln \frac{p}{1-p} = \beta_0 + \sum_{t=1}^{N} \beta_t \frac{I_{high}(t) - I_{low}(t)}{N} \tag{3.4}$$

The two approaches are equivalent for tasks with a fixed stimulus duration. However, the latter approach in a reaction time tasks does not account for the fact that different subsets of trials are used to estimate β_t for different time points in the stimulus. For example, subjects may be less attentive on trials with longer response times; this possibility is further explored below. Any such global variations in subjects' behavior will bias our estimates of the psychophysical kernel. Nevertheless, psychophysical kernels estimated using these two methods gave qualitatively similar results. We will from this point present the results of the method summarized in equation (3.3).

Using this approach we evaluated the behavioral impact of tones at depending on their timing relative to the onset of the stimulus (Fig. 3.5ace) or the rats' withdrawal from the center port (Fig. 3.5bdf). Psychophysical kernels computed for individual subjects' were noisy; standard error of the estimate increased with latency as fewer trials with sufficiently long response times were available. However, kernels for different subjects followed a stereotyped pattern (Fig. 3.5cd), which allowed us to combine data from multiple subjects (Fig. 3.5ef).

Several features are apparent from these measurements. The peak at the zero position of the psychophysical kernel indicates that the first tone in the stimulus is weighted disproportionately by the rats, having almost 5$\times$ the influence on subjects choices as tones later in the trial. At 30 ms into the trial the kernel decays to ~ 1, where it remains for as long as 400 ms, or almost twice the typical response time. Similarly, the withdrawal aligned kernel peaks at 140 ms before rats' response but remains >0 for the duration of the examined time interval. At first glance these results suggest that although rats give excess weight to tones at the beginning and at the end of the stimulus, they continue to integrate sensory evidence for the duration of

the trial. However, this analysis is confounded by the the fact that these psychophysical kernels combine trials with a wide range of response times.

To address this confound we estimated psychophysical kernels separately for trials with different response times (Fig. 3.6). On trials with typical response times (0.2-0.3 s), subject choices were indeed influenced by tones throughout the stimulus with a slightly higher weight given to tones at the onset. However, on trials with longer response times, only the tones in the last ∼0.2 s of the stimulus influenced subjects' behavior. This suggests that trials with these extended response times reflect momentary lapses of attention. Consistent with this interpretation, trials with response times >0.3 s were most common following brief pre-stimulus delays (Fig. 3.7), when the rat had just entered the center port.

We can further break down subjects' strategy by computing the psychophysical kernel for each of 18 tone frequencies in the stimulus:

$$\ln \frac{p}{1-p} = \beta_0 + \beta_1(r_{high}(t) - r_{low}(t)) + \beta_{f_1}\frac{I_{f_1}(t)}{N} + \cdots + \beta_{f_{18}}\frac{I_{f_{18}(t)}}{N} \tag{3.5}$$

Here I_{f_n} indicates the presence of an f_n Hz tone at this position in the stimulus. To measure the relative behavioral impact of tones of different frequencies across time, we compute their weights as follows:

$$w_{f_n,t} = \frac{\beta_{f_n}(t) - \dfrac{\sum_{i=1}^{18}\beta_{f_i}(t)}{18}}{\beta_1(t)}$$

This spectrotemporal psychophysical kernel for an example rat is shown in Fig. 3.8a. Since it appeared to change in magnitude but not its frequency content over time, we averaged it along the time axis (Fig. 3.8b). As tones in the middle octave (10-20 kHz) carry no information about the location of reward, an optimal kernel should give zero weight to these frequencies and equal in magnitude but opposite in sign weights to tones in the low and high octaves. Instead, in most subjects tones of the middle octave biased them toward the low frequency choice port (Fig. 3.8cd).

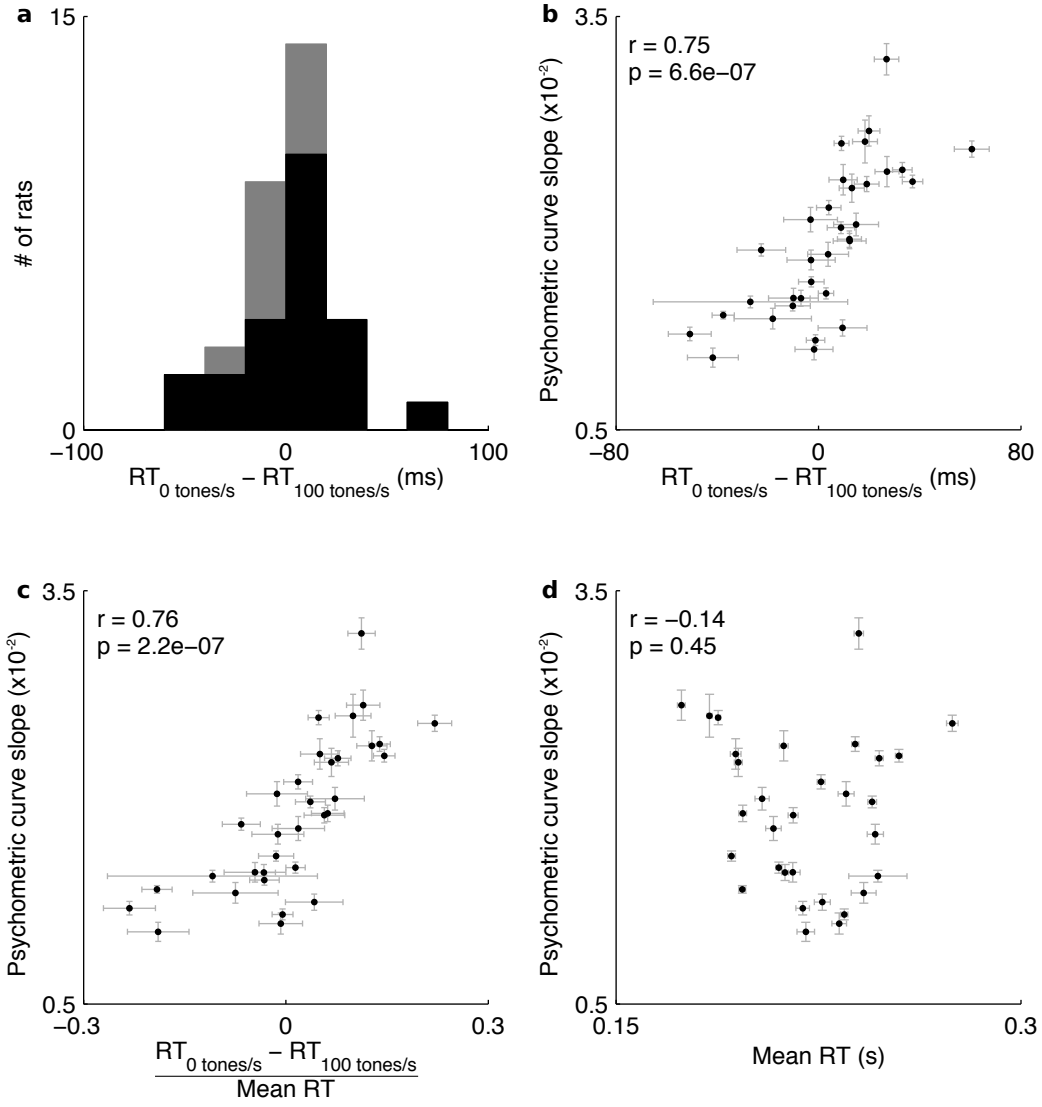

Figure 3.4: **Speed-accuracy trade-off in "cloud-of-tones" task. a,** Modulation of response time by stimulus strength across rats, estimated from linear regression fits of chronometric functions on correct trials. Black bars - rats, whose chronometric functions slope was significantly different from 0 ($p < 0.05$). **b,** Slope of chronometric function (difference of response time from 0 to maximum stimulus strength) predicts psychometric curve slope. **c,** Same as panel **b**, with response time modulation plotted as a fraction of mean response time. **d,** Psychometric performance does not vary with mean response time.

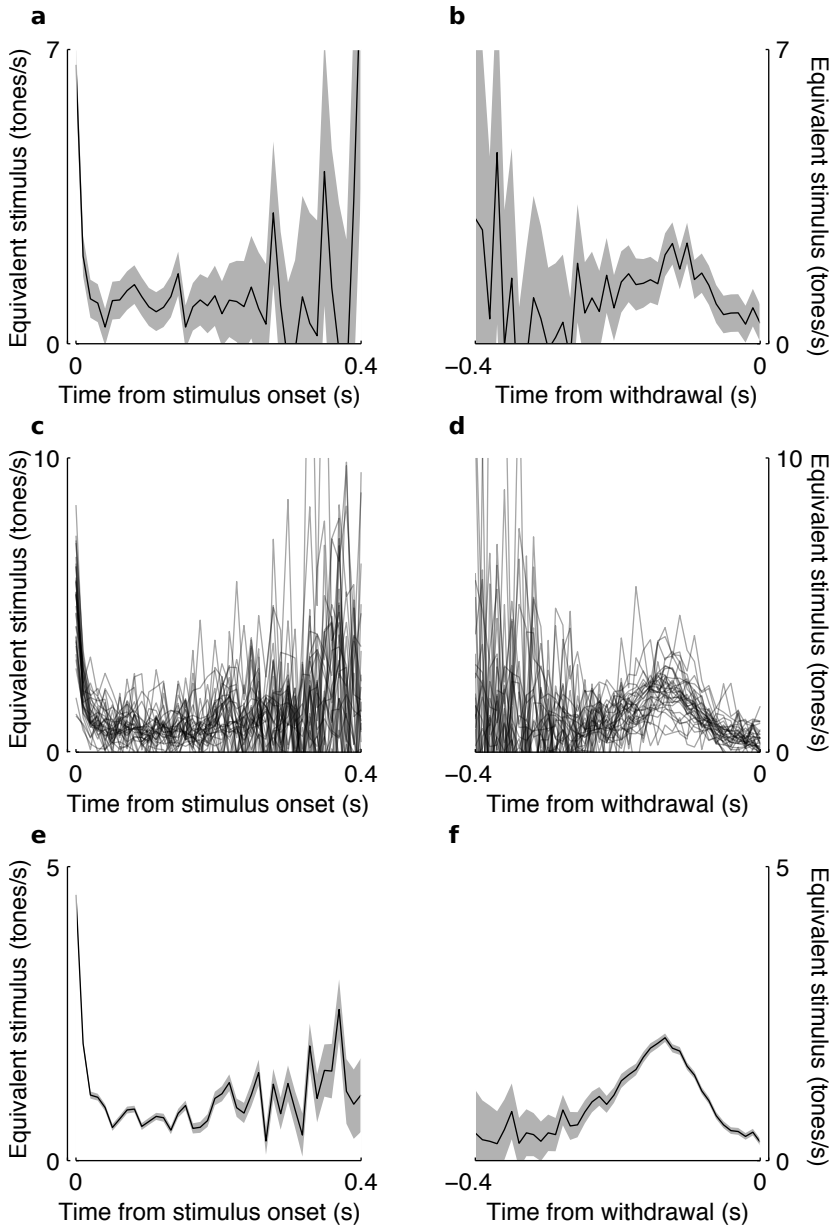

Figure 3.5: **Timecourse of psychophysical kernels. a,** Psychophysical kernel for an example rat estimating behavioral impact of tones aligned to stimulus onset. Gray shading is 95% confidence interval. **b,** Psychophysical kernel for an example rat estimating behavioral impact of tones aligned to rat's withdrawal from the center port. **c,** Psychophysical kernels 33 rats aligned to stimulus onset. **d,** Psychophysical kernels 33 rats aligned to withdrawal from the center port. **e,** Inverse-square error weighted mean of psychophysical kernels in panel **c**. Gray shading is 95% confidence interval. **f,** Inverse-square error weighted mean of psychophysical kernels in panel **d**.

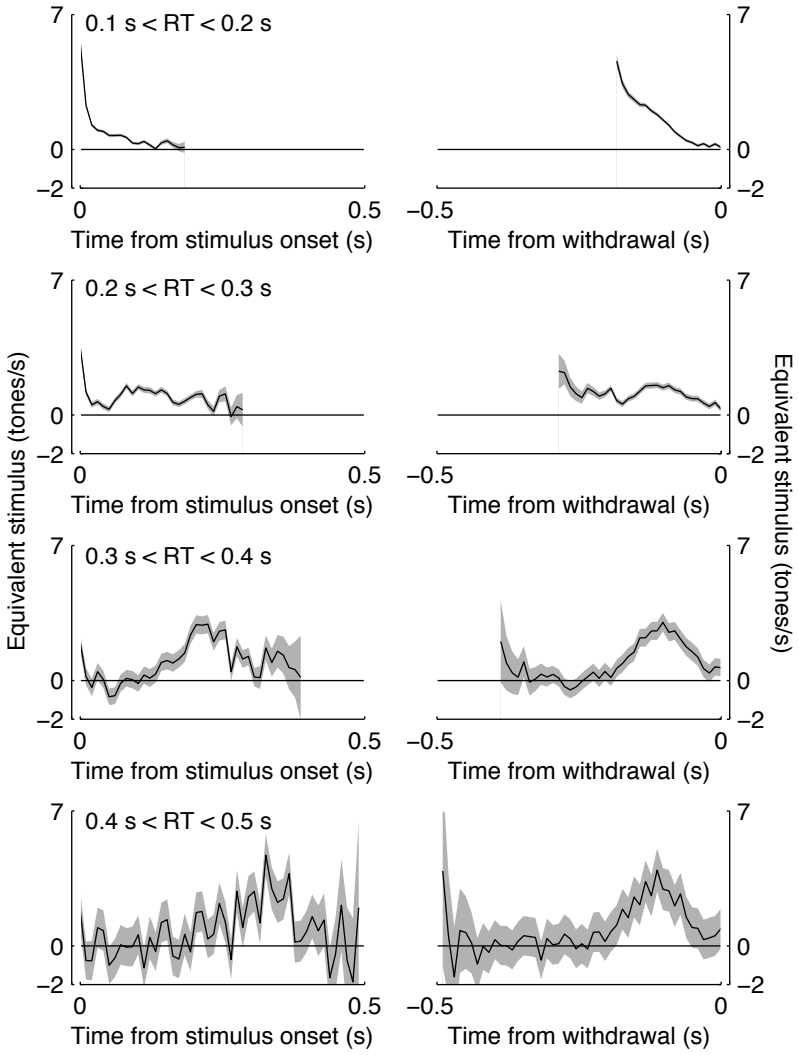

Figure 3.6: **Psychophysical kernels binned by response time.** Sound onset and withdrawal-aligned psychophysical kernels for trials where the rat responded 0.1-0.2 s, 0.2-0.3 s, 0.3-0.4 s or 0.4-0.5 s from stimulus onset.

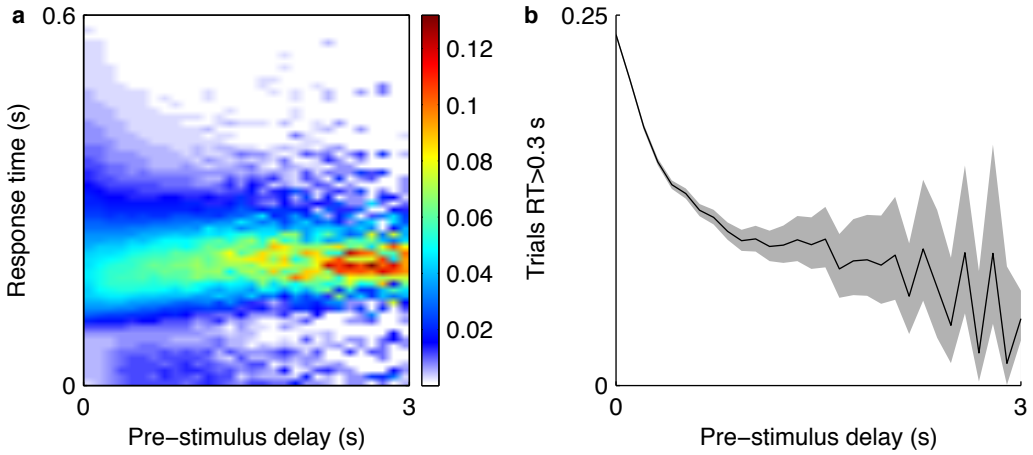

Figure 3.7: **a,** Distribution of response times as a function of pre-stimulus delay. **b,** Response times exceeding 0.3 s are most common on trials with brief pre-stimulus delays.

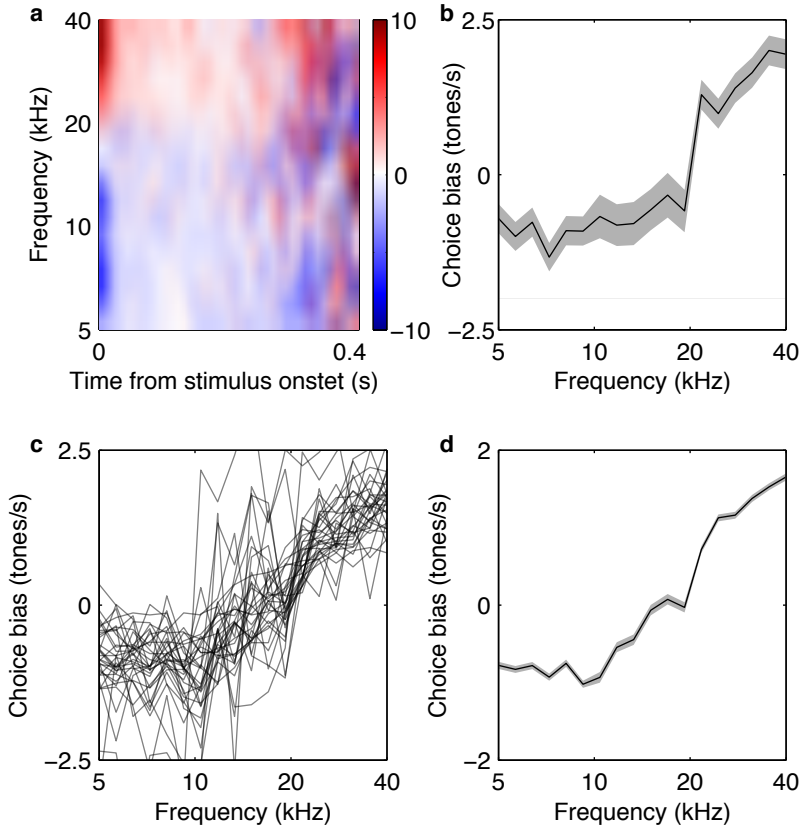

Figure 3.8: **Psychophysical kernels in the frequency domain.** **a,** Onset-aligned psychophysical kernel broken down by tone frequency for an example rat. **b,** Psychophysical kernel in panel **a** collapsed alogn the time dimension. **c,** Frequency kernels for 33 rats follow a stereotyped pattern with few exceptions. **d,** Inverse-square error weighted mean of psychophysical kernels in panel **c**.

4

Neuronal responses in the "cloud of tones" task

The acoustic world is represented in the activity of neurons in the auditory cortex. Individual cortical neurons differ in their selectivity to sounds. Responses in the auditory cortex are sparse, for a given sound only a minute fraction of the neurons respond vigorously (Hromádka et al., 2008). While "preferred" stimuli that can elicit reliable responses can be identified for most neurons (Wang et al., 2005), no general framework akin to orientation selectivy in visual cortex (Hubel and Wiesel, 1959) has been discovered to characterize the properties of auditory cortical cells. One principle that has been well-established is the tonotopic or cochleotopic organization of the auditory cortex. As discussed in Chapter 3, tonotopy was a key factor in the design of the "cloud-of-tones" task.

To understand how the "cloud-of-tones" stimulus is represented in the auditory cortex, we recorded the activity of single auditory cortical neurons in rats performing the task. We found a diversity of sound-evoked responses. While some neurons showed no modulation of firing in response to the stimulus, others showed transient or sustained responses. Furthermore, responses were modulated by the frequency content of the "cloud-of-tones" stimulus. A similar pattern of responses was observed in auditory striatal neurons.

The activity of a surprising number of cortical and striatal neurons was modulated by the rat's choice after the rat withdrew from the center port. Given the timing of these responses, they are unlikely to be causal in the animal's decision but probably constitute an

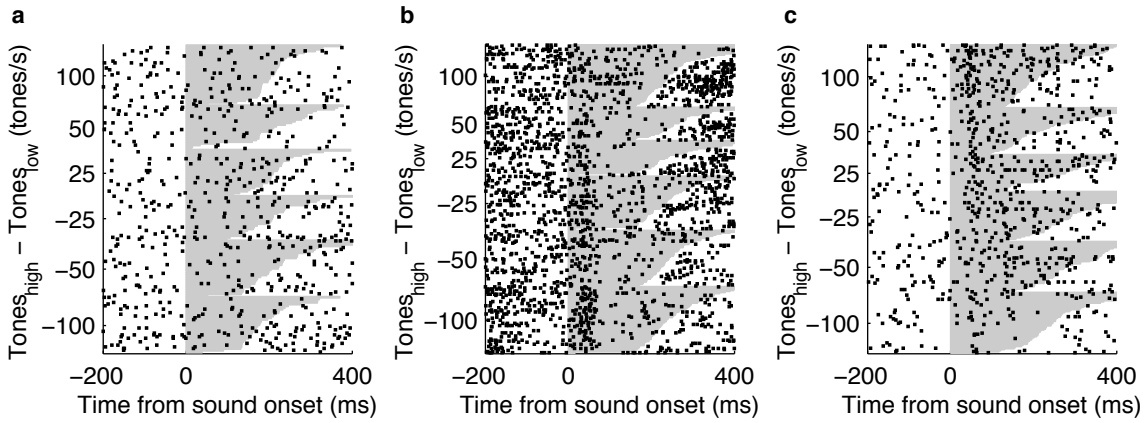

Figure 4.1: **Diversity of responses to the "cloud-of-tones" stimulus in the auditory cortex. a,** Raster from an example auditory cortex neuron, which shows no modulation in the response to "cloud-of-tones" stimulus. Gray shading indicates timing of the stimulus, dependent on rat's position at the center port. Trials at each stimulus strength are sorted by response time. **b,** Example neuron showing a transient frequency-selective response to the "cloud-of-tones" stimulus. **c,** Example neuron showing a sustained frequency-selective response to the "cloud-of-tones" stimulus.

efference copy of a motor command generates elsewhere. Choice selectivity during the movement period and stimulus selectivity during sound presentation appear to be related, depending on the association between sound frequency and choice established in the task.

The striatal neurons analyzed in this chapter were recorded during behavioral experiments described in Sec. 6.4. Our sample is small and due to the typically low firing rates of striatal MSNs measurements from single neurons are noisy. Therefore, beyond the fact that striatal neurons carry signals about the auditory stimulus, the results presented here should be treated as preliminary.

4.1 Auditory responses

Auditory cortical neurons showed a diversity of responses to the "cloud-of-tones" stimulus. The firing of many neurons was not modulated at all (Fig. 4.1a). This was to be expected since we made no attempt to fine tune the stimulus parameters to match the selectivity of individual neurons. Among cells that did respond to the sound stimulus, neurons differed in the temporal dynamics of their responses. Some neurons showed transient responses confined to the first few

10s of milliseconds of sound presentation (Fig. 4.1b), while responses of other neurons were sustained for the duration of the stimulus (Fig. 4.1c).

Generally, neuronal firing rates varied monotonically with changes in the rate of high and low tones in the "cloud-of-tones" stimulus (Fig. 4.2ab). To analyze the extent to which signals carried by single neurons carry sufficient information to perform the task, we computed their neurometric functions, quantifying how well an "ideal observer" would perform the discrimination given access to the spike trains of a given neuron. For each neuron, we determined its preference for high or low frequency "cloud-of-tones" stimuli and an optimal discrimination threshold. Trials, when the neuron produced a number of spikes greater than or equal to the threshold were assigned to responses associated with the prefered frequency of the neuron. To prevent over-fitting, we used *leave-one-out* cross-validation and excluded the trial under consideration from estimation of frequency preference and firing threshold. We then fit neuronal choices to using the same logistic model we previously used to fit subjects' psychometric functions (Eq. 3.1) to generate the neurometric function (Fig 4.2c). For each neuron, we compared the its neurometric slope to the slope of the rats' psychometric function measured during the recording session. In our sample of ACx neurons, individual cells rarely matched the performance of the rats, although most neurones could discriminate the stimulus above chance levels (Fig. 4.2d).

Auditory striatal neurons showed a similar distribution of responses (Fig. 4.3). The median neurometric slopes in auditory cortex and striatum were not significantly different (0.23 and 0.21 respectively, p = 0.76, Wilcoxon ranksum test).

4.2 Choice selective responses

For some auditory cortical neurons, firing rate was modulated by rat's choice after the rat withdrew from the center port (Fig. 4.4a). To quantify this modulation, we computed a choice modulation index, $\frac{FR_{contra} - FR_{ipsi}}{FR_{contra} + FR_{ipsi}}$, where FR_{contra} and FR_{ipsi} are firing rates 50 to 300 ms following withdrawal for contralateral and ipsilateral choices respectively. This choice index was significantly different from 0 for 99 of 155 neurons examined ($p<0.05$, signed-rank test).

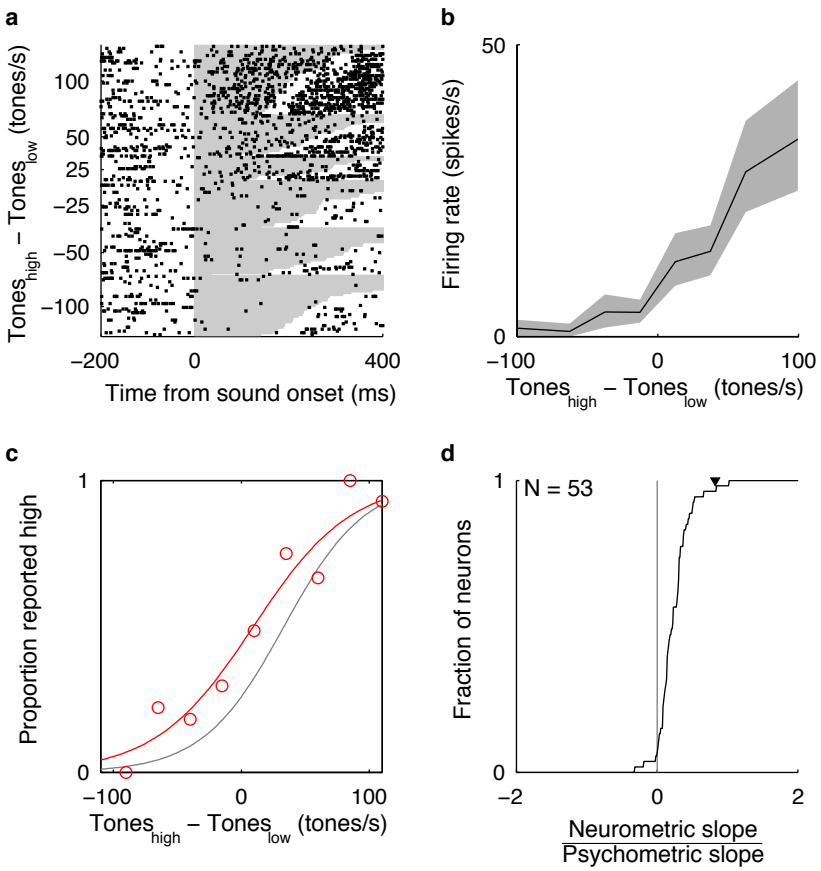

Figure 4.2: **Frequency-selective responses to the "cloud-of-tones" stimulus in the auditory cortex.** **a,** Raster from an example auditory cortex neurone shows a monotonic response to frequency content of the tonecloud stimulus. Gray shading indicates rat's position at the center port. **b,** Tuning curve of neuron in panel **a**. **c,** Neurometric performance of neuron in panel **b** (red) is similar to behavioural performance (gray). **d,** Distribution of the ratio of neurometric and psychometric curve slopes across the population of auditory cortical neurons. We used leave-one-out cross validation to get an unbiased estimate of neurometric performance, resulting in a small fraction of negative slopes. Majority of neurons have positive slopes. Triangle marks the example neuron in panels **a-c**.

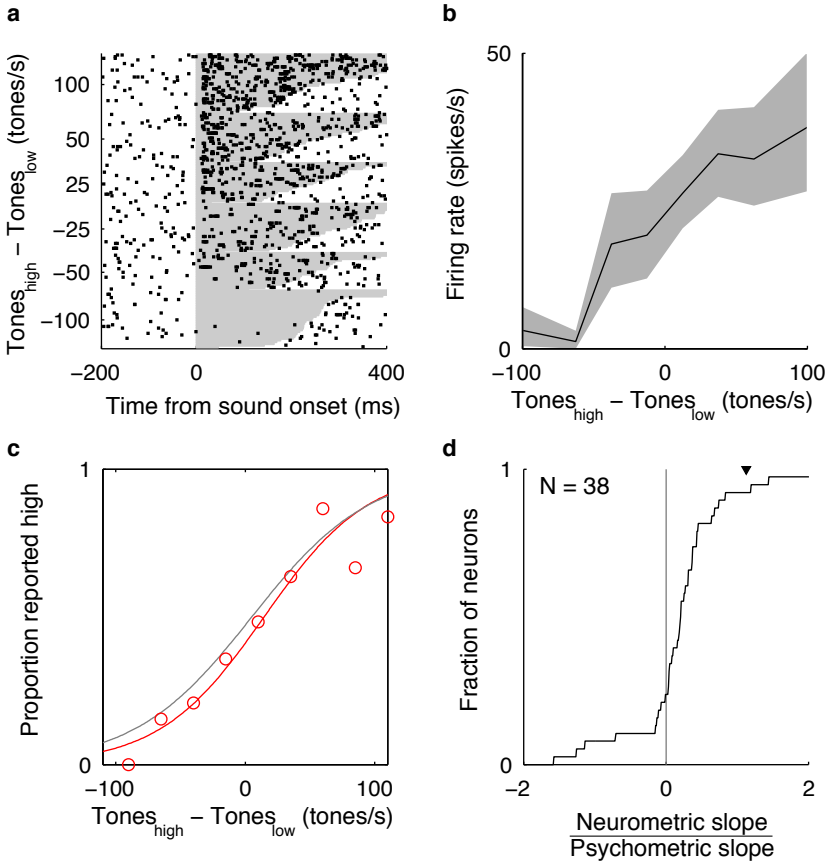

Figure 4.3: **Frequency-selective responses to the "cloud-of-tones" stimulus in the auditory striatum. a,** Raster from an example auditory striatum neuron shows a monotonic response to frequency content of the tonecloud stimulus. Gray shading indicates rat's position at the center port. **b,** Tuning curve of neuron in panel **b**. **c,** Neurometric performance of neuron in panel **b** (red) is similar to behavioural performance (gray). **d,** Distribution of the ratio of neurometric and psychometric curve slopes across the population of auditory striatal neurons. Triangle marks the example neurone in panels **a-c**.

Neurons preferring ipsilateral and contralateral choices were equally prevalent in the population (Fig. 4.4b).

To characterize the timing of these choice-related responses, we selected ACx neurons that showed significant choice selectivity ($p<0.01$, signed-rank test) and plotted their PETHs aligned to the onset of the rat's withdrawal from the center port (Fig. 4.4c). Across the population, these responses spanned the entire time of the rat's movement to the reward port.

To examine whether the preceeding stimulus had some impact on choice-related responses of auditory cortical neurons, we compared the neurons' choice selectivity on correct and error trials. In the extreme case, should the movement period responses actually reflect some residual activity produced by the auditory stimulus, we would expect the choice index to change its sign on error trials. However, we observed no systematic difference in choice selectivity indices estimated from correct and erroneous responses (Fig. 4.4d).

Finally, we examined whether a neuron's choice selectivity is related to its response selectivity during stimulus presentation. We calculated a stimulus modulation index, analogous to the choice index, by comparing firing rates during presentation of "cloud-of-tones" stimuli associated with contralateral and ipsilateral choices (Fig. 4.4e). Across the population, there was no correlation between stimulus and choice selectivity ($r = 0.09$, $p = 0.18$, 207 cells). However, among cells that showed significant stimulus selectivity ($p < 0.05$, signed-rank test), choice and stimulus indices were correlated ($r = 0.42$, $p = 0.0021$, 51 cells). Ignoring the magnitude and just considering the direction of choice and stimulus selectivity, 34 of 51 neurons fired more during movements toward the choice port associated with their preferred stimulus, more than would be expected by chance ($p = 0.012$, binomial test). Nevertheless, some of the neurons clearly violated this relationship. Among cells that were significantly modulated by both the auditory stimulus and rat's movement toward the reward port, 15 preferred movements toward the port associated with their preferred stimulus, while 8 had the opposite selectivity.

Since the association between stimulus and choice is arbitrary and established through training in the task, this correlation between stimulus and choice selectivity must be a consequence of plasticity during acquisition of the task.

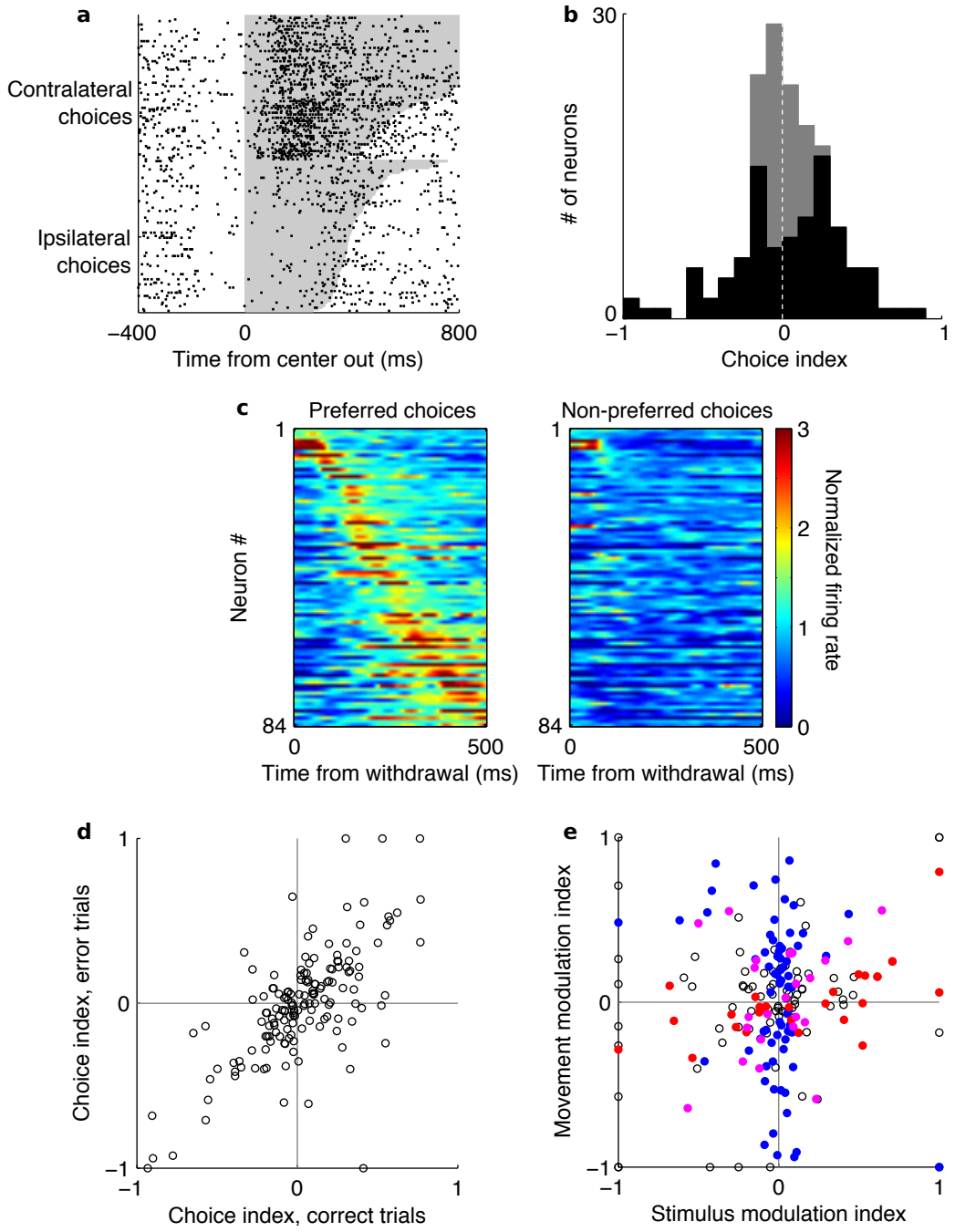

Figure 4.4: **Choice-selective responses in the auditory cortex during subjects' movement.** **a,** Spike raster from an example cortical choice selective cell. Shading indicates rat's travel time from the center port to the reward port. **b,** Histogram of choice selectivity indices calculated as $\frac{FR_{contra} - FR_{ipsi}}{FR_{contra} + FR_{ipsi}}$ using the period 50 to 300 ms following withdrawal for cells whose mean firing rate $(FR_{contra} + FR_{ipsi})/2 > 1$ Hz. Black - cells with significant choice-related modulation ($p < 0.05$, Wilcoxon rank-sum test). **c,** Normalized PETHs for all cells with significant ($p < 0.01$) choice-related modulation, sorted by their peak response timing. **d,** Choice selectivity indices on correct and error trials (N=155 neurons). **e,** Scatter plot of stimulus and choice selectivity indices (N=207 neurons). Blue - cells with evoked firing rates >0.5 Hz.

Similar choice-selective responses were observed during movement to the response port among auditory striatal neurons (Fig. 4.5a-c). As in the auditory cortex, there was no correlation between stimulus and choice selectivity ($r = -0.04$, $p = 0.75$, 70 cells). We did not have a sufficient sample of striatal cells with significant stimulus selectivity to carry out this analysis. Instead, we selected cells with evoked firing rates >0.5 Hz. For this population, stimulus and choice selectivity were correlated ($r = 0.41$, $p = 0.0036$, 48 cells), just as for stimulus selective neurons in the cortex.

4.3 Spike width and cell heterogeneity

Extracellular action potential waveforms can differ considerably between neurons. Neuronal populations often show a bimodal distribution of spike width, which has as a result been widely used to chatergorize neurons. Both in the cortex and the striatum, narrow spikes are primarily associated with parvalbumin-positive inhibitory interneurons (Barthó et al., 2004a; Berke et al., 2004; Kawaguchi, 1993; Lima et al., 2009).

In our cortical sample of auditory cortical spike waveforms, two distinct subpopulations were readily apparent (Fig. 4.6a). We classified narrow-spiking neurons as cells with peak-to-valley latencies no greater than 250 μs. These neurons had symmetric waveforms (spike peak and valley of similar amplitudes) and fairly consistent mean firing rates (Fig. 4.6ab). In contrast, broad-spiking neurons had asymmetric waveforms and were more heterogeneous in firing rate. Within this population, neurons with brief waveforms tended to have low firing rates, while those with broader waveforms fired at rates similar to narrow-spiking cells. Stimulus evoked firing rates were also greater for narrow-spiking neurons (Fig. 4.6c).

Narrow and broad spiking neurons could also be distinguished in auditory striatal recordings (Fig. 4.7ab). Unlike cortical narrow-spiking cells, the action potentials of these putative striatal interneurons are not symmetric (Fig. 4.7b). Their mean and evoked firing rates were much higher than that of broad-spiking putative MSNs (Fig. 4.7cd), consistent with published observations (Berke et al., 2004).

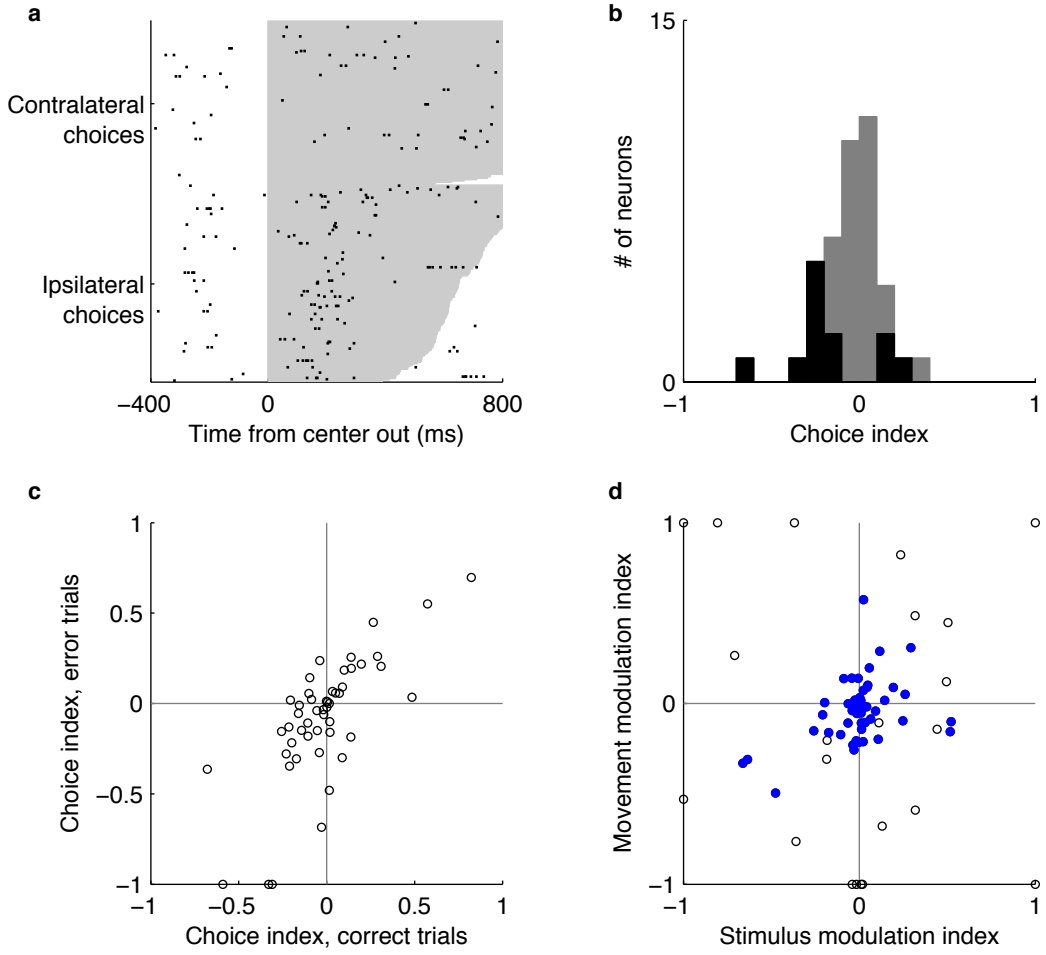

Figure 4.5: **Choice-selective responses in the auditory striatum during subjects' movement.** **a,** Spike raster from an example choice selective cell. Shading indicates rat's travel time from the center port to the reward port. **b,** Histogram of choice selectivity indices calculated as $\frac{FR_{contra} - FR_{ipsi}}{FR_{contra} + FR_{ipsi}}$ using the period 50 to 300 ms following withdrawal for cells whose mean firing rate $(FR_{contra}+FR_{ipsi})/2 > 1$ Hz. Black - cells with significant choice-related modulation ($p < 0.05$, Wilcoxon rank-sum test). **c,** Choice selectivity indices on correct and error trials (N=49 neurons). **d,** Scatter plot of stimulus and choice selectivity indices (N=70 neurons). Red - cells with significant stimulus-selective responses; blue - cells with significant choice-related responses; magenta - cells with significant selectivity for both stimulus and choice.

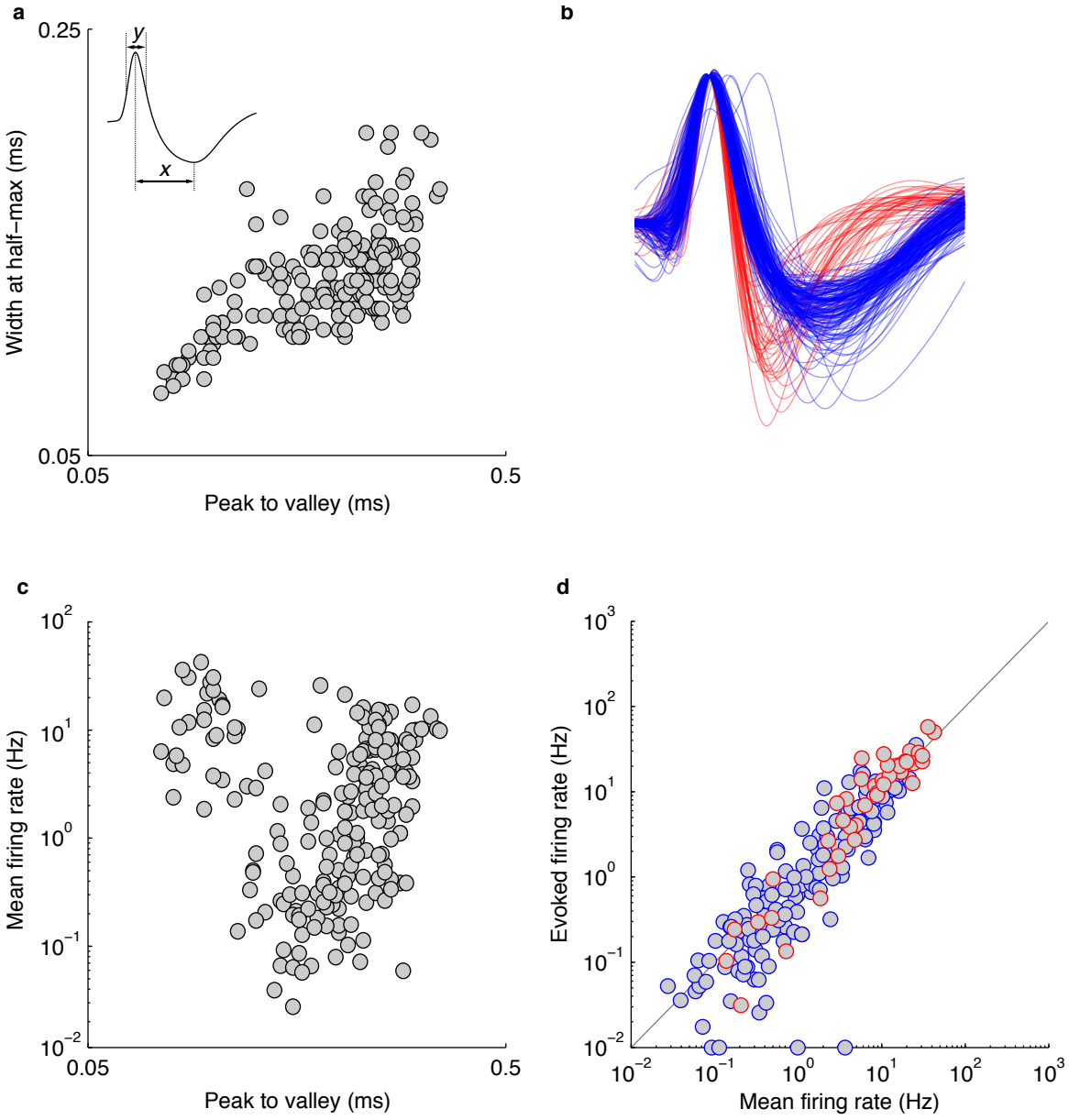

Figure 4.6: **Spike waveform heterogeneity in the auditory cortex.** **a,** Peak-to-valley duration (x in inset) and width at half-max (y in inset) of action potential waveforms of auditory cortical neurons. **b,** Mean waveforms of auditory cortical cells. Blue - broad-spiking cells with peak-to-valley duration >250 μs; red - narrow-spiking cells. **c,** Peak-to-valley duration and mean firing rate of cortical neurons. **d,** Mean and evoked firing rates of cortical neurons. Blue - broad spiking cells, red - narrow-spiking cells.

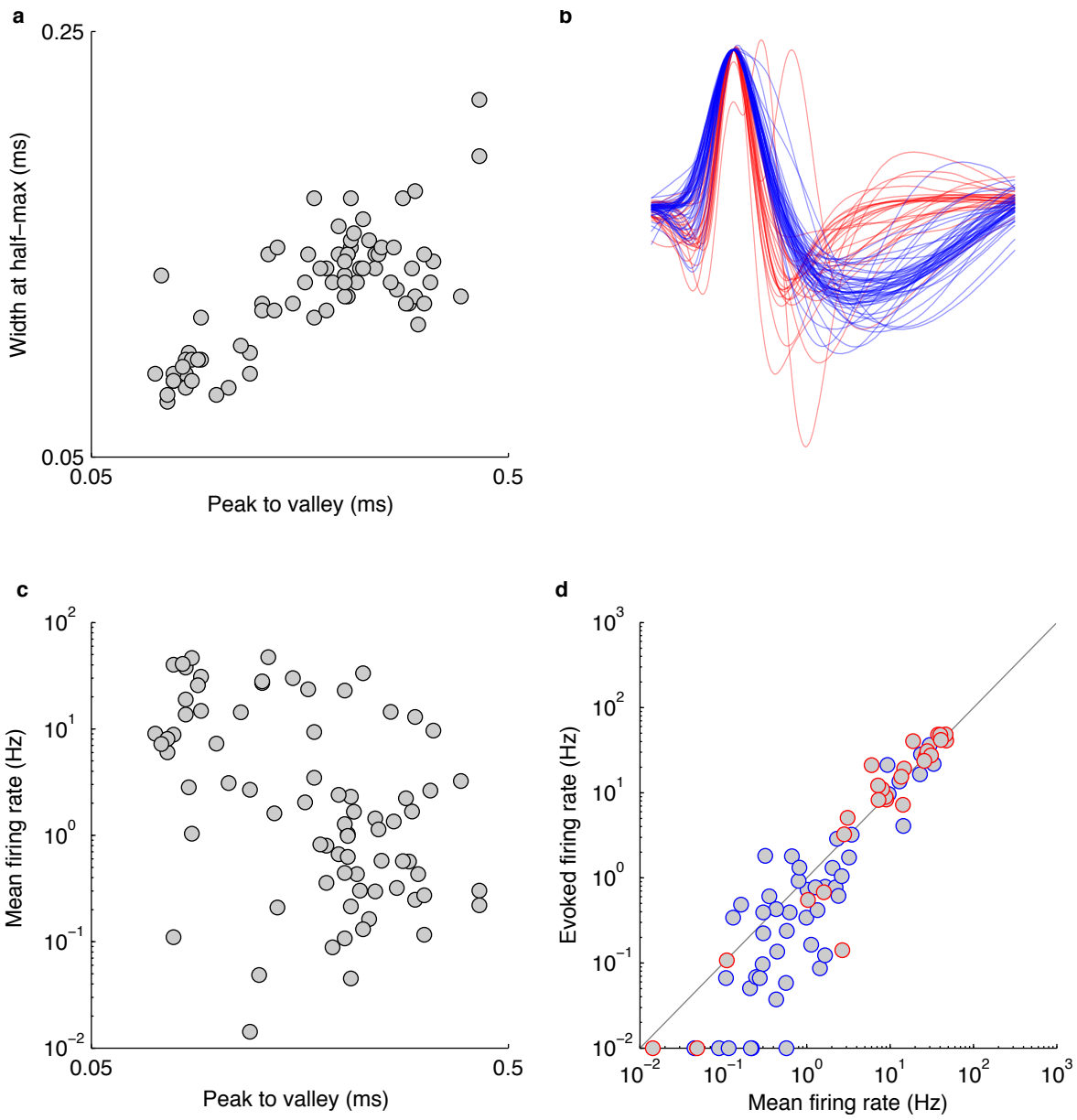

Figure 4.7: **Spike waveform heterogeneity in the auditory striatum. a,** Peak-to-valley duration and width at half-max of action potential waveforms of auditory striatal neurons. **b,** Mean waveforms of auditory striatal cells. Blue - broad-spiking cells with peak-to-valley duration >250 μs; red - narrow-spiking cells. **c,** Peak-to-valley duration and mean firing rate of striatal neurons. **d,** Mean and evoked firing rates of striatal neurons. Blue - broad spiking cells, red - narrow-spiking cells.

4.4 Correlated firing

Extracellular recordings offer no direct method of examining the connectivity of the neurons under study. However, indirect inferences can be made from the relative timing of the spikes of simultaneously recorded neurons (Barthó et al., 2004b; Ts'o et al., 1986). The firing of an excitatory neuron will produce a short latency increase in the firing rate of its post-synaptic targets. This elevation can be detected if spike trains of the post-synaptic cell are aligned with respect to the spike times of the pre-synaptic neuron. However, care should be taken when interpreting the resulting cross-correlograms as such interactions can arise from common inputs to the two neurons as well as monosynaptic connectivity between them. The firing rates of neurons may covary on slow time scales due to correlated changes in their excitability due to learning or changes to the animal's behavioral state and on faster timescales, due to stimulus evoked modulations.

Several methods, which take these confounds into account, have been proposed to distinguish different sources of spike synchrony (Aertsen et al., 1989; Brody, 1999). However, these methods rely on stimulus-locking of neuronal responses, which limits their applicability to recordings from freely moving behaving subjects. Furthermore, in the auditory cortex where stimulus-evoked as well as spontaneous activity is dominated by millisecond-timescale epochs of concerted neuronal firing (DeWeese and Zador, 2006; Hromádka et al., 2010), it may be impossible to distinguish between coordinate neuronal firing resulting from monosynaptic connectivity and shared sensory input.

Keeping these caveats in mind, we identified 21 neuronal pairs that showed significant millisecond-timescale spiking correlations among 125 cell pairs recorded on the same tetrode and 2 correlated cell pairs among 318 recorded on different tetrodes (Fig. 4.8).

We next examined stimulus and choice selectivity of significantly correlated neuronal pairs. Intriguingly, choice selectivities of these putatively connected pairs were correlated, although this was not the case for cells recorded on the same electrode that did not show significant spiking synchrony (Fig. 4.9a). We did not observe similar correlations for stimulus selectivities of putatively connected neurons (Fig. 4.9b). Typically, only one of the neurons in

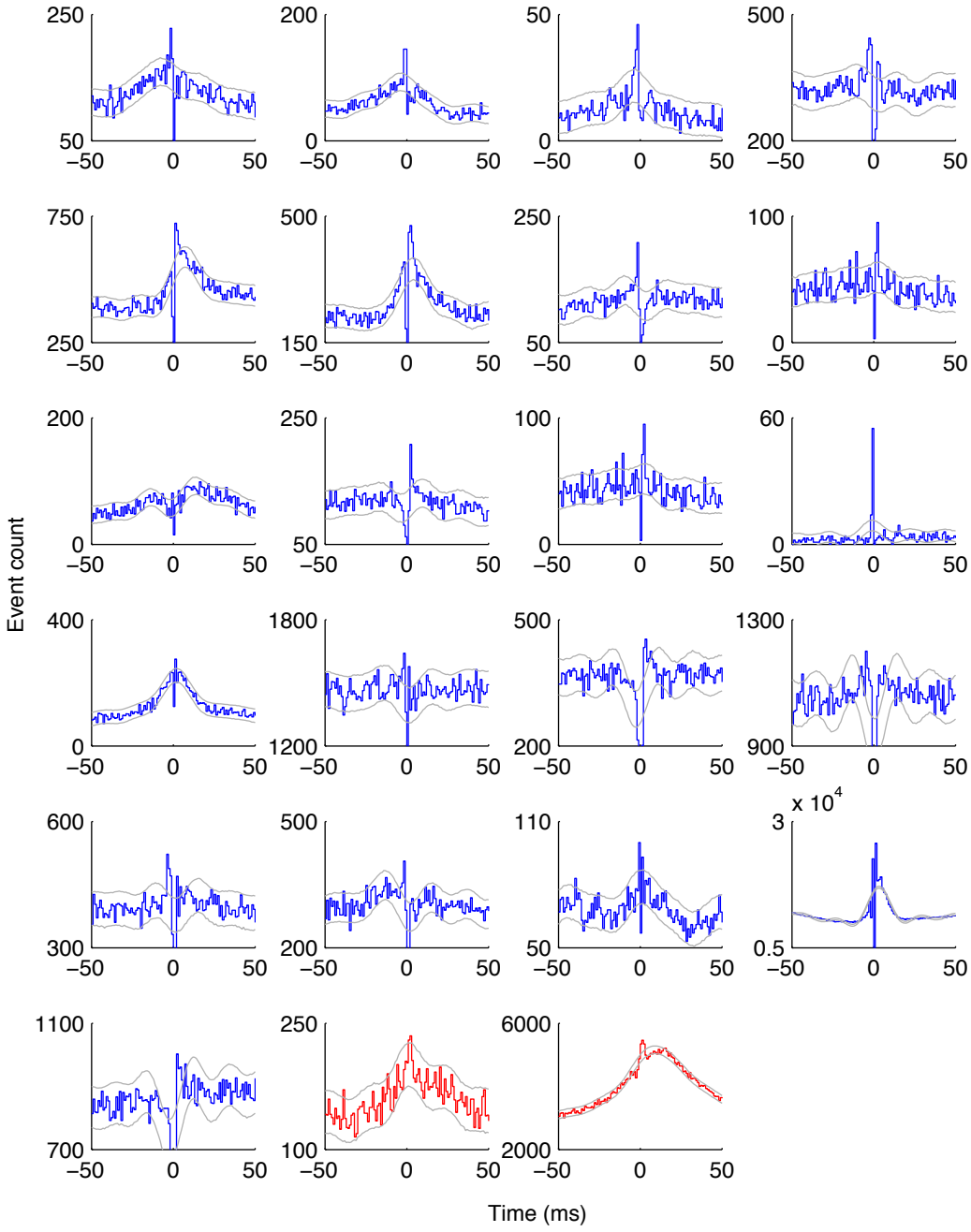

Figure 4.8: **Neuronal cross-correlations identify putative monosynaptic connections.** Crosscorrelograms of singificantly cross-correlated neuronal pairs in the auditory cortex. Blue - pairs recorded from the same tetrode; red - pairs recorded across different tetrodes. Gray - 99% confidence interval, see text.

the pair showed strong stimulus selectivity. This may be a reflection of the fact that robust stimulus-evoked responses are on the whole not as common as choice-related ones.

4.5 Discussion

We observed that both auditory cortical and striatal neurons carried signals about the frequency content of the "cloud-of-tones" stimulus that could be used to drive subjects' decisions. Frequency tuned sound-evoked responses have previously been reported in the auditory striatum of anaesthetized and passively listening animals (Bordi and LeDoux, 1992; Bordi et al., 1993). To our knowledge, ours is the first study examining auditory striatal activity during behavior. Our observations are simular to those made in somatosensory striatum of macaques performing a tactile discrimination task (Merchant et al., 1997). In the following chapters we will explore the role of these stimulus-evoked responses by measuring the behavioral effects of manipulating activity of neurons in the corticostriatal pathway during presentation of the stimulus.

Intriguingly, we observed that during subjects' movement toward the reward port many neurons in both areas encoded the direction of the response. Neurons tended to fire more during movements toward the port associated with their preferred stimuli, although this correspondence was not absolute and some neurons had the opposite choice preference.

Given that these responses occured after the initiation of movement, they could not have given rise to the choice itself. Instead they seem to represent an efference copy of the ongoing motor plan. These signals may arise from feedback projections from cortical areas involved in planning and execution of orientation movements, such as the secondary motor cortex (also known as the "frontal oriental field") or posterior parietal cortex. The function of these choice-selective signals is unclear. An attractive hypothesis is that they help establish associations between sensory stimuli and motor responses during learning. This hypothesis can be tested using optogenetic methods to silence the activity of cortical or striatal neurons during the choice execution.

We found neurons selective for both contralateral and ipsilateral choices in cortex as well as striatum. Since according to the conventional view striatal direct pathway D1 MSNs promote actions, while indirect pathway D2 MSNs suppress them, it is tempting to speculate

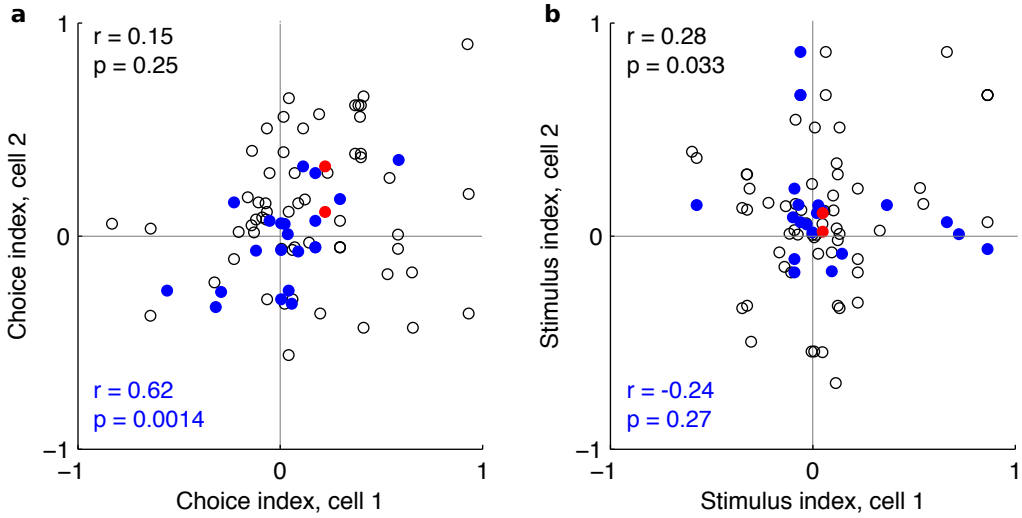

Figure 4.9: **Stimulus and choice selectivity of putatively connected neuronal pairs. a,** Choice modulation of simultaneous recorded neuronal pairs. A choice modulation index was calculated as $\frac{FR_{right} - FR_{left}}{FR_{right} + FR_{left}}$. Black - simultaneously recorded pairs from the same electrode; blue - correlated pairs on the same electrode; red - correlated pairs on different electrodes. **b,** Stimulus selectivity of simultaneously recorded neuronal pairs. Notation as in panel **a**.

whether contra- and ipsi-preferring responses arise from D1 and D2 neurons respectively. However, recent work using genetic tagging to distinguish D1 and D2 neurons has challenged this conventional view (Cui et al., 2013), showing evidence of preference for contralateral movements in both populations of neurons.

5

Non-specific optical stimulation of the auditory cortex

To understand how the activity of neurons in the auditory cortex contributes to subjects' choices in the "cloud-of-tones" task, we set out to measure the effects of artificial cortical stimulation on subjects' responses. The tonotopic organization of the auditory cortex implies that, first, nearby neurons have similar frequency selectivity and, second, that frequency preference changes gradually across the cortex. The former assertion appears to be true only in part. Recent studies employing calcium imaging to characterize frequency tuning of auditory cortical neurons have shown that while at the population scale frequency preference does change gradually across the cortical surface, the preferred frequency of nearby neurons can differ dramatically (Bandyopadhyay et al., 2010; Rothschild et al., 2010). Nevertheless, frequency preference of neurons activated by local cortical stimulation will vary along the tonotopic axis of the auditory cortex.

We hypothesized that activation of auditory cortical neurons in different regions of the tonotopic map would result in choice biases, the direction of which would depend on the frequency-response association the rat had been trained to make. To test this, we made use of the light-gated cation channel Channelrhodopsin-2 (ChR2) (Boyden et al., 2005; Nagel et al., 2003).

This chapter describes our approach for ChR2-mediated neuronal stimulation in freely moving behaving rats and summarizes the effects of non-specific optical stimulation of the

auditory cortex on rats' behavior in the "cloud-of-tones" task. We observed that although stimulation could bias subjects' choices in the task, the direction of the choice bias did not depend on the frequency tuning of the stimulation site. We discuss several possible technical and biological explanations for this surprising result.

5.1 ChR2 photostimulation *in vivo*

We expressed ChR2-Venus in the rat auditory cortex using a recombinant AAV carrying the gene encoding ChR2-Venus fusion under the control of the CAGS promoter(Niwa et al., 1991). With the goal of expressing ChR2 throughout the primary auditory cortex, we injected the virus in 4 separate penetrations along the cortical tonotopic axis. We used fluorescence of Venus to characterize the extent of ChR2 expression (Fig. 5.1a). We found 54% of labeled neurons were located in layers II-IV (<500 um from pia); 40% of cells were located in layer V(500-1000 um from pia); 6% of cells were found in layer VI (Fig. 5.1b). The sparse expression in layer VI likely resulted from our injection protocol rather than viral tropism, since we restricted injection depth to 800 μm below cortical surface to avoid viral spread to subcortical structures.

With the goal of delivering light to ChR2-expressing neurons at a defined location in the cortical frequency map in freely-moving rats, we designed a custom-made tetrode/optical fiber microdrive array carrying up to 6 individually movable 50 μm multimode optical fibers/electrodes (Fig. 5.2). Fibers were sharpened using a diamond wheel to improve tissue penetration and increase the effective numerical aperture of the fiber, maximizing the angle of the light exit cone. Each tetrode was cut to terminate <200 μm from the optical fiber tip. This arrangement allowed us to characterize the frequency tuning of the neurons near each stimulation fiber.

The spatial specificity of light activation is limited by the spatial spread of the light. Light intensity falls off with distance from the tip of the fiber due to geometrical spread of the light and its absorption and scattering by brain tissue. Due to the conical shape of the optical fiber tip, it radiates light in all directions acting approximately as a point light source. Therefore, light power drops off with the square of the distance to the fiber. The effects of

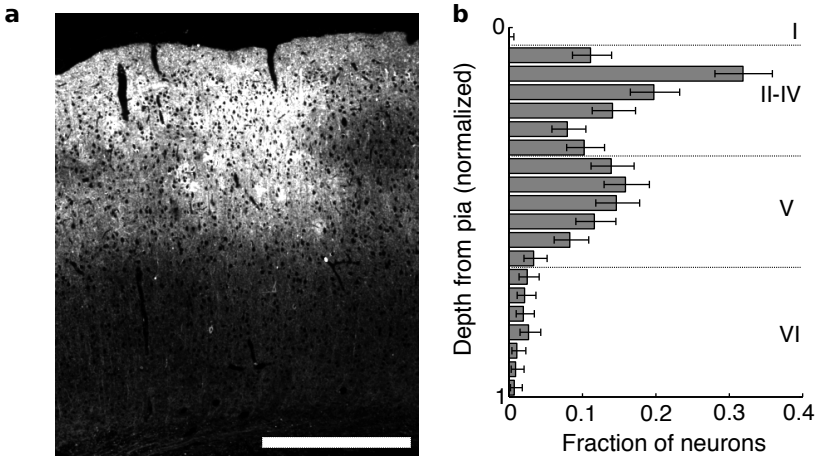

Figure 5.1: **Non-specific expression of ChR2 in the auditory cortex by AAV CAGS ChR2. a,** Fluorescence image of ChR2-Venus in the primary auditory cortex of a rat injected with the AAV CAGS ChR2-Venus virus. **b,** Depth distribution of ChR2-Venus positive neurons. Dashed lines mark approximate layer boundaries. Scale bar - 500 μm.

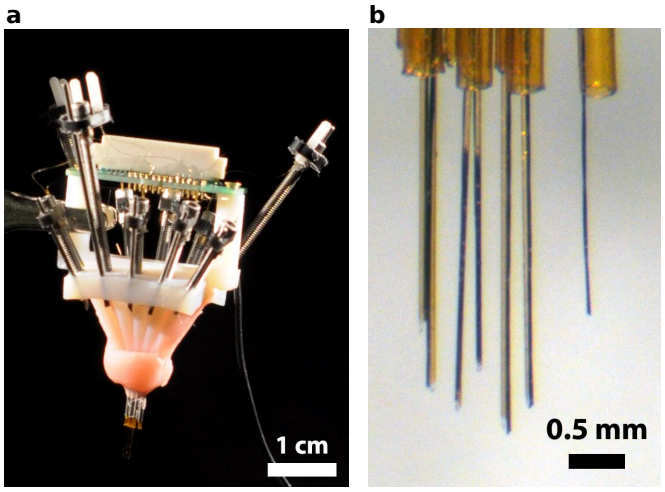

Figure 5.2: **Tetrode/optical fiber microdrive array. a,** Overview of the entire microdrive assembly. **b,** Close-up of the fiber/tetrode array. The single tetrode on the right is used as a reference channel.

absorption and scattering on light transmission T can be modeled as(Aravanis et al., 2007):

$$T = \frac{1}{Sx + 1}, \tag{5.1}$$

where x is the distance from the light source and S is the scatter coefficient of the tissue, ~ 10.3 mm$^{-}1$ for rat cortex(Aravanis et al., 2007). Putting effects of light transmission and geometric spread together, the theoretical distribution of light intesity I is

$$I \propto \frac{1}{x^2(Sx + 1)} \tag{5.2}$$

Together these factors result in a steep reduction in light power with distance from the fiber tip, with light intensity at 1 mm equal to $\sim 1\%$ of light intensity 200 μm from the fiber (Fig. 5.3a).

In addition to the extent of light penetration, the spatial profile of light-evoked activation is complicated by two additional factors: expression of ChR2 in neuronal processes and variability in ChR2 expression between neurons. Since ChR2 traffics throughout the cells' dendrites and axons, neurons may be activated even if their soma does not receive much light (Lewis et al., 2009). Finally, because we are using a virus to deliver the ChR2 expression cassette, neurons can carry a variable number of copies of this cassette, leading to substantial variation in ChR2 levels. The amount of light-evoked current generated at a given light intensity should vary linearly with ChR2 expression levels. Therefore, the minimal light intensity required to evoke spikes in a given neuron will be inversely proportional to its ChR2 levels.

To directly measure the spatial profile of light-evoked activity *in vivo*, we recorded light-evoked multiunit responses at different locations along the fiber/tetrode array. The largest light-evoked responses were observed at the tetrode immediately adjacent to the stimulation fiber (Fig. 5.3b). However, stimulation elevated firing rates as far as 1 mm away. These responses may be result from recurrent intracortical excitation as well as direct activation of neurons by light.

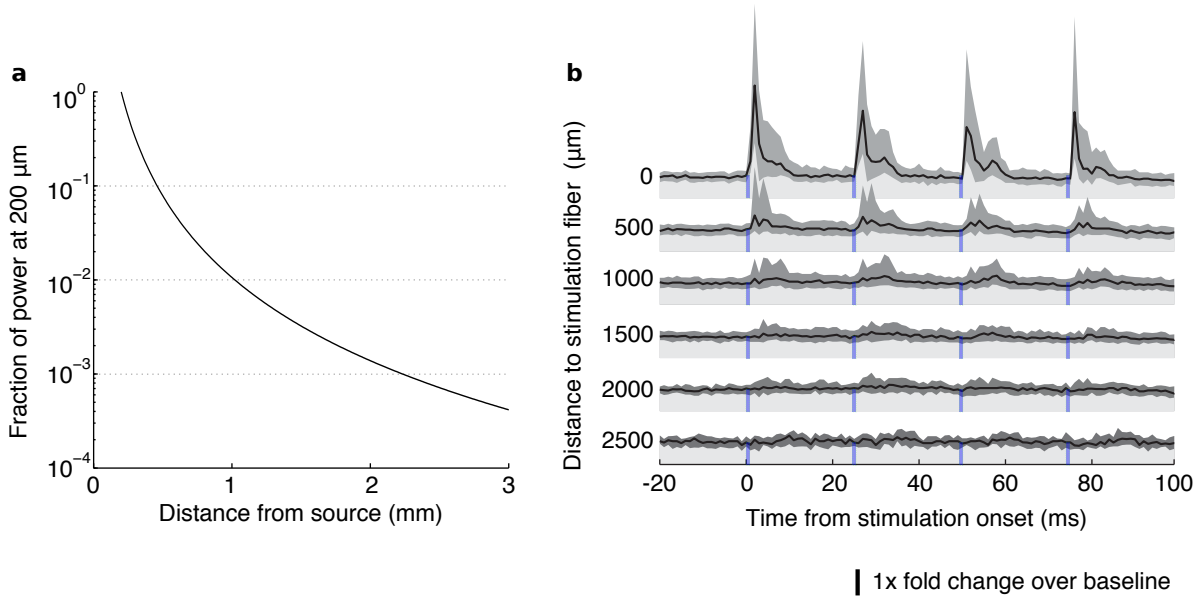

Figure 5.3: **Spatial spread of ChR2 activation. a,** Theoretical intensity distribution of light emitted from an optical fiber. **b,** Median baseline-normalized light-evoked multiunit PSTHs at varying distances from the stimulation fiber (N=128 stimulation experiments). Blue rectangles mark the timing of light pulses (2 ms, 3 mW power, 473 nm laser). Gray shading shows interquartile range across experiments.

5.2 Stimulation biases choices and disrupts psychophysical performance

At the start of each experimental session, we selected one of the optical fibers for stimulation. We delivered light to activate ChR2-expressing ACx neurons on a subset of trials, and compared performance on stimulated trials to that on control trials without light activation. To minimize behavioural adaptation to photostimulation we limited the number of stimulation trials to 25%, and rewarded the animal as on control trials according to the frequency content of the stimulus.

Activation of ChR2-expressing auditory cortical neurons induced substantial choice biases on individual sessions (Fig. 5.4ac). To estimate the location of the stimulation fiber along the cortical tonotopic map, we measured multiunit responses evoked by pure tones played in free field to the passively listening animal. Multiunit activity reflects the firing of a large number of neurons near the electrode and therefore provides a good estimate of frequency selectivity of the local neuronal population. Typically, pure tones evoked transient onset responses tuned to a sound frequency characteristic of primary auditory cortex (Fig. 5.4b). We defined the preferred frequency as the frequency that evoked the largest response at 70 dB-SPL. This differs from the definition of "characteristic frequency" (CF) employed in the auditory field, where CF is defined as the best frequency at threshold sound intensity. However, although the frequency tuning bandwidth in ACx tends to broaden with sound intensity, best frequency of multiunit responses does not change systematically (Pienkowski and Eggermont, 2011). Furthermore, as the stimuli used in the task are far above threshold (45-75 dB), responses at these sound intensities would better characterize the neurons' role in the task.

We hypothesized that stimulation would bias rats' choices, making them more likely to select the reward port associated with the preferred frequency of the stimulation site. While for some sites this was indeed the case (Fig. 5.4ab), surprisingly, we often observed significant biases in the opposite direction (Fig. 5.4cd).

To quantify the behavioral effects of photostimulation, we extended the logistic regression model in (3.1):

$$\ln \frac{p}{1-p} = \beta_0 + \beta_1(r_{high} - r_{low}) + \beta_2 S + \beta_3 S(r_{high} - r_{low}) \tag{5.3}$$

where S is 1 on manipulation trials and 0 on control trials. The inclusion of the interaction term β_3 allows us to evaluate whether stimulations alters the slope of the subjects' psychometric function, a measure of stimulus sensitivity. The shift of the psychometric function evoked by the manipulation, $\frac{\beta_2}{\beta_1+\beta_3}$ tones/s, which we refer to as the stimulation choice bias, estimates the change to the stimulus strength of the auditory stimulus $r_{high} - r_{low}$ that would produce an effect on choices equivalent to the effects of stimulation.

Across the population, we found no relationship between the frequency tuning of the stimulation site and the direction of stimulation-evoked choice biases (Fig. 5.5a). However, when we reexamined choice biases with respect to the stimulated hemisphere, we found that stimulation tended to bias subjects toward the contralateral choice port notwithstanding the preferred frequency of the stimulation site (Fig. 5.5bc).

Furthermore, we found that stimulation tended to decrease the subjects' sensitivity to the stimulus, quantified as the slope of the psychometric function (Fig. 5.6a). Extreme choice biases, which induce the rat to consistently choose the same reward port independent of the auditory stimulus, may manifest as an apparent reduction in psychometric slope. However, stimulation tended to reduce subjects' sensitivity even for sites where stimulation-evoked choice biases were minor (Fig. 5.6b).

5.3 Discussion

Although non-specific stimulation biased subjects' responses in the "cloud-of-tones" task, we observed no relationship between choice bias direction and frequency tuning of the stimulation site. Instead, biases were predominantly contralateral to the stimulated hemisphere. There are several plausible explanation for these effects.

First, since the CAGS promoter drives expression in inhibitory as well as excitatory neurons, stimulation may have inhibited cortical outputs, rather than specifically exciting outputs with specific frequency tuning. However, while this explanation would explain the decrease in psychophysical performance during stimulation trials, it seems incompatible with the contralateral trend of stimulation-evoked biases.

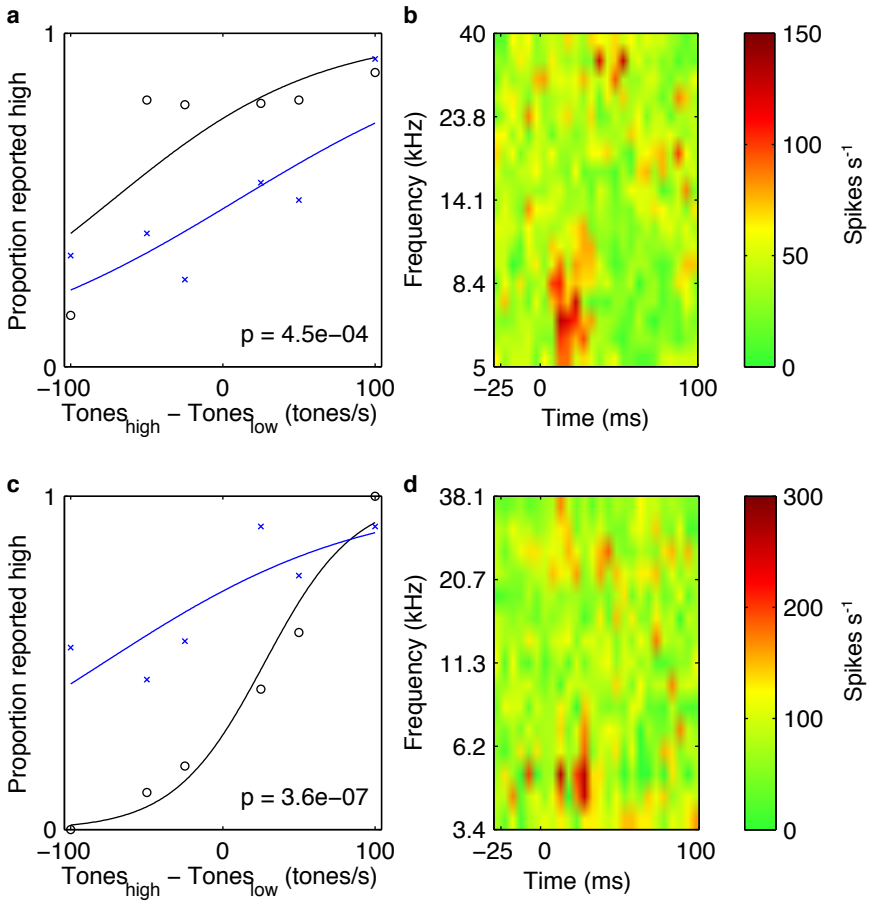

Figure 5.4: **Non-specific stimulation of auditory cortex biases choices. a,** Psychometric curves on control (black) and stimulation (blue) trials for a example stimulation session. **b,** Mutliunit tone-evoked responses for site in panel **a**. **c,d,** Psychometric curves and frequency tuning for a stimulation site, where choice bias contradicts frequency preference.

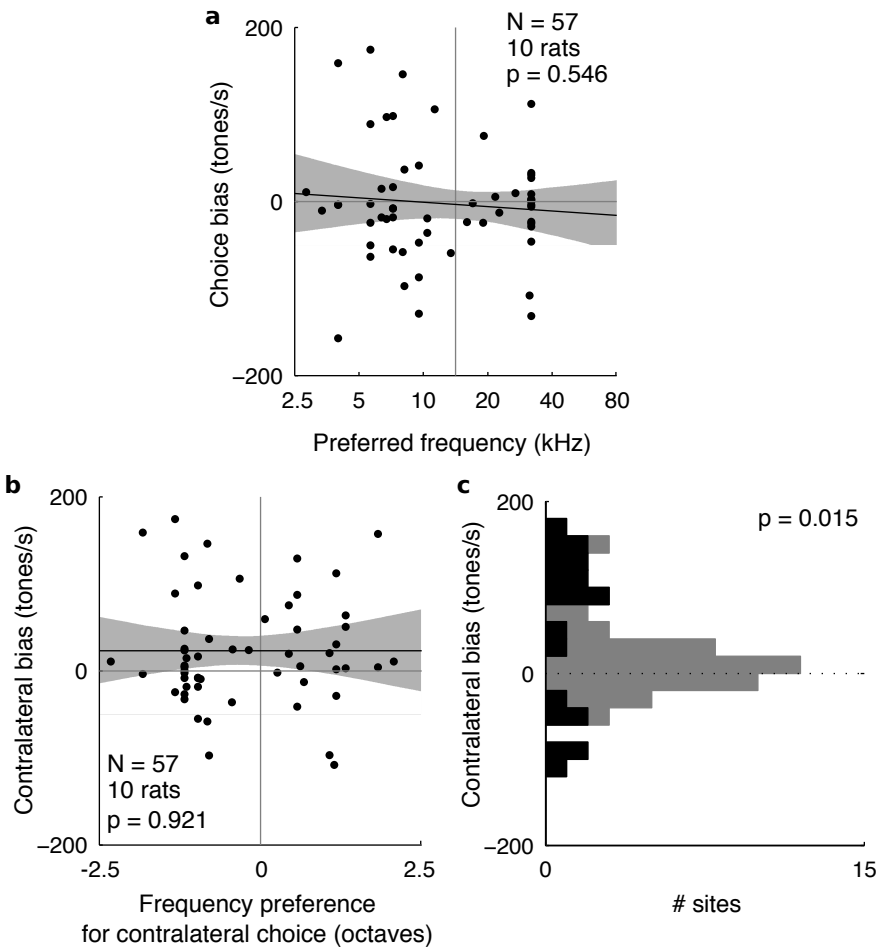

Figure 5.5: **Summary of stimulation-evoked choice biases. a,** Stimulation-evoked choice biases do not depend frequency of the stimulation site. **b,** We replotted choice biases replotted relative to the stimulated hemisphere and recalculated frequency preference such that positive values reflect tuning for frequencies associated with the contralateral choice port and 0 is the midpoint of the cloud-of-tones stimulus (14.1 kHz). **c,** Stimulation tended to bias responses toward the choice port contralateral to the stimulated cortex. Black bars indicate significant biases ($p<0.05$).

Second, biases that deviate from the port associated with preferred frequency of the stimulation site may arise from activation of neurons from other frequency bands. This may occur either through direct photoactivation of the passing axons of these neurons or their activation by recurrent cortical connections. To reconcile this explanation with the excess of contralateral choice biases, we would have to postulate that on average, activity of neurons, tuned to frequencies associated with contralateral choices, has a stronger impact on subjects' behavior.

Third, these effects may result from activation of competing output pathways, projecting to target areas with different functional roles. The predominantly contralateral biases may be the result of the activation of a lateralized motor pathway, such as one involved in sound localization. Projections to the posterior parietal cortex and superior colliculus, structures specialized for spatial processing, may have played this role. Another candidate is the projection to the posterodorsal auditory field(Kimura et al., 2004), which itself has extensive connections with those areas.

The failure of non-specific cortical stimulation to elicit consistent behavioral effects is not without precedent. For example, while stimulation of mPFC neurons projecting to the raphe nucleus increases rats' mobility in the force swim test, non-specific neuronal activation of ChR2-expressing neurons has no observable behavioral effect (Warden et al., 2012).

Somewhat optimistically, we interpreted these results to suggest that the auditory cortex plays a role in the task, but that the method of non-specific activation of diverse neuronal populations used in these experiments does not provide sufficient experimental control over the activity of the projection neurons actually driving subjects' choices during auditory discimination. We therefore hypothesized that targeted stimulation of corticostriatal neurons might yield more systematic effects. The following chapter is devoted to our tests of this hypothesis.

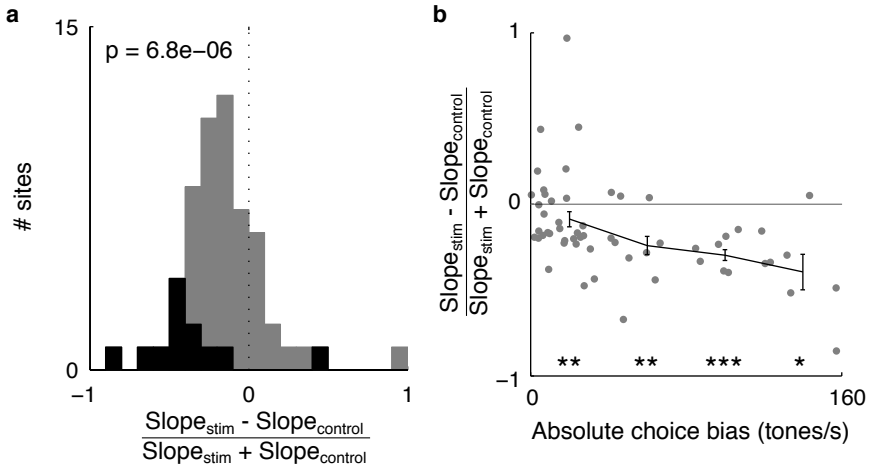

Figure 5.6: **Non-specific cortical stimulation disrupts discrimination performance. a,** Auditory cortex stimulation reduced psychometric performance measured as the slope of the psychometric curve. Back bars indicate sites with significant effects ($p<0.05$). **b,** Stimulation reduced the slope of the psychometric curve even for sites where stimulation-evoked choice bias was minor. Error bars - s.e.m., * - $p < 0.05$, ** - $p < 0.01$, *** - $p < 0.001$, signed-rank test.

6

Stimulation of corticostriatal neurons

We hypothesized that the projection from the auditory cortex to the striatum carries acoustic information that drives behavioral choices during auditory discrimination. Three key lines of evidence suggest that the striatum is ideally positioned to transform sensory representations in auditory cortex into motor commands. First, the striatum is one of the major long range targets of the auditory cortex (Allen Brain Institute, 2012). The auditory cortex projects to a specific region of the striatum(McGeorge and Faull, 1989), which does not receive input from other cortical areas and contains neurons sensitive to auditory stimuli (Bordi and LeDoux, 1992; Bordi et al., 1993). Second, through downstream structures of the basal ganglia, the striatum influences the activity in the motor thalamus(Beckstead et al., 1979) as well as superior colliculus(Hopkins and Niessen, 1976), a structure which has been implicated in driving behavioural choices in 2-AFC tasks (Felsen and Mainen, 2008). Third, corticostriatal connections are plastic and are the proposed site of dopamine-dependent reinforcement learning (Reynolds et al., 2001). This plasticity may enable them to encode the arbitrary stimulus-response associations acquired in such tasks (Kreitzer and Malenka, 2008).

We tested whether activity of corticostriatal neurons could influence subjects' judgments in the "cloud-of-tones" task by specifically exciting these neurons using two independent targeting strategies. The first strategy relied on retrograde infection by a virus to drive ChR2 expression specifically in corticostriatal cells. The second strategy specifically activated corti-

costriatal neurons by delivering light in the striatum, stimulating their axons. Both of these approaches demonstrated that activity of corticostriatal neurons contributes to subjects' responses in the task. Activation of neurons with different preferred frequencies mimicked the behavioral effects of adding more tones of this frequency in the auditory stimulus. We demonstrate that choice biases produced by stimulation are driven by long-range projections of these neurons and not their recurrent intracortical connections.

6.1 Targeting ChR2 expression to corticostriatal neurons

To specifically target ChR2 expression to corticostriatal neurons, we employed a binary strategy using a Cre-dependent ChR2 expression vector and a retrogradely transported virus to specifically express Cre recombinase in corticostriatal neurons (Fig. 6.1) We targeted Cre expression to corticostriatal neurons using the Herpes Simplex Virus-1 (HSV1) engineered to express Cre recombinase (Ciocchi et al., 2010; Lilley et al., 2001; Lima et al., 2009). This virus, when injected into the auditory striatum, was transported retrogradely along the axons and drove Cre expression in corticostriatal neurons. We then injected rAAV EF1a FLEX ChR2-YFP, which expresses ChR2 only after activation by Cre (Atasoy et al., 2008). This results in expression of ChR2 only in neurons infected by both the HSV1-Cre and the rAAV-ChR2.

Distribution of ChR2-expressing neurons resembled that of corticostriatal neurons in other sensory areas in rats (Reiner et al., 2003). Most neurons (84%) were located in layer V with a smaller population in other layers (Fig. 6.2).

In extracellular recordings, we identified a small population of neurons where brief pulses of blue light reliably drove action potentials (Fig. 6.3ab, 4 of 201 cells responded on >50% of trials). Properties of these presumed corticostriatal neurons are described in Appendix A. As we varied light intensity, these neurons displayed step-like activation functions (Fig. 6.3c) characteristic of cells activated directly by ChR2-mediated currents. In contrast, cells activated by light indirectly through recurrent excitatory connections gradually increase their firing over ∼10 range of light powers (S.G. Koh, personal communication). Activation threshold of these putative corticostriatal neurons increased with distance from the stimulation fiber (Fig. 6.3c).

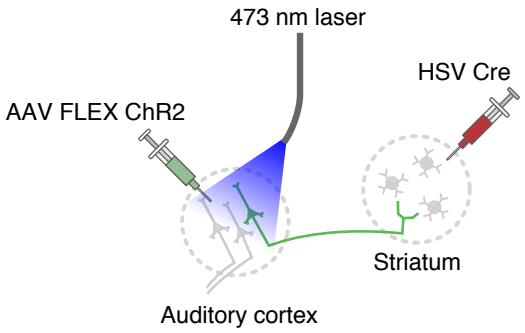

Figure 6.1: **Strategy for specific stimulation of corticostriatal neurons.**

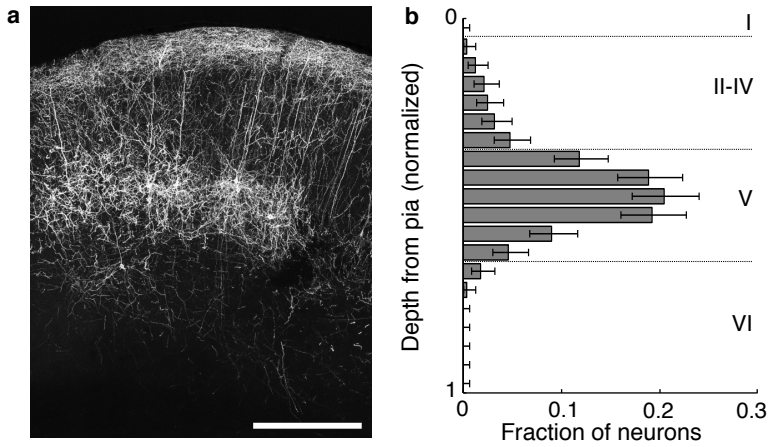

Figure 6.2: **Targeted expression of ChR2 in corticostriatal neurons. a,** Fluorescence image of ChR2-YFP expression in corticostriatal neurons in the auditory cortex. Scale bar - 500 μm. **b,** Depth distribution of corticostriatal neurons labeled by HSV-1. Dashed lines mark the approximate location of layer boundaries. Error bars - 95% confidence intervals.

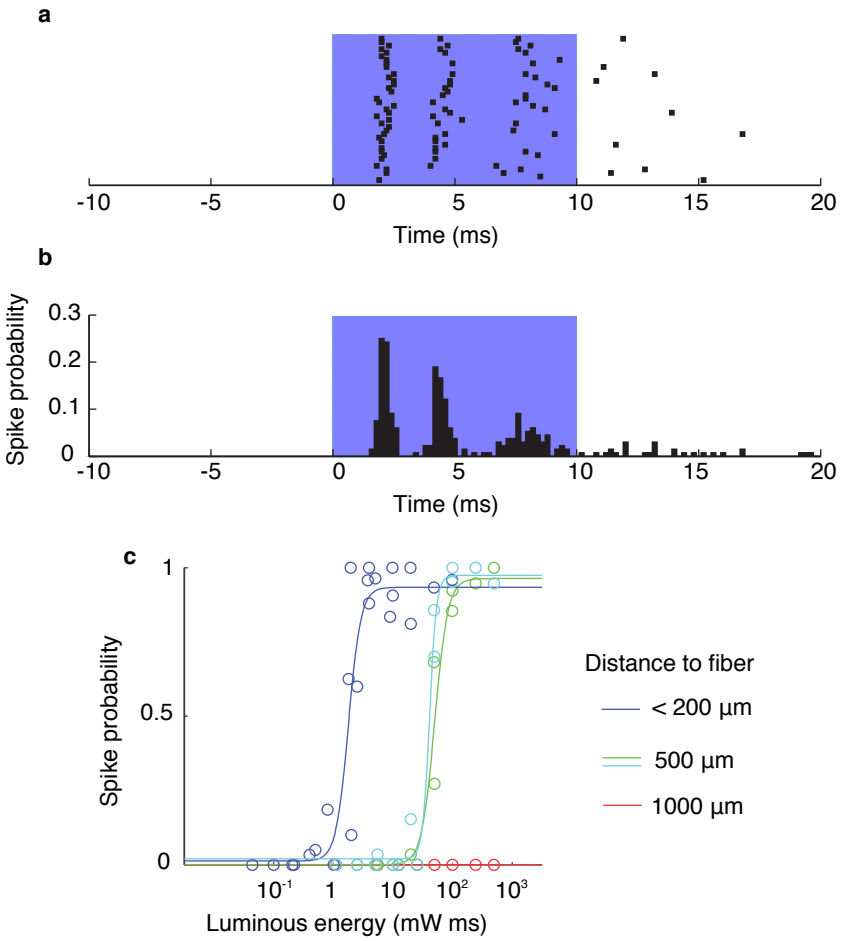

Figure 6.3: **Light-evoked responses of putative corticostriatal neurons. a,** Raster of a light-evoked response in a putative corticostriatal neuron. Blue shading marks timing of light stimulation. **b,** PSTH of responses in panel **a**. **c,** Light-evoked response probability for neuron in panels **a,b** as a function of light intensity and distance to stimulation fiber.

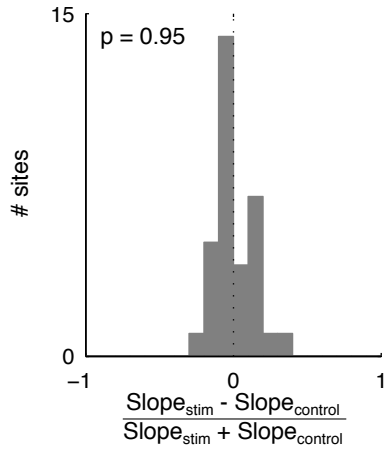

Figure 6.4: **Stimulation of corticostriatal neurons does not decrease discrimination performance.** Stimulation of corticostriatal neurons does not affect psychometric performance measured as the slope of the psychometric curve.

6.2 Stimulation of corticostriatal neurons biases choices

We measured the effects of activation of corticostriatal neurons on rats' choices in the "cloud-of-tones" task using the same approach as we applied previously to characterize the effects of non-specific stimulation of auditory cortical neurons (Sec. 5.2). We first fit subjects' responses to the full logistic regression model (5.3):

$$\ln \frac{p}{1-p} = \beta_0 + \beta_1(r_{high} - r_{low}) + \beta_2 S + \beta_3 S(r_{high} - r_{low})$$

However, we observed that stimulation had no systematic effect on the slope of subjects' psychometric functions (Fig. 6.4). Therefore, we eliminated the interaction term from subsequent analyses:

$$\ln \frac{p}{1-p} = \beta_0 + \beta_1(r_{high} - r_{low}) + \beta_2 S \tag{6.1}$$

The shift of the psychometric function produced by photostimulation, β_2/β_1 tones/s, measures the change to stimulus strength $r_{high} - r_{low}$ that would produce an effect on choices equivalent to the effects of stimulation.

Across sites, stimulation consistently biased subjects' choices toward the choice port associated with the preferred frequency of the stimulation site (Fig. 6.5a-c). The biases were not significant on individual sessions ($p<0.05$ on 1/33 sessions), in part because the number of

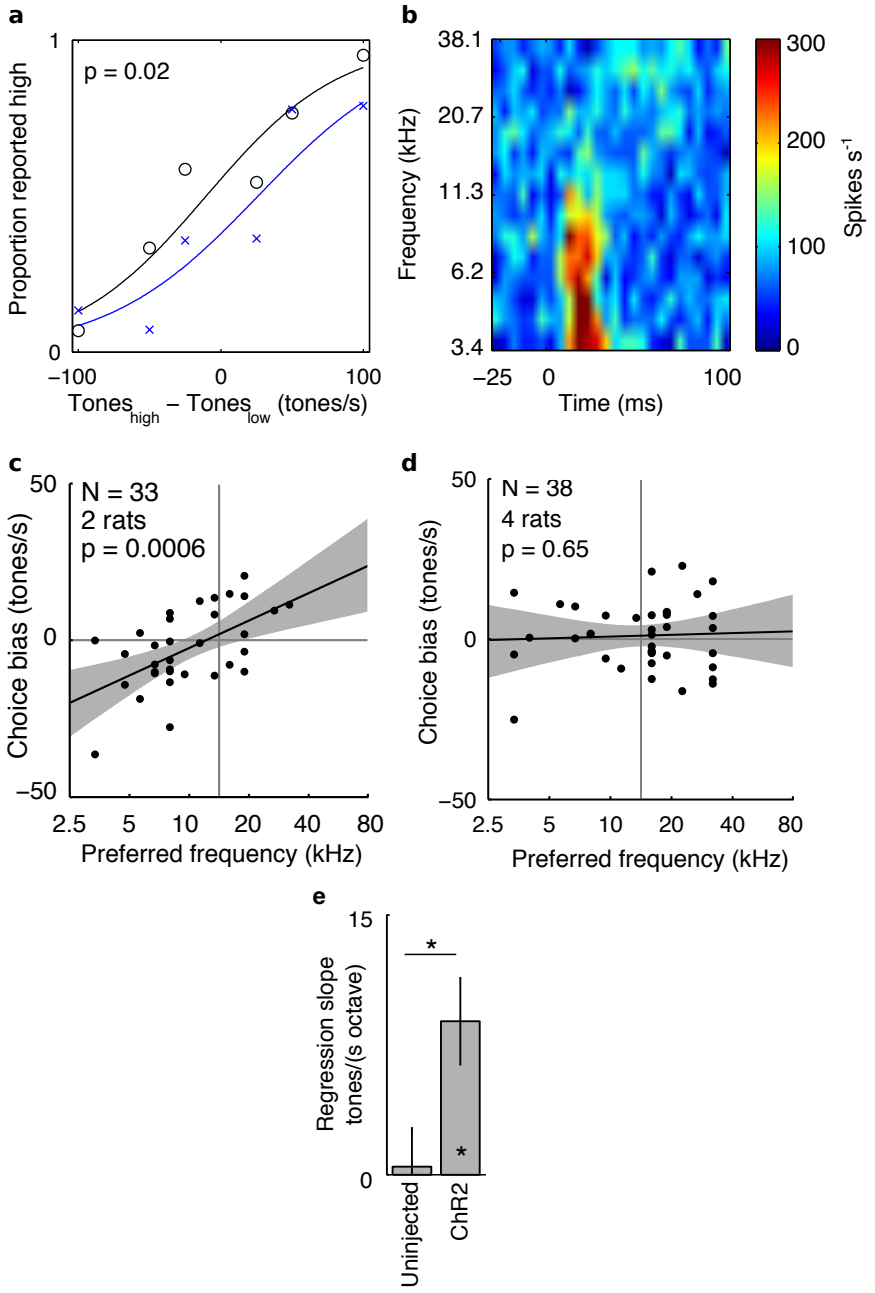

Figure 6.5: **Stimulation of corticostriatal neurons biases choices.** **a,** Psychometric performance during a single behavioural session on control (black) and stimulation of corticostriatal neurons (blue) trials. **b,** Mutliunit tone-evoked responses for site in panel **a**. **c,** Across the population, direction and magnitude of choice biases evoked by stimulation depends on the frequency preference of the stimulation site. Gray shading shows 95% confidence interval for regression line. **d,** Consistent choice biases were not observed in control animals that did not express ChR2. **e,** Slope of the regression line relating choice bias to preferred frequency is significantly greater in ChR2 animals than uninjected controls.

stimulated trials per session was typically small (70±24 (s.d.) trials). However, the magnitude and direction of the bias varied systematically with the preferred frequency of the stimulation site (Fig. 6.5a-c). In contrast to non-specific stimulation, contralateral and ipsilateral biases were observed with similar frequency (12/33 contralateral sites, p = 0.31 signed-rank test).

To confirm that these choice biases resulted from ChR2-mediated activation of corticostriatal neurons and not non-specific effects of light delivery, we repeated these experiments in uninjected animals. Choice biases were not observed in these control rats' (Fig. 6.5de). Together these results demonstrate that activation of corticostriatal neurons biases subjects' responses in a manner predicted by the frequency tuning of the stimulated neurons.

6.3 Stimulation of corticostriatal neurons inhibits cortical activity

The behavioural effects of photostimulation could arise either directly through excitation of striatal neurons by their cortical inputs, or indirectly through excitation of other output pathways of the auditory cortex through recurrent cortical connections of corticostriatal neurons. To distinguish between these possibilities we examined the responses of auditory cortical neurons to activation of corticostriatal cells.

Surprisingly, we found that most cortical neurons were suppressed by stimulation of corticostriatal cells (Fig. 6.6ab). To quantify these effects, we calculated a stimulation modulation index $\frac{FR_{light}-FR_{pre}}{FR_{light}-FR_{pre}}$, where FR_{light} and FR_{pre} are firing rates in a 20 ms window during and immediately preceeding a light pulse (Fig. 6.6c). The stimulation modulation index was negative for 72% of the neurons in our sample (112/155 cells).

What is the source of this light-evoked inhibition? Its rapid onset suggests that it is mediated by local inhibitory interneurons activated by inputs from corticostriatal neurons (Fig. 6.6e-g). Consistent with this, among cells activated by light with low reliability characteristic of synaptic rather than direct stimulation some had narrow spike waveforms characteristic of inhibitory PV interneurons (Fig. 6.6d). Alternatively, it is plausible that subset of corticostriatal neurons themselves may mediates this inhibition. Corticostriatal neurons expressing inhibitory

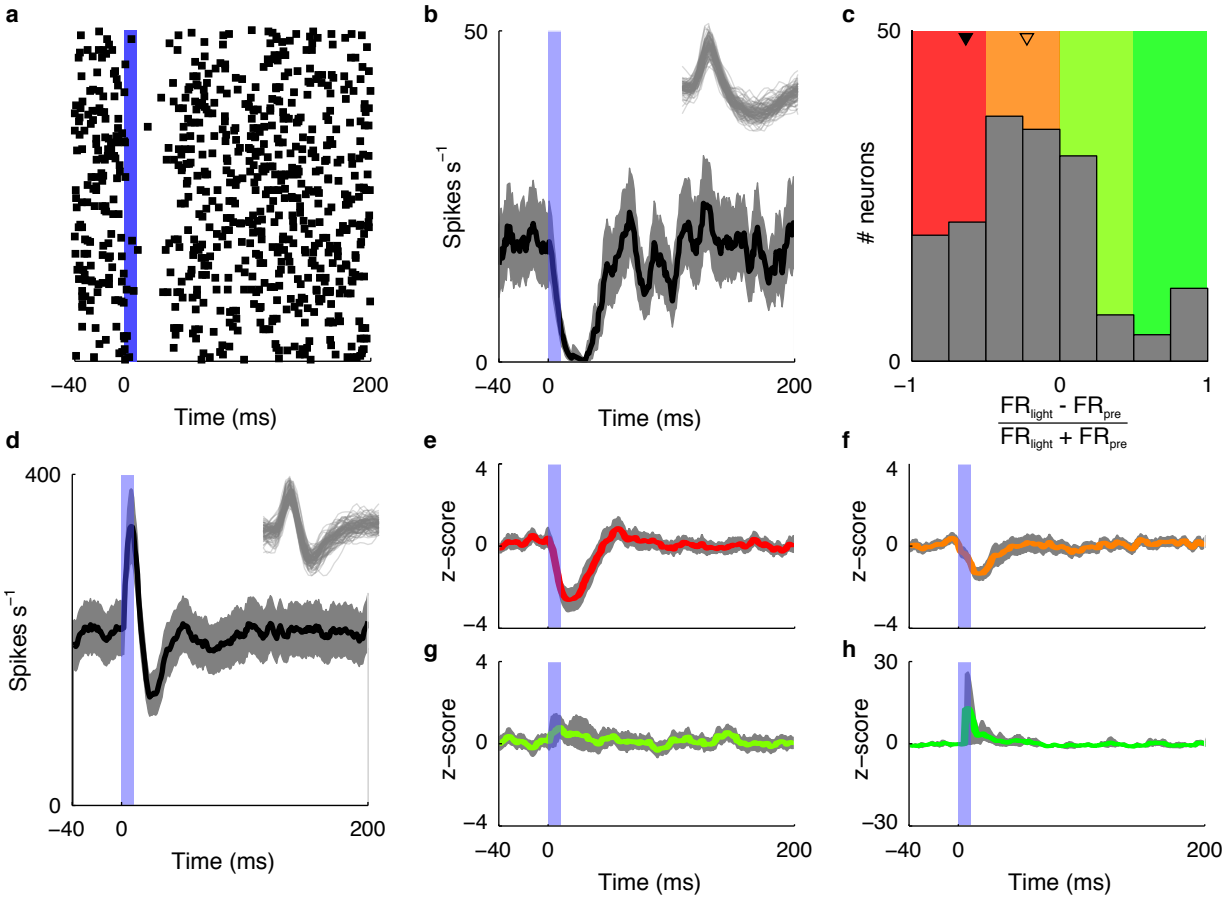

Figure 6.6: **Stimulation of corticostriatal neurons suppresses the firing of auditory cortical cells.** **a,** Activity of an auditory cortex neuron inhibited by photostimulation of corticostriatal neurons. Blue light (473 nm) was presented for 10 ms at 5 mW (blue bar). **b,** PSTH of the neuron in panel **a**. **c,** Most cortical neurons are inhibited by stimulation of corticostriatal cells. Light modulation index was calculated comparing firing rates during 20 ms following and preceding the onset of the light pulse. Open triangle - median light modulation; filled triangle - cell in panel **a**. **d,** PSTH of a putative narrow-spiking interneuron activated by stimulation of corticostriatal neurons. **e-h,** Mean standardized PSTHs for neurons grouped by light modulation index, as highlighted in panel **c**

.

markers parvalbumin and glutamic acid decarboxylase (GAD) have been found in mouse somatosensory cortex(Jinno and Kosaka, 2004). However, these cells appear to be absent in the auditory cortex.

6.4 Axonal stimulation of corticostriatal neurons biases choices

The observation that activation of corticostriatal neurons generally supresses cortical activity favors the hypothesis that biases evoked by stimulation are mediated by their long-range rather than local connections. To test this hypothesis directly, we developed a second strategy which did not rely on cortical stimulation and thus would allow us to test whether stimulation of corticostriatal neurons could bias subjects' choices when recurrent cortical activity is blocked.

We expressed ChR2 non-specifically in the auditory cortex and stimulated the axons of corticostriatal neurons in the striatum (Fig. 6.7a). Light stimulation drove neurotransmitter release from corticostriatal terminals, resulting in excitation of postsynaptic striatal neurons (Fig. 6.7b). Due to backpropagation of action potentials, antidromic responses were observed in the auditory cortex with $\sim$2 ms latency due to axonal conduction delays (Fig. 6.7c).

This approach did not allow us to *directly* access the cortical tonotopic map. However, we could still define the frequency tuning of stimulated fibers, exploiting the topography of corticostriatal projections. This topography is well established in the somatosensory cortex; projections of neurons from different regions of the somatotopic map remain segregated in the striatum(Alloway et al., 1999). A similar organization has been described in the auditory cortex of the cat(Reale and Imig, 1983) but somehow missed in earlier studies of the rat auditory cortex(Roger and Arnault, 1989). To determine whether the striatal projections of the auditory cortex in the rat are topographic, we injected viruses driving expression of fluorescent proteins mCherry and Venus at different locations along the cortical tonotopic axis. The axons of neurons labeled by these injections terminated in the striatum in two distinct bands (Fig. 6.8a). The axons originating from the caudal injection site targeted medial and dorsal regions of the auditory striatum, while those arising from the rostral site targeted more ventral and lateral regions. We further validated the topography of corticostriatal projections by injecting HSV-1 mCherry at different locations in the auditory striatum and examining the distribution

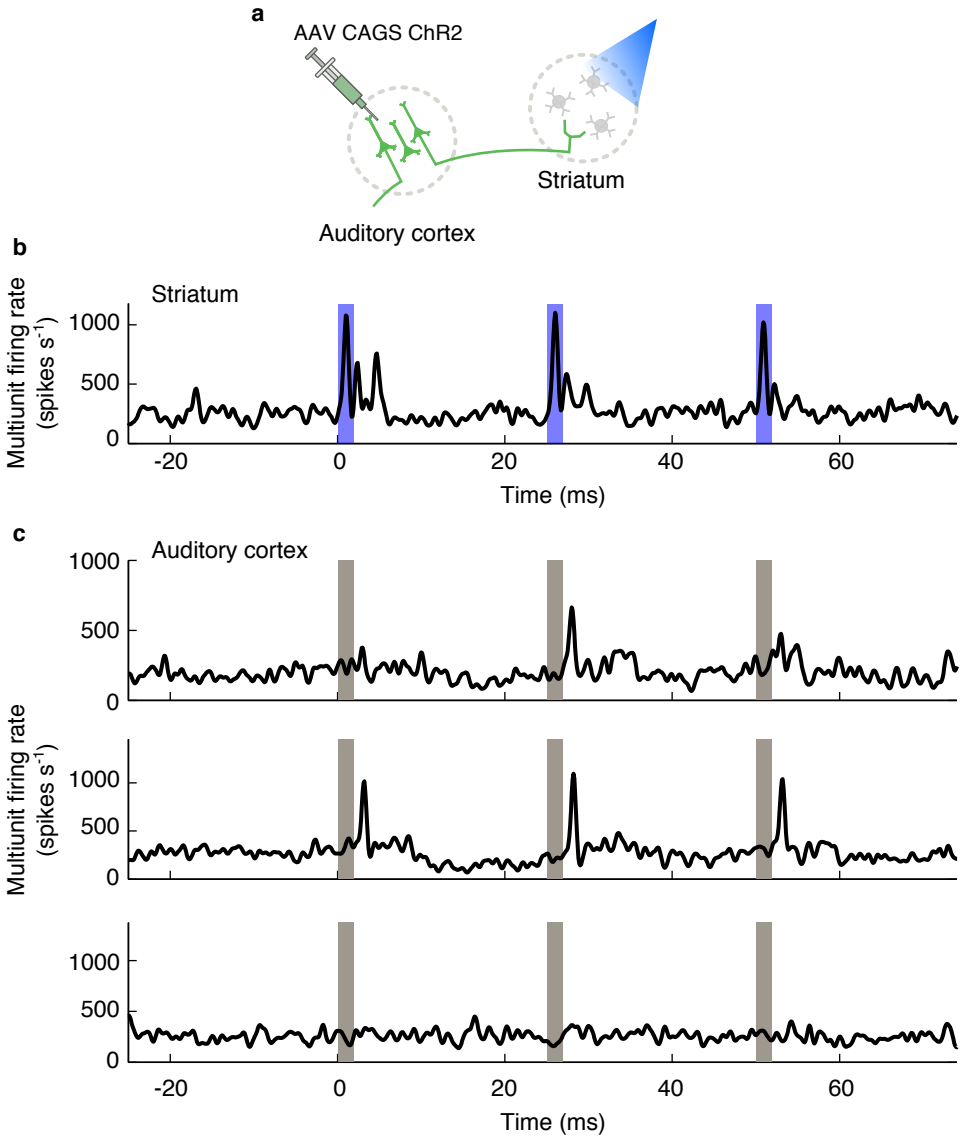

Figure 6.7: **Photostimulation of corticostriatal axons. a,** Targeting strategy for photostimulation of corticostriatal axons. **b,** Multiunit PSTHs of responses evoked by light stimulation of corticostriatal axons at the striatal stimulation site and, **c,** 3 recording sites in the auditory cortex.

of retrogradely labeled neurons in the auditory cortex. Neurons labeled by injection in the dorsal region of the auditory striatum were concentrated in the caudal part of the primary auditory cortex, while those labeled by a more ventral injection were mostly found rostrally (Fig. 6.8b-d).

Owing to this topography, focal light stimulation in the striatum is expected to excite corticostriatal axons arising from a restricted region of the tonotopic map. We used striatal multiunit activity to characterize the frequency preference of the stimulation site. Stimulation of corticostriatal axons biased subjects' choices toward the choice port associated with the preferred frequency of the stimulation site (Fig. 6.9a). While axonal stimulation occasionally produced large choice biases, its effects appeared less consistent than that of targeted stimulation of corticostriatal somata described in Section 6.2. It seems likely that due to the anatomy of the corticostriatal projection, axonal stimulation affords us less control over the frequency preference of the stimulated neurons. Figure 6.8a illustrates this point. While the tracer virus injections into low and high frequency regions of the auditory cortex lie 1.5 mm apart, their axons terminate in two bands separated by only $\sim$300 μm. Therefore, an optical fiber placed near the boundary of the two domains could excite fibers tuned to low and high frequencies in similar numbers.

Stimulation also had a modest but significant effect on the subjects' performance, reducing the slope of their psychometric functions (Fig. 6.9c). In contrast to non-specific cortical stimulation, these effects were only found for sites with large choice biases (Fig. 6.9d).

Reexamining choice biases with respect to the stimulated hemisphere (Fig. 6.9b) confirmed the relationship between frequency preference and choice. It also appears that stimulation as sites associated with contralateral choices resulted in more consistent choice biases than at sites associated with ipsilateral choices. This appears at odds with results of HSV-mediated targeting of corticostriatal neurons (Fig. 6.5c). All the subjects included in that dataset were trained to associate low frequencies with ipsilateral choices. Stimulation at low frequency sites was no less efficient in biasing choices than at high frequency sites. This may reflect a difference in how corticostriatal neurons are recruited by axonal and somatic stimulation. For

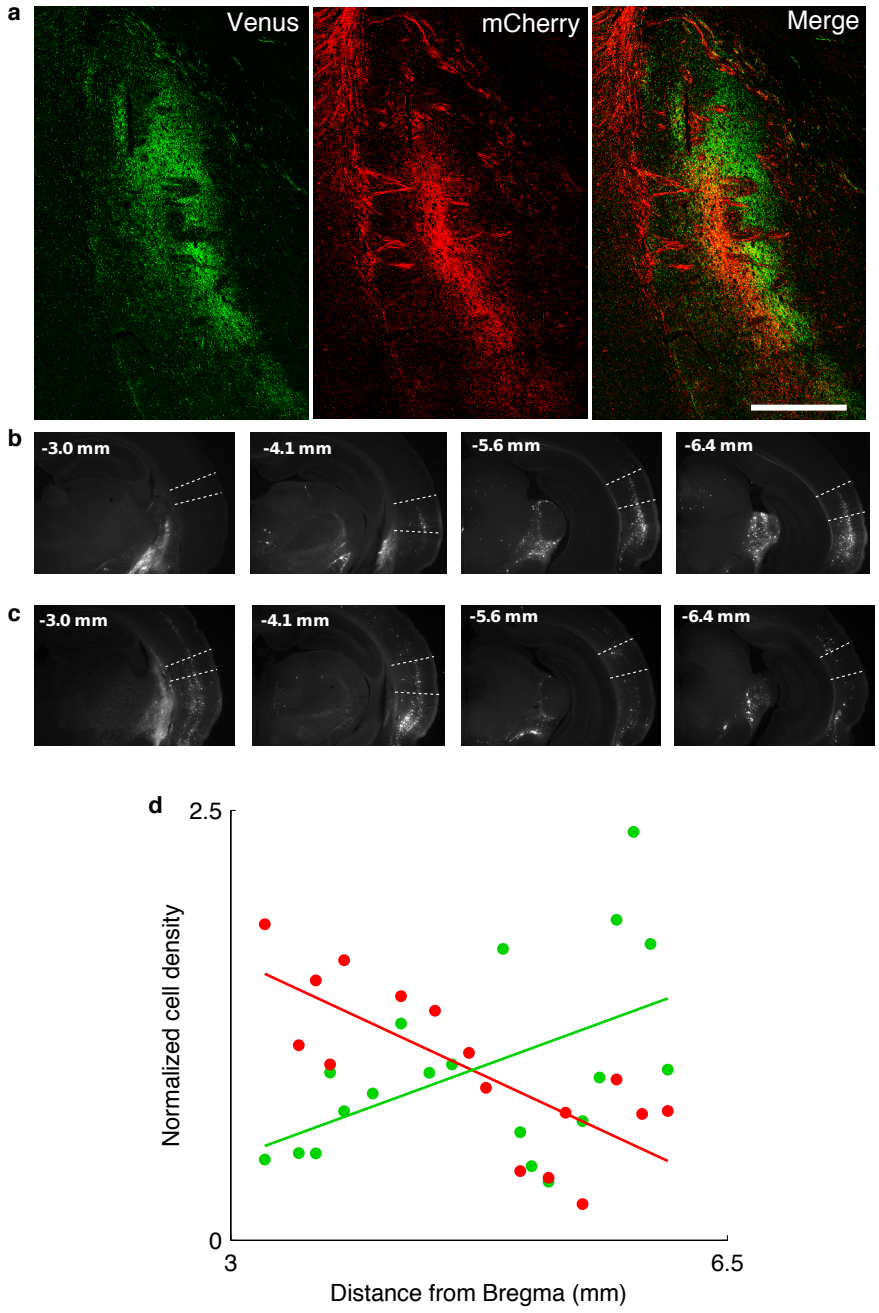

Figure 6.8: **Topography of corticostriatal projections.** **a,** Injections of AAV mCherry (red) and AAV ChR2-Venus were made at different locations along the tonotopic axis of the auditory cortex (1 mm and 2.5 mm caudal from the rostral border of the temporoparietal suture) and result in distinct bands of axonal projection in the striatum. Scale bar - 500 um. **b-c,** Retrograde labeling of corticostriatal neurons following injections of HSV-1 mCherry into dorsal (top) and ventral (bottom) auditory striatum. **d,** In each section, we quantified the number of labeled corticostriatal neurons in the primary auditory cortex per mm^3 of tissue. We then normalized these values by the mean density across all section in a given brain. Density of corticostriatal neurons in primary auditory cortex followed a caudal gradient for injection in panel **b** (green) and a rostral gradient for injection in panel **c** (red).

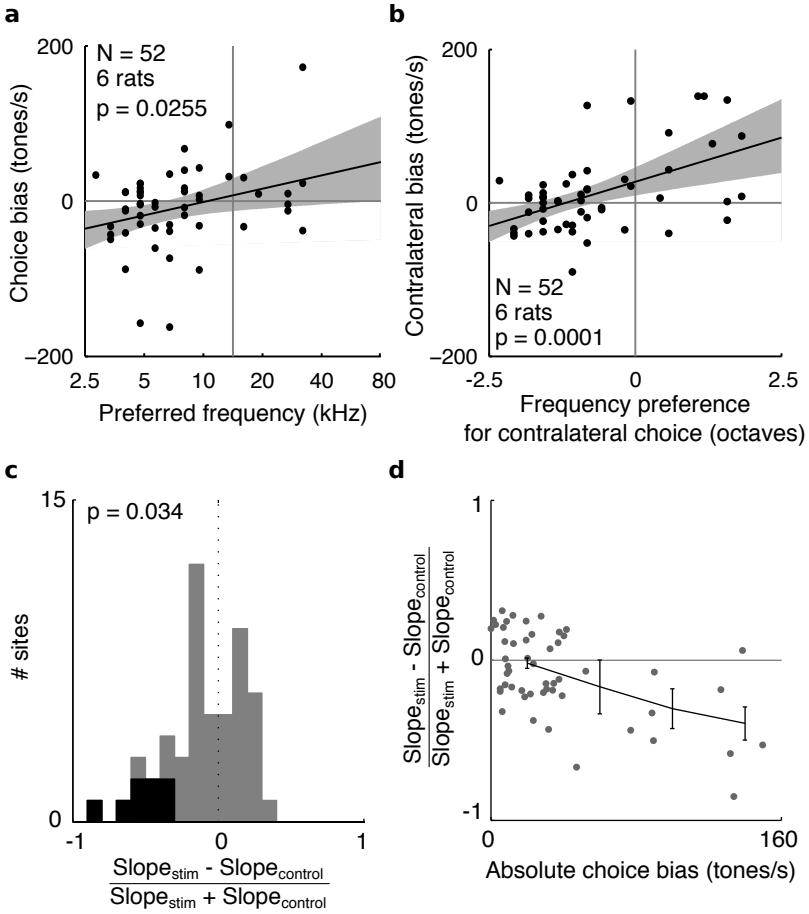

Figure 6.9: **Stimulation of corticostriatal axons biases choices.** **a,** Choice biases for individual sites during axonal stimulation. Stimulation biased rats toward the choice port associated with the preferred frequency of the stimulation site. **b,** Effects of axonal stimulation with respect to stimulated hemisphere. **c,** Axonal stimulation of corticostriatal neurons had a modest but significant effect on performance quantified as the slope of the psychometric function. **d,** During axonal stimulation, psychometric slope was reduced only for sites with large choice biases. Error bars - s.e.m.

instance, ipsilateral biases may be mediated by corticostriatal neurons that send collaterals to the contralateral striatum, which may differ in the topography of their ipsilateral projections.

6.5 Choice biases are mediated by long-range rather than local outputs of corticostriatal neurons

We next tested whether stimulation of the axons of corticostriatal neurons could bias subjects' choices in the absence of cortical recurrent activity. We selected striatal sites whose stimulation produced significant ($p<0.05$) biases in subjects' choices and repeated stimulation after pharmacologically inactivating the ipsilateral auditory cortex (Fig. 6.10a). Cortical inactivation (2% lidocaine N=2 sites, 125 μM tetrodotoxin N=5 sites) successfully blocked antidromic light-evoked responses, as demonstrated by local field potential recordings (Fig. 6.10b). Photostimulation of corticostriatal axons still biased choices in the absence of cortical activity ($p=0.016$, signed-rank test, Fig. 6.10c, 6.11), demonstrating that these biases are mediated directly by long-range outputs of corticostriatal neurons. Biases evoked by stimulation were reduced on inactivation sessions but the difference was not statistically significant ($p=0.30$, Wilcoxon ranksum test). This reduction in choice bias persisted following recovery from inactivation ($p<0.05$, Wilcoxon ranksum test, compared to pre-inactivation sessions) and likely reflects subjects' adaptation to repeated stimulation of the same site. Consistent with this, we observed that the magnitude of stimulation-evoked choice biases decayed during single stimulation sessions (Fig. 6.12). Similar effects weree observed during stimulation of area MT in macaques (Salzman et al., 1992).

6.6 Stimulation-evoked choice biases are reflected by subjects' response times

We next examined the effects of stimulation of corticostriatal neurons on rats' response times. Although individual rats varied in how they weighed response speed versus response accuracy (Sec. 3.2), most rats used in the stimulation experiments showed small but significant (of order 20-50 ms) increases in response times on challenging trials (one of the axonal stimulation rats was an exception). We fit chronometric functions to single behavioral sessions obtained from

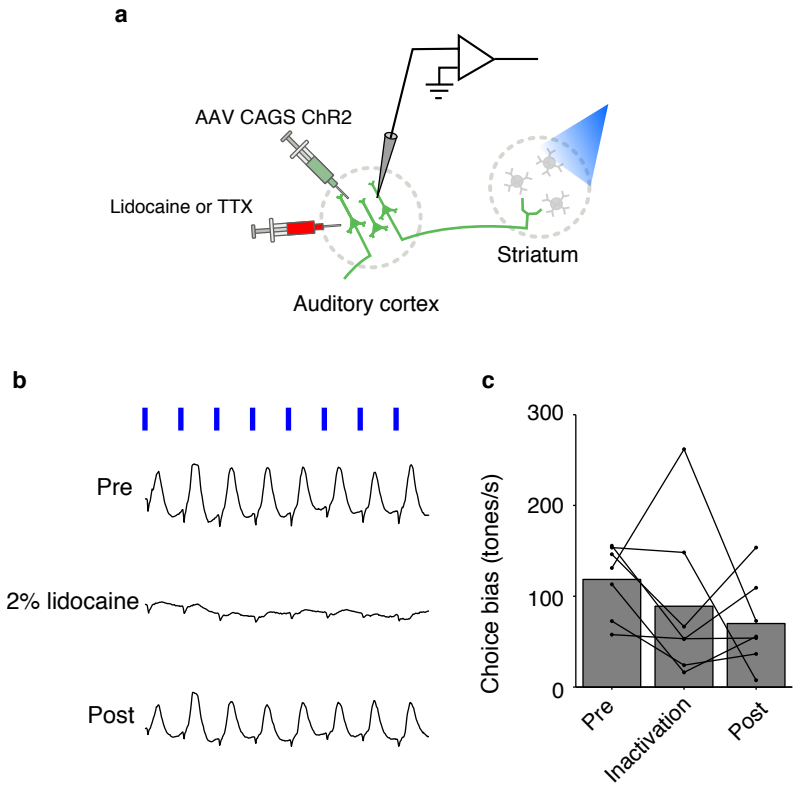

Figure 6.10: **Choice biases evoked by stimulation of corticostriatal neurons do not depend on recurrent cortical excitation. a,** Recurrent cortical activity was pharmacologically inactivated during stimulation of striatal axons. **b,** Lidocaine infusion into the auditory cortex reversibly abolishes antidromic light-evoked LFP responses. **c,** Inactivation of cortical recurrent excitation does not abolish light-evoked choices biases.

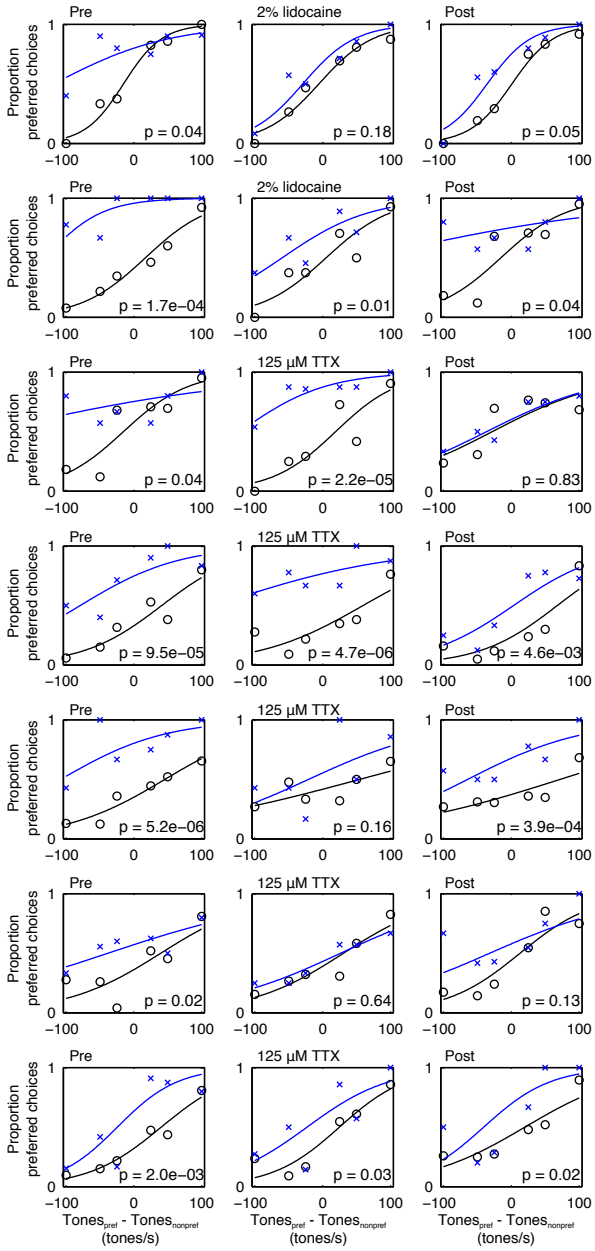

Figure 6.11: Psychometric curves from control (black) and stimulation (blue) trials on for behavioral session before inactivation (left column), during the inactivation session (center column) and following recovery from inactivation (right column). The p-values quantify significance of the stimulation-evoked choice biases.

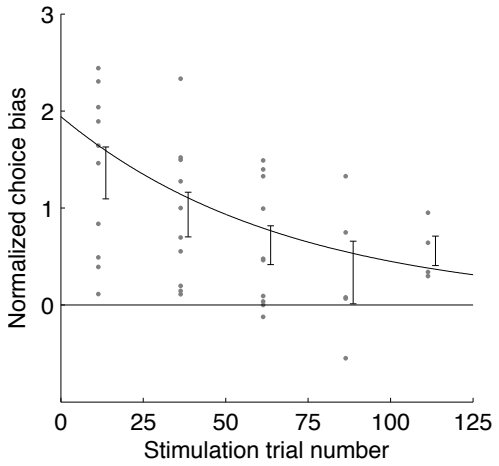

Figure 6.12: **Behavioral adaptation during stimulation of corticostriatal neurons.** For sites where we collected at least 75 stimulation trials and stimulation produced a choice bias of at least 15 tones/s, we binned the stimulation trials in blocks of 25 trials and independently measured the stimulation-evoked choice bias in each block. We normalized these measurements by the mean choice bias during that session. Error bars are s.e.m. and the line is an exponential fit to the data. Effects of stimulation were greatest at the start of the session and decayed with a time constant of 68 stimulation trials (95% confidence interval, 39-265 trials).

these rats and quantified the shift of the chronometric curve produced by stimulation of corticostriatal neurons (Fig. 6.13ab). Due to the fact that stimulus strength accounts for only a fraction of the variance in response times, our estimates of these shifts from single sessions were noisier than those of stimulation-evoked choice biases. Nevertheless, across sessions chronometric shifts depended on the frequency tuning of the stimlation site (Fig. 6.13c) and were correlated with stimulation-evoked choice biases (Fig. 6.13d). Thus, stimulation mimicked the effects on response times of adding acoustic evidence favoring the choice associated with the preferred frequency of the stimulation site.

6.7 Discussion

The experiments above that the activity of corticostriatal neurons influences subjects' decisions in the "cloud-of-tones" task. The effects of stimulation of these neurons on choice depend on the frequency preference of the stimulated neurons and mimic the effect of increasing the occurence of tones of this frequency in the stimulus. Choice biases produced by corticostriatal neurons are mediated by their long-range rather than local intracortical connections. Some corticostriatal

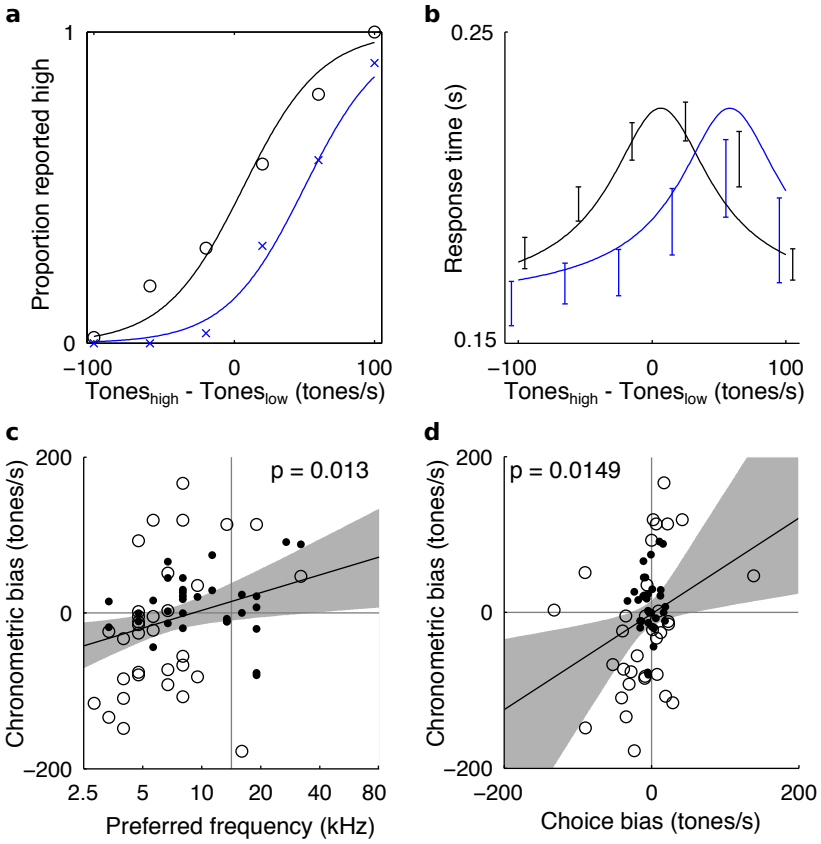

Figure 6.13: **Effects of stimulation of corticostriatal neurons on response times. a-b,** Psychometric and chronometric functions from a single session during stimulation of corticostriatal axons. Black - control trials; blue - stimulation trials; error bars - s.e.m. **c,** Shifts of the rats' chronometric curves evoked by stimulation of corticostriatal neurons depended on the frequency tuning of the stimulation site. Filled circles - HSV-mediated targeting of corticostriatal neurons; open circles - axonal stimulation. **d,** Stimulation-evoked chronometric shifts were correlated with stimulation-evoked choice biases.

neurons send axon collaterals to other brain structures, the contralateral auditory cortex and inferior colliculus (Moriizumi and Hattori, 1991). The role of these outputs in the behavioral effects of photostimulation is unclear. The inactivation approach described in Section 6.5 could be applied in the striatum to measure the relative contribution of striatal and other projections of corticostriatal neurons. If behavioral effects of stimulation indeed result from excitation of striatal neurons, choice biases will be abolished if the target striatal cells are inactivated during stimulation.

Naturally, our method of stimulation of corticostriatal neurons cannot reproduce their normal patterns of activity. Therefore, it is not unreasonable to question whether the effects of photostimulation reflect the normal function of these cells in the task. This question is addressed in Chapter 7, where we examine behavioral effects of specific inactivation of corticostriatal neurons.

Since the association between sound frequency and behavioral response is established arbitrarily during training in the task, downstream circuits must learn to decode the activity corticostriatal cells. This task may be accomplished by plasticity of corticostriatal connections. Evidence of this plasticity is presented in Chapter 8.

7

Inactivation of corticostriatal neurons

We have shown in Chapter 6 that specific stimulation of corticostriatal neurons biases rats' choices in the "cloud-of-tones" task. However, since artificial stimulation cannot replicate the natural firing patterns of these neurons, it remains to be seen whether the activity corticostriatal neurons contributes to subjects' responses during normal performance of the task. To answer this question, we used Archaerhodopsin-3 (Arch)(Chow et al., 2010), a light-activated proton pump, to selectively supress the endogenous activity of corticostriatal cells during auditory discrimination. Rather than attempting to inactivate all corticostriatal cells—a technically difficult feat whose interpretation might be obscured by the compensatory plasticity common to lesion studies—we sought instead to silence corticostriatal neurons within a restricted region of the tonotopic map. We hypothesized that local inactivation of corticostriatal neurons would produce a behavioral effect, equivalent to a reduction in the presentation rate of tones of the preferred frequency of the inactivation site. In other words, it would bias subjects' responses in the direction opposite of the bias produced by stimulation.

We find that Arch-inactivation of corticostriatal neurons results in an "anti-bias" away from the choice port associated with the preferred frequency of the inactivation site. GFP fluorescence of the Arch-GFP fusion allowed us to estimate the number of neurons affected by inactivation. We found that the magnitude of stimulation evoked-biases correlated with the number of Arch-expressing cells near the inactivation fiber.

7.1 Arch-inactivation of corticostriatal neurons

We targeted Arch expression to corticostriatal neurons using the same HSV-based approach we previously used to express ChR2 (Fig. 7.1a). The depth distribution of Arch expression (Fig. 7.1bc) was similar to that previously seen for ChR2 (Fig. 6.2).

Pulses of green light in inhibited spiking of putative corticostriatal neurons (Fig. 7.2a). To estimate the spatial extent of Arch-inactivation, for each neuron that was supressed by light we determined the maximum distance where light delivery could reduce the neuron's firing by at least 50%. We took this distance to be the mean of the distances to the furthest fiber where inactivation was >50% and the closest fiber where inactivation was <50%. The likelihood inactivation decreased with distance from the fiber. An exponential fitted to the data had a space constant λ of 564 μm.

7.2 Local inactivation of corticostriatal neurons biases choices

We inactivated corticostriatal neurons during stimulus presentation in the "cloud-of-tones" task on a subset of trials and measured the behavioral effects of inactivation subjects' responses. Stimulation had no effect on the slope of subjects' psychometric functions (Fig. 7.3). Therefore, we used the same approach as applied for specific stimulation of corticostriatal cells (Eq. 6.1) to measure the choice biases produced by inactivation.

As predicted, inactivation of corticostriatal neurons biased subjects' choices away from the reward port associated with the frequency band of the inactivation site (Fig. 7.4a-c). Pulses of green light did not affect the behavior of uninjected control animals (Fig. 7.4d). These results indicate that stimulus-evoked responses of corticostriatal neurons in the auditory cortex are used by rats to make decisions driven by auditory stimuli.

The same trend was observed for shifts for subjects' chronometric functions but did not reach significance (Fig. 7.5).

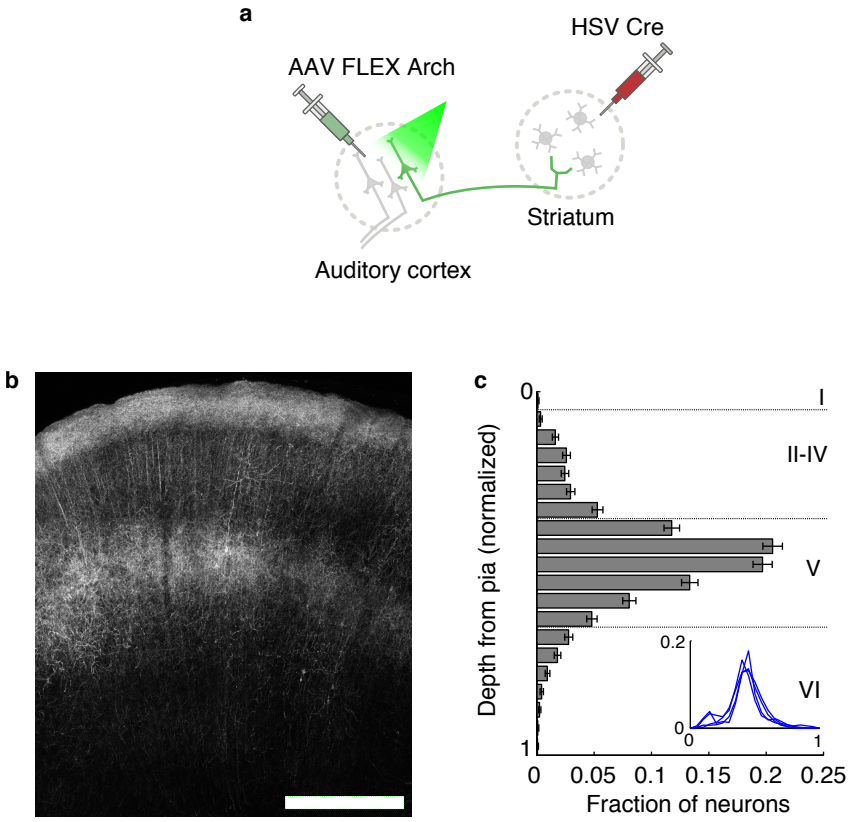

Figure 7.1: **Targeted expression of Arch in corticostriatal neurons.** **a,** Strategy for specific inactivation of corticostriatal neurons. **b,** Fluorescence image of Arch-GFP expression in corticostriatal neurons in the auditory cortex. Scale bar - 500 μm. **c,** Depth distribution of Arch-GFP expression. Dashed lines mark the approximate location of layer boundaries. Error bars - 95% confidence intervals. Inset - depth distribution of Arch in 4 rats.

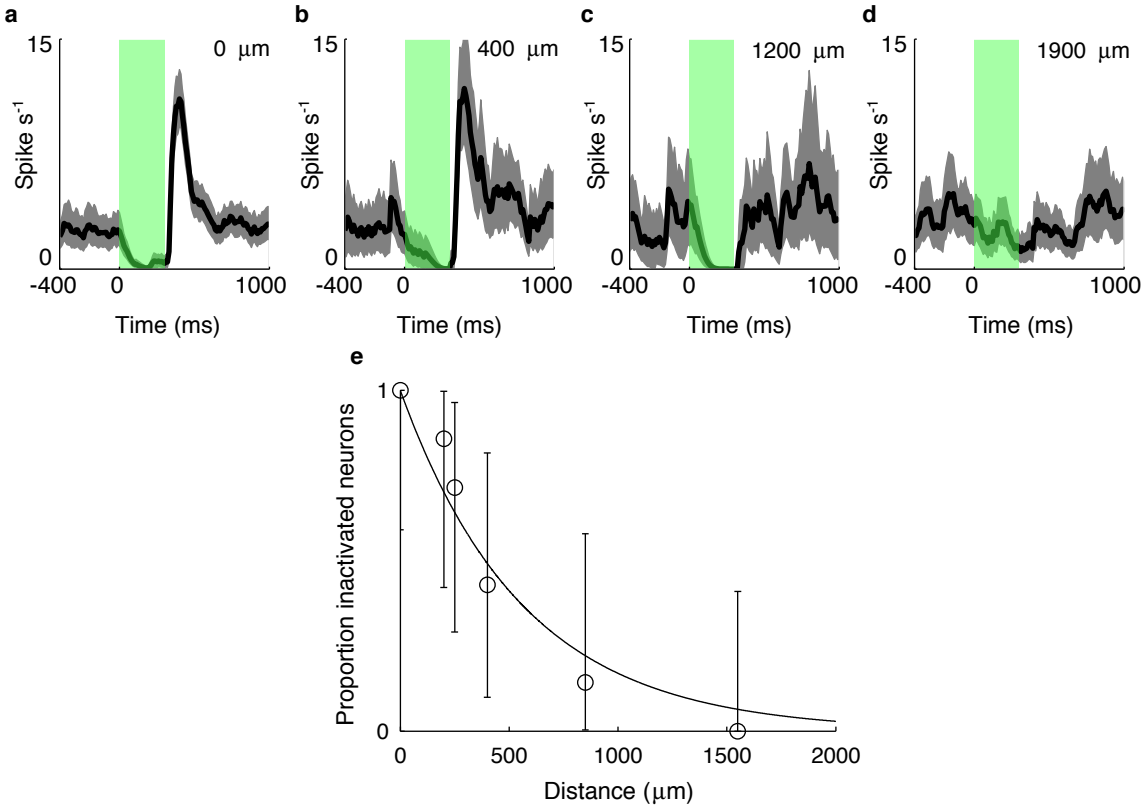

Figure 7.2: **Spatial extent of Arch-inactivation. a-d,** PSTH of an example putative corticostriatal neuron, illuminated with green light (5 mW) at fibers 0, 400, 1200 and 1900 μm from the recording electrode. Inactivation persists up to 1200 μm away. Green bar shows timing of light delivery. **e,** The likelihood of silencing for Arch-expressing corticostriatal neurons as a function of distance from the fiber. For each neuron (N=7), we determined the maximum distance where light delivery could reduce the neuron's firing by at least 50%. The likelihood of inactivation at a given distance was estimated as the fraction of neurons inactivated at that point (space constant $\lambda = 564\mu$m). Error bars are 95% binomial confidence intervals.

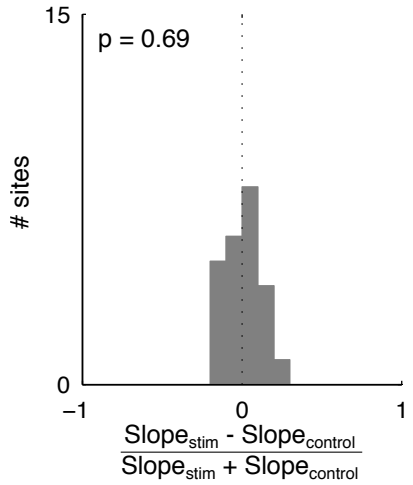

Figure 7.3: **Inactivation of corticostriatal neurons does not decrease discrimination performance.** Inactivation of corticostriatal neurons does not affect psychometric performance measured as the slope of the psychometric curve.

7.3 Effects of inactivation are correlated with Arch expression levels

We used Arch-GFP fluorescence to estimate the number of neurons silenced in each experiment. The locations of Arch+ neuronal somata were identified in fluorescence images of brain sections from experimental animals (Fig. 7.6a). Consecutive sections were then aligned using rigid registration maximizing the cross-correlation of fluorescence signals of adjacent sections (Fig. 7.6b) and cell coordinates were reconstructed in three dimensions.

We first quantified the number of Arch-expressing neurons within a radius of 1 mm from the inactivation fiber for each session [1]. The magnitude of choice biases depended on the number of corticostriatal neurons expressing Arch near the fiber (Fig. 7.6c). The number of Arch-expressing cells within 1 mm of the fiber in our experiments did not exceed 2444, or 0.83% of neurons in that volume. In two rats cell counts were consistently low (Fig. 7.6c, gray circles), likely as a consequence of poor retrograde HSV infection. The median choice bias for sites recorded from these rats was not significantly different from 0 ($p = 0.60$, signed-rank test). The variance of choice biases in these animals is accounted for by sampling error due to the

[1] Since submitting the paper describing this work (Znamenskiy and Zador, 2013), we have modified the method through which we estimate the location of the inactivation sites. Therefore, these cell counts differ slightly from those reported in the paper.

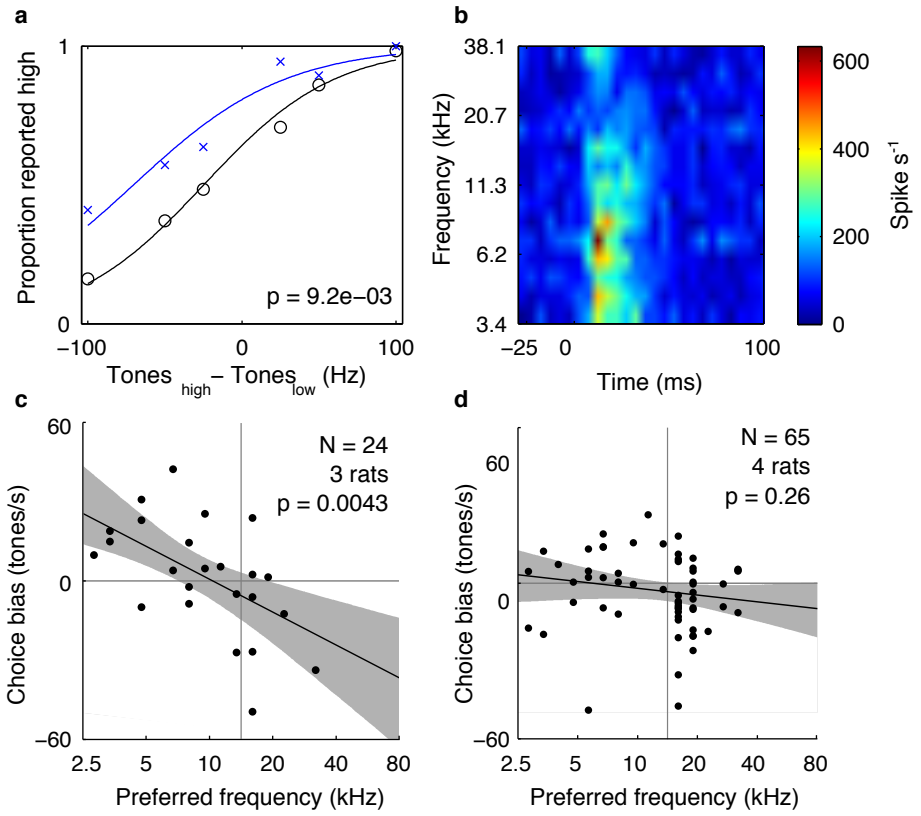

Figure 7.4: **Arch-inactivation of corticostriatal neurons biases choices. a,** Psychometric performance during a single behavioural session on control (black) and inactivation (blue) trials. **b,** Mutliunit tone-evoked responses for site in panel **a**. **c,** Across the population, direction and magnitude of choice biases evoked by inactivation depends on the frequency preference of the inactivation site. Gray shading shows 95% confidence interval for regression line. **d,** Consistent choice biases were not observed in control animals that did not express Arch.

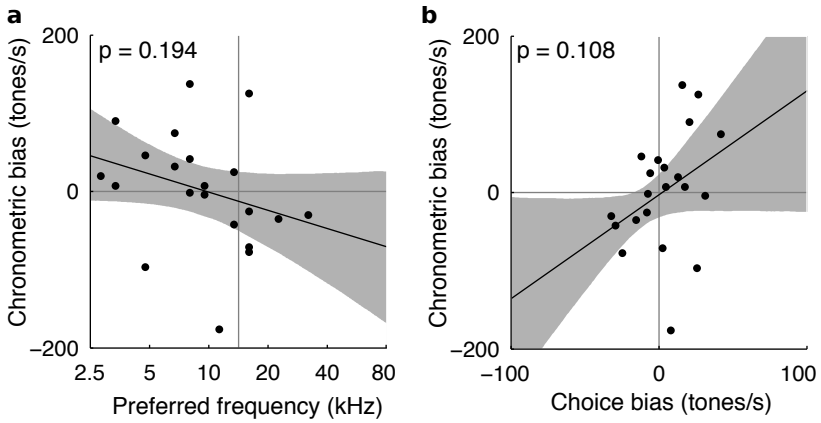

Figure 7.5: **Effects of Arch-inactivation of response times. a,** Shifts of the rats' chronometric curves evoked by inactivation of corticostriatal neurons and frequency tuning of the inactivation site. **b,** Inactivation-evoked chronometric shifts in relation to inactivation-evoked choice biases.

limited number of inactivation trials during a single behavioral session.

Perhaps a more accurate way to estimate the number of neurons affected by inactivation is to directly use our *in vivo* measurements of the spread of Arch-inactivation (Fig. 7.2e) to define the probability of inactivation for each cell based on its distance from the fiber. The number of the inactivated neurons n is then given by:

$$n = \sum_{i=1}^{N} e^{-d_i/\lambda} \tag{7.1}$$

where N is the total number of Arch+ neurons, d_i is the distance from the fiber to ith neuron and λ is the measured space constant of inactivation (564 μm). The neuron counts obtained using this method are $\sim$ 2-fold lower than those using a simple 1mm cutoff. However, the relationship between cell count and inactivation-evoked choice biases holds (Fig. 7.6d).

There are a number of limitations to these estimates. The biggest is the assumption that all the neurons included in the count are tuned to the same sound frequencies as cells at the stimulation site. While this assumption is true for cells within 100s of μm from the fiber, it is certainly violated for cells millimeters away.

Consider for instance the sites with low cell counts from animals that overall have high levels of Arch expression. Light delivered at these sites inactivates a small number of cells near the fiber. The large pool of neurons further away receives little light, but a subset of these cells

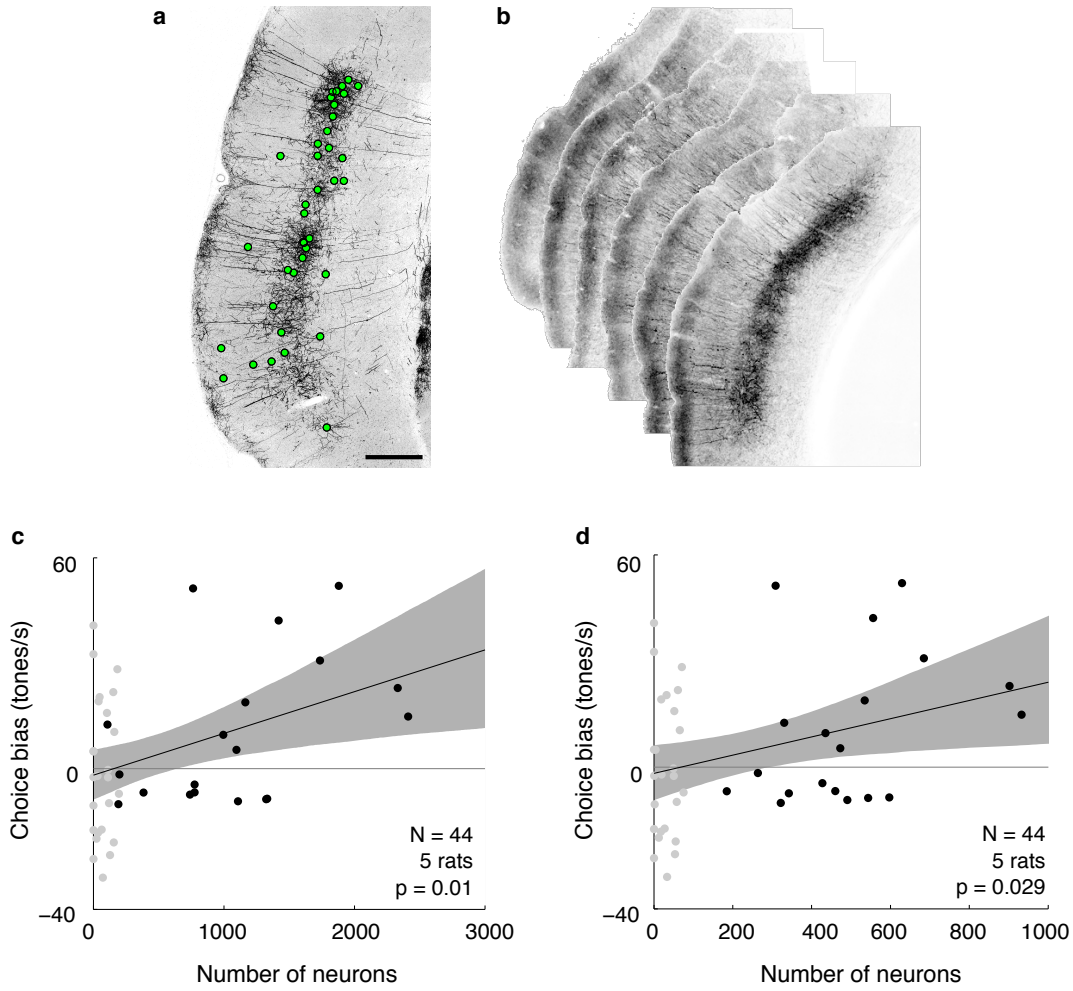

Figure 7.6: **Quantification of numbers of neurons affected by inactivation. a,** Somata of neurones expressing Arch-GFP (green circles) identified in a fluorescence image of the auditory cortex at the end of an inactivation experiment. Scale bar - 500 μm. **b,** Consecutive sections from a single rat aligned using rigid registration. **c,** Effects of inactivation were correlated with the number of Arch-expressing neurones within 1 mm, or approximately 2λ, from the fiber. Data for 2 of 5 rats, for which Arch expression was low throughout the auditory cortex (on average 72±69 cells per site), is shown in gray. **d,** Same notation as in **c** with cells counted according to the exponential drop off in Fig. 7.2e.

with high Arch expression levels will still be affected. Since the preferred frequency of these distant neurons will tend to differ from the recording site, their inactivation will diminish the observed choice biases. This may explain why the number of neurons within a 1 mm sphere around the inactivation site (Fig. 7.6c) better predicts the magnitude of choice biases than estimates based on exponential drop-off of inactivation probability (Fig. 7.6d). Certainly, as a consequence of variation in tuning among inactivated neurons our experiments underestimate the contribution single neurons.

7.4 Implications for neuronal pooling models

The results described in Sec. 7.3 relate the behavioral effects of inactivation to the numbers of affected neurons. These measurements provide a constraint to neuronal models of decision-making. This section will briefly explore the implications of our results for simple neuronal pooling models.

Consider an observer (or a downstream circuit) trying to discriminate the "cloud-of-tones" stimulus on the basis of the firing of a corticostriatal neurons in the auditory cortex. One approach is to assign each neuron to a high or low frequency pool depending on its stimulus selectivity and compare the total number of spikes emitted in each pool. In the simplest version of this model the variability in subjects' behavioral responses stems from the Poisson noise in spike counts of neurons in the pool.

Let the firing rate in the high frequency pool f_{high} and low frequency pool f_{low} vary as follows as a function of stimulus s, which we normalize to vary from -1 to 1:

$$f_{high}(s) = f_0(1 + \alpha s)$$

$$f_{low}(s) = f_0(1 - \alpha s)$$

Here the parameter α, which can take values from 0 to 1, sets the average selectivity of the neurons for their preferred stimulus. The difference in the number of spikes generated by Poisson processes with these rates is approximated by a normal distribution with mean $\mu(s)$

and standard deviation $\sigma(s)$:

$$\mu(s) = f_{high}(s) - f_{low}(s) = f_0(1+\alpha s) - f_0(1-\alpha s) = 2\alpha f_0 s \tag{7.2}$$

$$\sigma(s) = \sqrt{f_{high}(s) + f_{low}(s)} = \sqrt{f_0(1+\alpha s) + f_0(1-\alpha s)} = \sqrt{2f_0} \tag{7.3}$$

Applying normal approximation, since μ is large, the probability of subjects' choices is described by the cumulative normal distribution:

$$\Pr(\text{right}|s) = \Phi\left(\frac{\mu(s)}{\sigma}\right) = \Phi\left(\frac{2\alpha f_0 s}{\sqrt{2f_0}}\right) = \Phi(\alpha s\sqrt{2f_0})$$

By fitting subjects' psychometric curves with a probit model $\Pr(\text{right}|s) = \Phi(\beta s)$, we can measure $\beta = \alpha\sqrt{2f_0}$.

Experiments described in Sec. 7.3 allowed us to measure the number of neurons n, whose inactivation produces a choice bias equivalent to increasing stimulus s by 1 (or 100 tones/s in units used in the task). We can use this measurement to estimate the total size of the neuronal pool consistent with this basic pooling model. If the mean number of spikes fired by each corticostriatal neuron per trial is ρ, then

$$\Pr(\text{right}|s+1) = \Phi\left(\frac{\mu(s+1)}{\sigma}\right) = \Phi\left(\frac{\mu(s)+2\alpha f_0}{\sigma}\right) = \Phi\left(\frac{\mu(s)+n\rho}{\sigma}\right)$$

therefore, $2\alpha f_0 = n\rho$, and as $\alpha = \sqrt{\frac{\beta^2}{2f_0}}$

$$\sqrt{2f_0\beta^2} = n\rho \tag{7.4}$$

We can then estimate $f_0 = \frac{(n\rho)^2}{2\beta^2}$. From experiments $n \approx 5\times10^3$ (Fig. 7.6d). Since the mean evoked spike rate in auditory cortex is ≈ 2.5 Hz (Hromádka et al., 2008), and stimulus presentation typically lasts 200 ms, $\rho \approx 0.5$ spike/trial. From psychometric fits we can measure $\beta \approx 2$, for a well-trained subject. The mean number of spikes in each neuronal pool that is consistent with these parameters, $f_0 = 7.8\times10^5$, the output of some 1.56×10^6 neurons, or the approximate number of neurons in the entire auditory cortex of both hemispheres.

The analysis above assumed that the only source of noise in the task is Poisson firing of neurons. We will consider the neuronal pool to be made up of N neurons with mean spike

count ρ, such that $f_0 = N\rho$. To allow for other sources of noise, we add an additional parameter E to (7.3) such that $\sigma = \sqrt{2N\rho + E}$. Let $\epsilon = 1 + {}^{E}/_{N\rho}$, then $\sigma = \sqrt{2\epsilon N\rho}$. Amending (7.4),

$$\sqrt{2\epsilon N\rho\beta^2} = nr \quad \Rightarrow \quad \epsilon = \frac{n^2\rho}{2N\beta^2}$$

By assuming that N is the total number of corticostriatal neurons ($\approx 5 \times 10^4$), we can estimate $\epsilon = 31.25$. In other words, the contribution of E to behavioral variabilty is $30\times$ that of Poisson spiking noise. There are many possible sources of this increased variability. One possible interpretation of E, is that it reflects "memory noise", or fluctuations in the decision threshold across trials. Another possibility is that it reflects signals unrelated to the sensory stimulus, for example driving response variability to encourage exploration, or "pooling noise" arising during integration of neuronal signals (Shadlen et al., 1996).

We have so far assumed that the responses of neurons are statistically independent. Non-independence of responses is another factor that can inflate the variability of pooled spike counts. What would be the consequences if responses of single neurons are correlated with a correlation coefficient c? Covariance of the responses of any pair of neurons

$$\mathrm{Cov}(x_i, x_j) = c\sqrt{\mathrm{Var}(x_i)\mathrm{Var}(x_j)} = c\sqrt{\rho^2} = c\rho$$

The variance of the sum of their responses is then given by

$$\begin{aligned}
\mathrm{Var}\left(\sum_{i=1}^{N} x_i\right) &= \sum_{i=1}^{N}\sum_{j=1}^{N} \mathrm{Cov}(x_i, x_j) \\
&= \sum_{i=1}^{N} \mathrm{Var}(x_i) + \sum_{i\neq j} \mathrm{Cov}(x_i, x_j) \\
&= Nr + (N^2 - N)c\rho = N\rho(1 + (N-1)c)
\end{aligned}$$

Assuming responses are correlated within each pool but the low and high frequency pools are independent, we can ammend (7.3) to

$$\sigma = \sqrt{2N\rho(1 + (N-1)c)} \approx \sqrt{2N\rho(1 + Nc)}$$

Since $\sigma = \sqrt{2\epsilon N\rho}$,

$$c = \frac{\epsilon - 1}{N} = \frac{\dfrac{n^2\rho}{2N\beta^2} - 1}{N} = \frac{n^2\rho}{2N^2\beta^2} - \frac{1}{N}$$

Given our estimates of n and N, $c = 0.0006$ would account for behavioral performance. Clearly, the all-to-all correlations within neuronal pools and 0 correlation across pools assumed here are an over-simplification. Between-pool correlation will decrease σ^2 proportional to the covariance low and high pool spike rates. Therefore, any further analysis requires a detailed understanding of the correlation structure of auditory cortical responses, specifically that of corticostriatal neurons.

7.5 Discussion

We demonstrated that specific inactivation of corticostriatal neurons biases subjects choices, mimicking the behavioral effects of reducing the rate of presentation of tones at the preferred frequency of the inactivation site. These results show that the activity of corticostriatal neurons contributes to subjects' decisions under control conditions.

These experiments provided us with an opportunity to quantify the contribution of the output of single corticostriatal cells to behavior. We observed robust choice biases at sites with 1040-2444 Arch-expressing neurones within 1 mm of the fiber, comprising 0.35-0.83% of neurones in that volume. Inactivation of this minute fraction of cells targeted to corticostriatal neurones could affect behavior, suggesting a privileged role of these cells in auditory discrimination.

Earlier studies using ChR2- or electrical stimulation demonstrated that subjects can be trained to detect the activation of as few as 6-197 neurons (Huber et al., 2008) or even a single neuron (Houweling and Brecht, 2008). However, these studies differ from ours in several important ways. First, stimulation increased neurones' firing as much as 25-fold over spontaneous rate (Houweling and Brecht, 2008). Second, previous work examined subjects' ability to detect stimulation in the absence of any background sensory stimulation. Our experiments allowed us to estimate the contribution of single neurones to behaviour during normal auditory perception. Third, as responses in the auditory cortex are sparse (Hromádka et al., 2008), only a fraction of the neurones we silenced were activated by the auditory stimulus.

While our results show that the activity of corticostriatal cells instructs subjects' choices, they do not address the question whether corticostriatal neurons are essential for auditory

discrimination or act in parallel with other pathways. Owing to technical limitations of light delivery and the large area of the auditory cortex in rats, this question is difficult answer using optogenetics. Instead, pharmacological approaches such as designer receptors exclusively activated by a designer drug (DREADDs) (Armbruster et al., 2007) seem a more suitable tool to answer this question. DREADDs could be virally expressed in corticostriatal cells and activated by intraperitoneal injection of the ligand (Ferguson et al., 2011), reversibly silencing corticostriatal neurons. This approach could test whether subjects can still perform auditory discrimination when the majority of corticostriatal cells in the auditory cortex are inactivated.

8

Plasticity of corticostriatal connections

We have shown in Chapters 6 and 7 that the behavioral effects of manimulation of corticostriatal neurons depend on the association between the their preferred frequency and motor response implicit in the task. Since these associations are selected arbitrarily by the experimenter during behavioral training, these results imply circuits downstream from corticostriatal cells learn to select the appropriate motor action on the basis of their activity.

The plastic nature of corticostriatal connections is well established. Therefore, we hypothesized that training in the "cloud-of-tones" task changes the strength of cortical inputs into the auditory striatum. To test this hypothesis, we developed a novel recording paradigm to measure corticostriatal synaptic weights *in vivo*. The topographic organization of corticostriatal projections allowed us to track how corticostriatal connectivity depends on the frequency preference of cortical inputs.

We found that training in the "cloud-of-tones" task potentiates corticostriatal connections. Moreover, this potentiation occured specifically at sites whose preferred frequency was associated with contralateral choices in the task.

8.1 Measuring corticostriatal connectivity *in vivo*

To assay the strength of corticostriatal connections *in vivo*, we virally expressed ChR2 in the cortex and implanted optical fibers coupled to tetrodes in the striatum, targeting the axons of

corticostriatal neurons (Fig. 8.1a). Light stimulation drove neurotransmitter release and generated excitatory currents in striatal neurons, which could be detected in extracellular recordings (Fig. 8.1b). Because the striatum, like the CA1 region of the hippocampus, lacks recurrent excitatory connections, we could interpret the light-evoked local field potential (LFP) as a measure of evoked synaptic current.

The light-evoked LFP is composed of a presynaptic and a postsynaptic component. Consistent with their synaptic origin, light-evoked responses peaked 3 ms after light onset and adapted to high frequency stimulation (Fig. 8.1b). AMPA and NMDA glutamate receptor blockers reduced this component (Fig. 8.1c). Its incomplete inactivation may be the result of limited diffusion of the drugs *in vivo*. Tetrodotoxin completely abolished the synaptic component of the response, presumably by blocking spiking in corticostriatal axons. Light-evoked currents in the axons conducted by ChR2 itself give rise to the remaining component of the LFP. The decay rate of this component is consistent with the closing rate of the channel (Nagel et al., 2003).

8.2 Corticostriatal connectivity in trained animals reflects frequency-response associations

We first examined the magnitude of light-evoked respones in fully trained animals as a function of frequency preference of the stimulation site. These data were collected during the course of experiments measuring the behavioral effects of stimulation of corticostriatal axons (Sec. 6.4).

In animals trained to associated high frequencies with contralateral choices, the magnitude of light-evoked corticostriatal responses increased with preferred frequency of the stimulation site (Fig. 8.2a). In rats which learned the opposite association, responses were highest at sites preferring low frequencies (Fig. 8.2b). Thus the association between sound frequency and choice that the rats were trained to make was encoded in the weights of corticostriatal connections. It appears that training selectively reinforced cortical inputs from neurons responding to sounds associated with contralateral choices.

However, we are cautious in the interpretation of these results. Since the data were collected once the rats were already trained, we weren't able to track the plasticity as it occured.

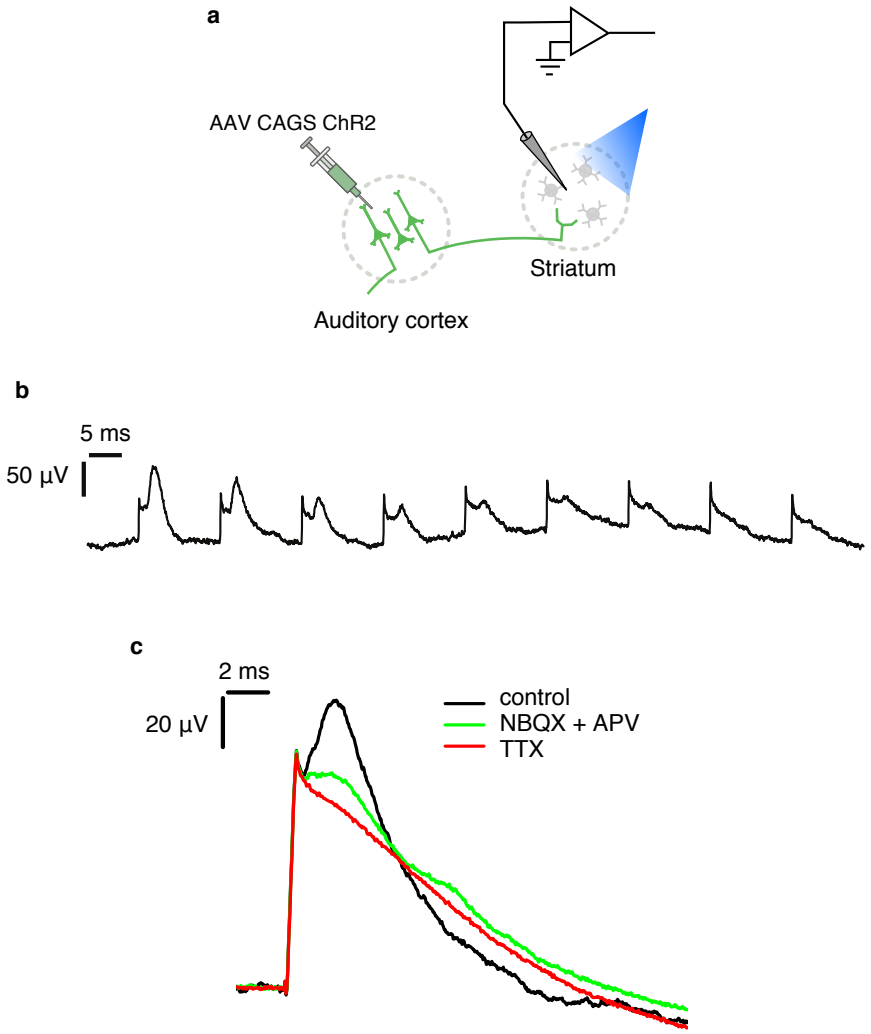

Figure 8.1: **Assaying corticostriatal connectivity *in vivo*.** **a,** Experimental setup for measuring corticostriatal connections. **b,** Example striatal light-evoked LFP in response to an 80 Hz stimulation train. **c,** Synaptic component of the LFP is blocked by application of glutamatergic blockers.

Difference in the density of ChR2-expressing axons from site to site and between animals could contribute to variation in light-evoked responses. It is difficult to imagine how such variation could give rise to frequency-dependent trends that we observed. Nevertheless, we wanted to confirm that we could observe the potentiation of corticostriatal connection at single sites during behavioral training.

8.3 Training potentiates corticostriatal connections

Since our measurement of the strength of corticostriatal connections relies of the local field potential, we can use it monitor changes in corticostriatal connectivity across multiple behavioral sessions. We implanted naïve animals with the fiber/tetrode array and lowered fibers into the auditory striatum. To best approximate the state of the animal during training, the animal was water restricted and received free water once daily while placed in the behavioral chamber. At this time we measured frequency tuning and baseline light-evoked responses for each fiber. By monitoring the baseline response for several consecutive days we confirmed that it was stable and that our stimulation protocol itself did not elicit plasticity. We than began training and measured light-evoked responses after the end of each behavioral session in awake animals not engaged in the task. We conducted our measurements outside the context of the task to minimize possible effects of stimulation on behavior and corticostriatal plasticity.

Training resulted in a rapid and persistent increase in corticostriatal transmission in the auditory striatum, evident from the first training session during which the rat performed the task above chance levels, typically either the first or the second training session (Fig. 8.3a). We next asked whether this plasticity is task and modality specific. To do this, we trained rats in a simple visual task requiring them to select the choice port lit up by an LED before starting training in the "cloud-of-tones" task. Corticostriatal responses were unchanged after training in the visual task even at sites that later showed potentiation after training in the "cloud-of-tones" task (Fig. 8.3b).

We next characterized how training altered corticostriatal transmission across the striatal frequency axis. To quantify the effects of training, we measured the slope of the rising

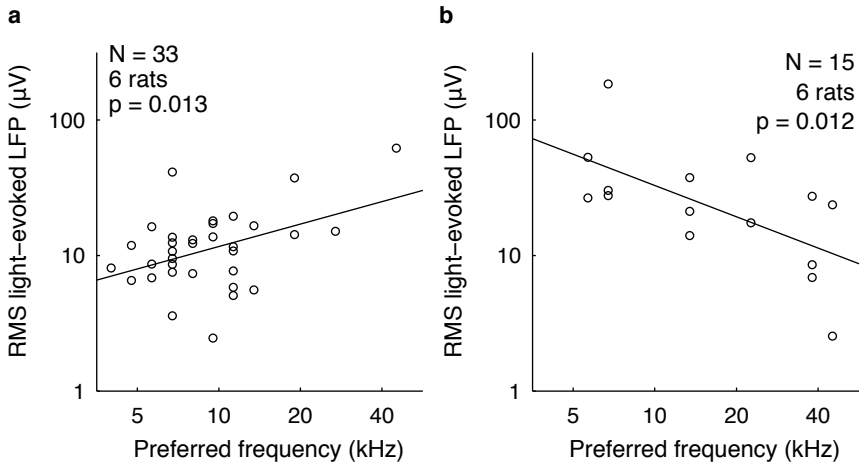

Figure 8.2: **Corticostriatal connectivity in trained animals reflects frequency-response associations. a,** In subjects trained to associate high frequencies with contralateral choices, striatal light-evoked responses were positively correlated with preferred frequency. **b,** The opposite trend was observed in subjects trained to associate low frequencies with contralateral choices.

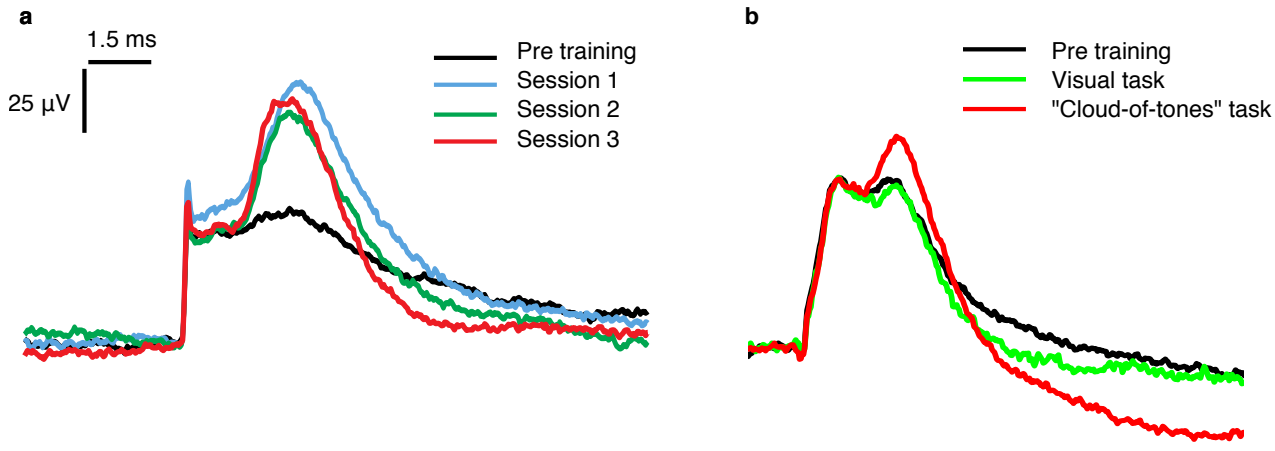

Figure 8.3: **Training in an auditory task potentiates corticostriatal transmission. a,** Striatal light-evoked field potentials at a site before behavioral training and following the first three training session. **b,** Light-evoked responses showed no change after training in a simple visual task but were enhanced after training in the "cloud-of-tones" task.

phase of the light-evoked LFP normalized across sites and sessions to the peak of the presynaptic ChR2-evoked response. In this cohort of rats trained to associated low frequencies with contralateral choices, training selectively potentiated striatal connections of cortical neurons tuned to low frequencies, while the outputs of high frequency neurons remained unchanged (Fig. 8.4a). No such effect was observed after training in the control visual task (Fig. 8.4b).

8.4 Discussion

We observed that training in the "cloud-of-tones" task potentiated corticostriatal connections. Potentiation was specific to inputs tuned to frequencies associated with contralateral choices and was not observed after training in a simle visual discrimination task. These changes persisted for days and could be observed outside the context of the behavioral task, suggesting that the potentiation was mediated by changes in corticostriatal synaptic weights and not effects of neuromodulation.

Thus in the context of a two-alternative choice task, learning reinforces corticostriatal synaptic weights of neurons predicting contralateral rewards. This suggests a simple mechanism through which auditory striatum might drive action selection in the task. The auditory stimulus will create an imbalance in striatal activity in the left and the right hemisphere, which will drive the selection of the choice associated with the frequency of the sound.

Here we only examined projections of the auditory cortex to the ipsilateral striatum. A projection to the contralateral striatum exists but is significantly weaker. A tempting speculation is that synaptic plasticity in the other hemisphere will follow the opposite pattern with respect to sound frequency, such that inputs associated with choices contralateral to the striatal recording site and not the source of cortical projections are potentiated. This collateral projection may provide a pathway for the auditory cortices in both hemispheres to drive choices in both contralateral and ipsilateral directions.

Since we used light-evoked LFPs as a measure of corticostriatal connectivity at the population level, we cannot determine which the striatal cell-types undergo plasticity. Since D1 MSNs are associated with promoting actions, the naïve prediction would be that potentiation at site associated with contralateral responses specifically reinforces their inputs. This question

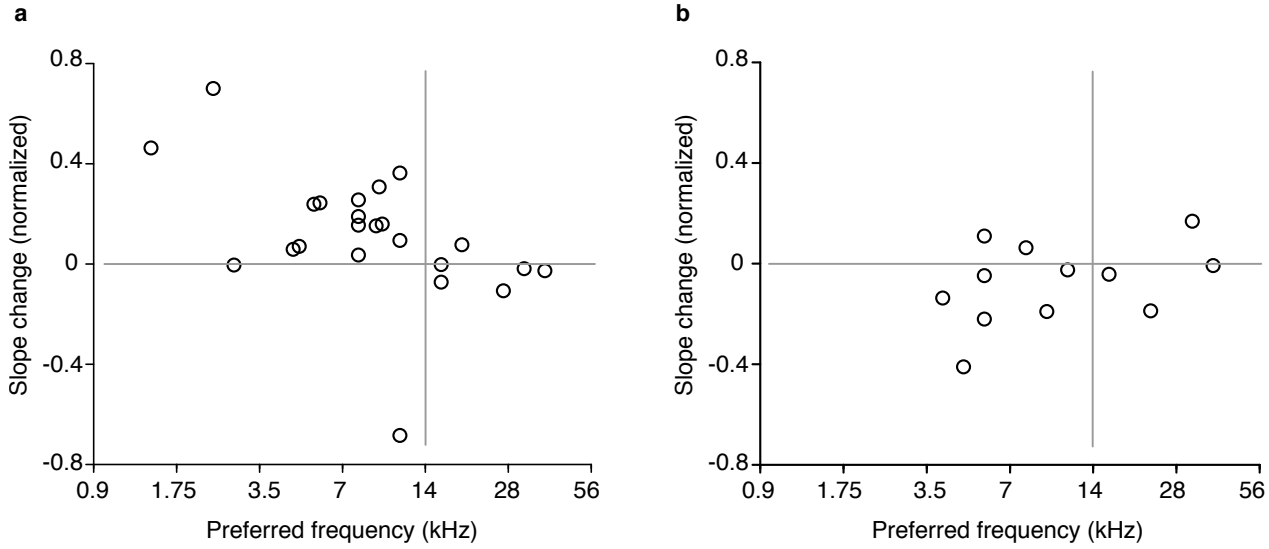

Figure 8.4: **Potentiation is specific to inputs associated with contralateral choices. a,** Change in slope $Trained - Control$ of the rising phase of the light-evoked response in rats, which learnt to associate low frequencies with contralateral choices. **b,** No consistent changes after training in the control visual task.

could be answered through *in vitro* recordings comparing the strength of cortical input onto D1 and D2 MSNs in trained animals at different locations along the striatal frequency axis.

Finally, we do not know how this plasticity affects *in vivo* firing patterns of striatal neurons. Given the rapid timecourse of plasticity, it should be possible to track how responses of single neurons change during the course of learning within a single session. This would be particularly informative if combined with optogenetic methods to specifically identify D1 and D2 MSNs (Lima et al., 2009).

9

Materials & methods

9.1 Plasmid and BAC contruction

PRV BACs HF22a and pBecker were provided by Dr. L. Enquist (Princeton University). BAC recombineering was done using the Counter Selection BAC Modification Kit (Gene Bridges). BACs were prepared using the NucleoBond BAC 100 kit (Clontech). Restriction cloning was done using standard molecular biology techniques.

9.2 Viral production

RVG-pseudotyped EIAV was a kind gift of Dr. P. Osten (Cold Spring Harbor Laboratory). The AAV CAGGS ChR2-Venus plasmid was a provided by K. Svoboda (HHMI Janelia Farm). AAV FLEX ChR2-YFP construct was provided by K. Deisseroth (Stanford University). AAV FLEX Arch-GFP construct was generated subcloning Arch-GFP from an AAV CAG Arch-GFP plasmid (provided by E. Boyden, MIT) into AAV FLEX backbone from AAV FLEX ChR2-YFP. The plasmid DNA was prepared using standard maxiprep protocols (Qiagen). AAV serotype 2/9 was packaged by the University of North Carolina viral core at the titer of 1-2 $\times 10^{12}$ particles per ml. HSV-mCherry-IRES-iCre construct was provided by Andreas Luthi (Friedrich Miescher Institute, Switzerland) and packaged by BioVex (Biovex Group Inc.) at the titer of 2.4 $\times 10^{10}$ transducing units per ml. PRV was packaged in-house by transfection or infection of PK15 cells according to established protocols (Curanovic and Enquist, 2009).

9.3 Animal subjects

Animal procedures were approved by the Cold Spring Harbor Laboratory Animal Care and Use Committee and carried out in accordance with National Institutes of Health standards. Male Long Evans rats (Taconic Farms) were housed with free access to food, but were water restricted following the start of behavioural training. Water was available during task performance (24 μl for each correct trial) and freely available for 15-30 min after the end of each behavioural sessions and for at least 1 hour on days when behavioural sessions were not conducted.

9.4 Viral injection

Three to five week old rats were anaesthetised with mixture of ketamine (60 mg/kg of body weight) and medetomidine (0.24 mg/kg) and placed in a stereotaxic apparatus. To target the auditory cortex, part of the temporalis muscle was resected to expose the temporoparietal suture, which was used as a landmark to target injections. For optogenetic experiments, 4 injections were made unilaterally spanning primary auditory cortex at 0.5, 1.5, 2.5 and 3.5 mm from the rostral edge of parietal bone and 1.2 mm from its ventral edge. A small craniotomy was made for each injection and a glass micropipette was inserted perpendicular to the surface of the brain. Two injections were made at the depths of 400 and 800 μm expelling $\sim$250 nl of virus at each depth. To target the auditory striatum, two small craniotomies were made 2.0 and 2.5 mm caudal of Bregma and 4.5 mm lateral of the midline. Injections were made at depths between 3.5 and 6 mm, 0.5 mm between injection sites, $\sim$100 nl per site. Injections were performed by delivering brief pulses of pressure using Picospritzer II (Parker), each pulse delivering $\sim$2 nl at 0.2 Hz. Rats were monitored during their recovery from surgery and returned to group housing.

9.5 Behavioral training

Upon reaching the weight of 200-250 g rats were placed on a water deprivation schedule and commenced behavioural training. The rats were placed in a soundproof behavioural chamber and presented with 3 choice ports. The rats were trained to first poke into the center port, wait for the onset the auditory stimulus and select one of the other two ports to receive a water

reward (24 ul). Rats were shaped to carry out this sequence using the following procedure. During the first phase of training, water was delivered at the correct choice port as soon as the stimulus was played. The duration of the pre-stimulus delay, during which the rat was required to remain in the center port, was drawn from an exponential distribution whose mean was gradually increased from 0.05 s to 0.3 s. The next phase of training required to the rat to poke at the correct choice port to trigger water delivery, however, the rat was allowed to correct his choice if it made a mistake. Once rats learned to perform the discrimination above chance, they were required to make the correct choice on the first attempt. Error trials were punished with a 4 s timeout (2 s during recording sessions).

The "cloud-of-tones" stimulus consisted of stream of 30 ms overlapping pure tones presented at 100 Hz (i.e. with 10 ms between tone onsets). Eighteen possible tone frequencies were logarithmically spaced between 5 and 40 kHz, a range where rats' hearing thresholds are low and relatively constant (Kelly and Masterton, 1977). For each trial either the low (5-10 kHz) or the high (20-40 kHz) octave was selected as the target octave. Stimulus strength r determined the difference in the rate of high and low octave tones in the stimulus. Tones were drawn from the target octave with a probability of $\frac{1+{}^{2r}/_{100}}{3}$. Initially, rats were trained to discriminate tone cloud stimuli composed of tones entirely either in the high or the low octave ($r = 100$) and were gradually introduced to more and more difficult stimuli.

Sound intensity of individual tones was constant during each trial. To discourage subjects from using loudness differences in discrimination, tone intensity was randomly selected on each trial from a uniform distribution 45-75 dB (SPL) during training. During manipulation and recording sessions, sound intensity was kept constant at 60 dB.

9.6 Electrophysiology and optogenetics

Custom-built optical fiber/tetrode arrays were assembled in-house. Each array carried 6 multimodal optical fibers 62.5 μm in diameter with 50 μm core. The fiber tips were sharpened to point using a diamond wheel to improve tissue penetration and increase the angle of the light exit cone. Each fiber was glued to a tetrode and the tetrode tip was cut to terminate within $\sim$100 μm of the fiber tip. The fiber/tetrode assemblies were mounted on individually

movable microdrives. The tetrodes were gold-plated to an impedance of 1 kΩ at 1 kHz and the tetrode/fiber tips were coated with DiI to assist with the identification of fiber tracks in brain tissue.

To implant the fiber/tetrode array, rats were anaesthetised with a mixture of ketamine (40 mg/kg of body weight) and medetomidine (0.16 mg/kg) and placed in a stereotaxic apparatus. A craniotomy was made over the target area (for auditory cortex, 3.5-6.0 mm caudal of Bregma and 6.5-7.0 mm lateral from the midline; for auditory striatum, 2.5-3.5 mm caudal of Bregma and 4-5 mm lateral from the midline). All rats, with the exception of 1 Arch-expressing and 1 uninjected control animal, were implanted in the left hemisphere. The dura was removed and the implant was placed over the target area and fixed in place with dental acrylic. The tetrodes were then lowered until first action potentials were encountered.

To characterize the frequency tuning of stimulation and inactivation sites, the rats were placed in a soundproof chamber and pure tones were played in free field at ∼0.5 Hz. Tone frequencies spanned from 1 to 64 kHz and were played in a random order at 30, 50 or 70 dB-SPL. Only sites that significantly responded to sounds (p ¡ 0.01, signed-rank test comparing firing rate 5-55 ms following sound onset to 0-50 ms preceding sound onset) were included in the analysis of stimulation and inactivation experiments. To determine the preferred frequency, firing rates in the window 5-55 ms following sound onset were computed for each frequency at 70 dB. The resulting tuning curve was smoothed with a 1/2 octave sliding window. The peak of the smoothed tuning curve was selected as the preferred frequency. Sites tuned to frequencies more than an octave outside the range used in the task (below 2.5 kHz) were excluded from analysis.

For optogenetic manipulations, laser light was coupled into a FC/PC parch cord using a FiberPort Collimator (Thor Labs). Laser power was adjusted to produce the desired output at the end of the patch cord. A single implanted fiber was selected for manipulation and coupled to the patch cord. For ChR2 activation, 473 nm laser light (10 mW) was delivered in 1 ms pulses at 40 Hz while the rat remained in the center port. For Arch, 530 nm laser light (50 mW) was delivered in 1 ms at 100 Hz, yielding the average power of 5 mW. To decrease the ability of the rat to detect the stimulation light, a mask LED of a wavelength similar to that of the laser was

placed above the center port in the behaviour chamber. The mask LED was activated on control as well as stimulation trials in the same temporal pattern as the laser. Manipulation trials were randomly interleaved among control trials. The optical fiber was advanced approximately 300 μm between manipulation sessions.

For action potential recordings, signals were filtered 600-6000 Hz and recorded using the Neuralynx Cheetah 32 system and Cheetah data acquisition software.

9.7 Pharmacological inactivation

Two PEEK tubing cannulas (Plastics One) were implanted into the auditory cortex with a separation of $\sim$1 mm. Six stereotrodes were implanted alongside the cannulas spanning 3-4 mm of the auditory cortex to confirm the efficiency of inactivation. One hour before the start of the behavioural session, the animal was briefly anaesthetised with 2% isofluorane and 0.4 μl of drug (during inactivation sessions) or 9 g/l NaCl (during control sessions) was injected at the rate of 0.08 μl/min in both cannulas.

9.8 Data analysis: electrophysiology

To isolate single units, spikes were manually clustered using MClust (MClust-3.5, A.D. Redish et al.). Neurometric functions were computed using the first 175 ms of the auditory response and only included trials where the rat remained in the center port for at least that period of time. We selected neurons whose firing rate during that epoch was $\geq$ 0.5 Hz. We used leave-one-out cross-validation to determine neurometric thresholds and frequency preference for each neuron. Specifically, for each trial we used ROC-analysis including firing rates on all other trials in the recording session to select a firing rate threshold that best discriminated the frequency content of the auditory stimulus and determine whether the neuron prefers high or low frequency stimuli. Trials where the firing rate was greater than or equal to the discrimination threshold were scored as reporting the preferred frequency of the neuron. The neuronal choices were then fit with a logistic regression model.

Cells included in the neurometric are the subset of the cells previously included in the manuscript summarizing this work. Other analyses described in Chapter 4 included an expanded dataset. For analyses of stimulus and choice selectivity, we selected neurons whose firing rate was > 0.5 Hz during the stimulus presentationa and movement period respectively.

To calculate peristimulus time histograms (PSTHs) neuronal firing rates were smoothed with a causal half-Gaussian kernel ($\sigma = 5$ ms). Confidence intervals were derived through bootstrap resampling. For each Arch-expressing corticostriatal neuron we encountered, we delivered light at different fibers along the array to estimate the maximum distance at which light delivery could reduce the neuron's firing by 50%. We took this distance to be the mean of the distances to the furthest fiber where inactivation was >50% and the closest fiber where inactivation was <50%. The likelihood of inactivation at a given distance was estimated as the fraction of neurons inactivated at that point.

To calculate the confidence intervals for cross-correlograms, we first digitally high-pass filtered the raw cross-correlogram at 50 Hz to remove slow co-variation in firing rates. We then randomly shifted the filtered cross-correlogram by 100-2000 ms to generate a resampled distribution. The 2.5% and 97.5% quantiles of this distribution were used as the 95% confidence interval. For comparison with the raw cross-correlogram, we readded the slow (<50 Hz) component of cross-correlogram to the confidence interval. Any point of the cross-correlogram with 5 ms of 0 that fell outside the 95% window was deemed significant.

9.9 Histology and cell count analysis

At the end of the experiment, rats were deeply anaesthetised with ketamine/medetomedine. Small electrolytic lesions were made by passing 30 μA direct cathodal current through each tetrode for $\sim$10 s, marking the final position of the tetrode tip. The rats were then perfused with 4% paraformaldehyde (PFA), their brains were extracted and postfixed in 4% PFA overnight. The brains were cut into 100 μm sections and mounted using Vectashield (Vector Laboratories) for confocal microscopy. To ensure that HSV-mediated labeling was confined to corticostriatal neurons, we verified that viral expression was absent in adjacent brain structures.

To quantify the depth distribution of opsin expression, we measured the distance of from each fluorescent cell soma to the pia as a fraction of total cortical thickness. To estimate the number of neurons affected by optogenetic manipulations, confocal stacks 50 μm in depth were acquired from alternate sections. The sections were registered using rigid registration maximizing the cross-correlation of fluorescence images of adjacent sections. The locations of ChR2-YFP or Arch-GFP expressing neurons were identified manually. Fiber tracks were identified with the help of electrolytic lesions and DiI labeling. Using the locations of the ends of the tracks, we estimated that processing resulted in $\sim$10% shrinkage of the tissue. We estimated the location of the fiber tip during each manipulation session and counted the number of expressing neurons within 1 mm. Since we only identified cells within a 50 μm stack every 200 μm, our estimate of the total number of manipulated cells is 4$\times$ this count.

10

Conclusions and perspectives

We have developed a novel behavioral task optimized for the study of the function of the auditory cortex and its long-range outputs in auditory decisions. Using this task, we demonstrated that corticostriatal neurons contribute to subjects' decisions driven by sounds. We found that the weights of corticostriatal connections are shaped by learning and encode the associations between sensory stimuli and motor responses. Our results have opened the door for further studies of mechanisms of auditory decisions at the cellular level.

Our key result is that stimulation of corticostriatal neurons in the auditory cortex biases subjects' responses in a two-alternative choice frequency discrimination task, mimicking the effects of presenting tones at the preferred frequency of the stimulation site. Inactivation of corticostriatal neurons has the opposite effect, demonstrating that these neurons play a role in subjects' choices under control conditions. This, to our knowledge, is the first demonstration to date of the causal role of a defined population of projection neurons in a perceptual decision-making task. Our results demonstrate the promise of this projection-specific manipulation approach in illucidation of neural circuits controling perceptual decision.

Our results do not exclude the participation of other parallel pathways in auditory decisions. However, owing to the the ubiquity of corticostriatal projections in cortex, they may play a role in sensorimotor transformations in other modalities, providing a general mechanism for control of motor decisions by sensory context (Jiang et al., 2011). Corticostriatal projections are conserved across mammals. In macaques, both primary and secondary auditory cortical

areas send projections to the striatum (Yeterian and Pandya, 1998). In visual cortex, they are found in extrastriate but not striate areas (Saint-Cyr et al., 1990).

How do auditory corticostriatal neurons influence rats' choices in our task? Direct pathway output of the auditory striatum targets the lateral regions of substania nigra reticulata and substantia nigra lateralis (Deniau et al., 1996), which in turn provide inhibition to the superior colliculus (Ficalora and Mize, 1989). Whether auditory striatal output also feeds into the motor thalamus like the output of motor striatal regions is unclear. Superior colliculus in rats is controls action selection in orienting decisions (Felsen and Mainen, 2008). By suppressing the activity of substantia nigra neurons, the auditory striatum may disinhibit the ipsilateral superior colliculus encouraging the selection of contralateral responses.

We also found that auditory corticostriatal connections are potentiated during acquisition of the "cloud-of-tones" task specifically at sites whose preferred frequency is associated with contralateral choices. The observation of corticostriatal plasticity during learning is not in itself novel (Yin et al., 2009). However, previous studies were not able to relate synaptic changes to firing properties of pre- or postsynaptic neurons. By measuring potentiation of corticostriatal connections *in vivo* and exploiting the tonotopy of striatal projections of the auditory cortex, we were able to demonstrate that potentiation occurs specifically for inputs which respond to stimuli that predict contralateral rewards.

An open question is how direct and indirect pathway MSNs act together to direct subjects' choices. One possibility is that D1 neurons are the main target of potentiation of cortical inputs during learning and are preferentially excited by sounds associated with contralateral choices; D2 neurons, on the other hand, could allow auditory corticostriatal projections to produce ipsilateral biases (Fig. 10.1a). This model could be tested directly by measuring the strength of cortical inputs onto D1 and D2 MSNs *in vitro*.

In experiments described in this thesis we have focused on the cortical projection to the ipsilateral striatum. Although much weaker, a projection to the contralateral striatum also exists. Since the contralateral projecting neurons also target the ipsilateral striatum, our manipulation experiments also affected this cell population and may given rise to choices biases

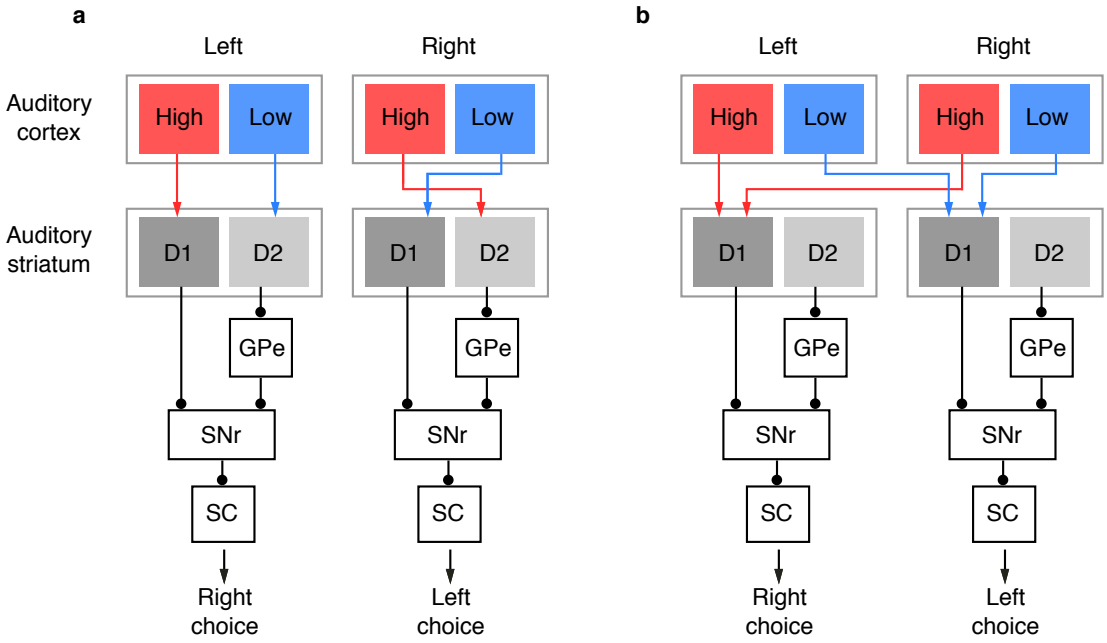

Figure 10.1: **Possible mechanisms for action selection in the auditory striatum.** Cartoon of corticostriatal connections in a rat trained to associate high frequencies with rightward choices. **a,** Action selection through differential connectivity onto D1 and D2 MSNs. **b,** Action selection through contralateral striatal projections.

arising from manipulations at site associated with choices ipsilateral to the cortical hemisphere (Fig. 10.1b).

In our experiments we exploited cortical tonotopy to target neurons based on their frequency preference but were not able to further define selectivity of manipulated neurons. New techniques for patterned excitation of ChR2 (Anselmi et al., 2011; Papagiakoumou et al., 2010) could be combined with *in vivo* calcium imaging to specifically target individual neurons based on their functional properties (O'Connor et al., 2009). For instance, neurons could be selected not only based on their frequency preference but on reliability with which they can predict the correct response. In principle, if sufficient numbers of neurons can be targeted using this method, it could be applied to directly map the rules through which activity of sensory neurons gives rise to animals' decisions.

Patterned light stimulation methods could also be used to extend our results beyond frequency discrimination to study the role of the auditory cortex in perception to more complex features of sounds. The auditory cortex in rats plays a role in discrimination of frequency, but is not absolutely essential (Pai et al., 2011; Tai, 2008). This is not surprising given that sound frequency is already represented at the very first stage of auditory processing in the auditory nerve. Examining how auditory cortex neurons contribute to perception of higher order features of sounds will help pinpoint the computational function of this "pariah of sensory cortices" (Hromadka, 2007).

Appendix A

Properties of corticostriatal neurons

This appendix documents the properties of presumed corticostriatal neurons that were excited by light in photostimulation experiments described in Section 6.1. Since excitatory cortical neurons have extensive local recurrent connections, identifying cells activated by light directly rather than through synaptic inputs is not trivial. Cells expressing ChR2 and activated by light directly can be unambiguously distinguished from indirectly activated cells through pharmacological blockade of synaptic transmission (Lima et al., 2009). However, this technique is generally not suitable for chronic *in vivo* recordings. Another approach takes advantage of the fact that cells directly driven by light tend to have step-like responses to changes in light intensity, while synaptically activated neurons respond in a graded fashion (S.G. Koh, personal communication). Unfortunately, this method is only applicable to cells that can respond to light with high reliability. In our recordings, many of the neurons we encountered (e.g. see Fig. A.8) had precisely time-locked low latency light-evoked responses but responded low probability even for the highest light powers tested. This phenotype is expected for ChR2-expressing neurons with low levels of expression.

In our small sample, presumed corticostriatal neurons did not appear to be any less heterogeneous in their response properties than the general population of auditory cortical cells. While some were robustly modulated by the frequency content of the "cloud-of-tones" stimulus (Fig. A.9), others showed not response to sound (Fig. A.5). We computed the mean stimulus tuning curve by aligning the tuning curve for each cell to its preferred frequency (Fig. A.1). As typical of auditory cortical neurons, responses of corticostriatal cells had a monotonic

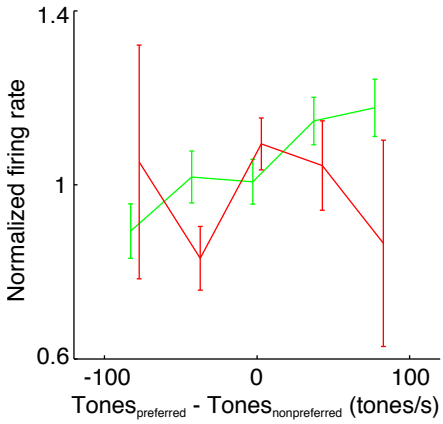

Figure A.1: **Mean stimulus tuning of presumed corticostriatal neurons.** For each neuron we determined its frequency preference and calculated its tuning for correct and error trials as in Fig. A.2-A.9c. We then computed the inverse variance weighted mean across neurons.

response to frequency content of the "cloud-of-tones" stimulus. We did not have enough data to conclusively compare responses on correct and error trials.

The spike waveforms of corticostriatal neurons fell into two classes: broad asymmetric spikes typical of cortical pyramidal neurons (Fig. A.2) and broad symmetric spikes (Fig. A.3). These subpopulation may correspond to different electrophysiological classes of layer V neurons.

Figure A.2-A.9: **Properties of presumed striatal projection neurons.** **a,** Raster of responses aligned to the onset of the "cloud-of-tones" stimulus. Gray shading indicates rat's position at the center port. **b,** Raster of responses aligned to onset of the rat's withdrawal from the center port. Shading indicates rat's travel time from the center port to the reward port. **c,** Neuronal tuning to the frequency content of the "cloud-of-tones" stimulus estimated from the first 175 ms of stimulus presentation. Green – correct trials; red – error trials. Error bars – standard error, estimated as the standard deviation of the bootstrap distribution. **d,** Raster of responses aligned rat's arrival at the reward port, sorted according to trial outcome. **e,** PSTH of neuronal response to light stimulation at the fibre adjacent to the recording electrode at the largest power tested. **f,** Light-evoked spike probability as a function of light intensity and duration. **g,** Example (gray) and mean (black) spike waveforms.

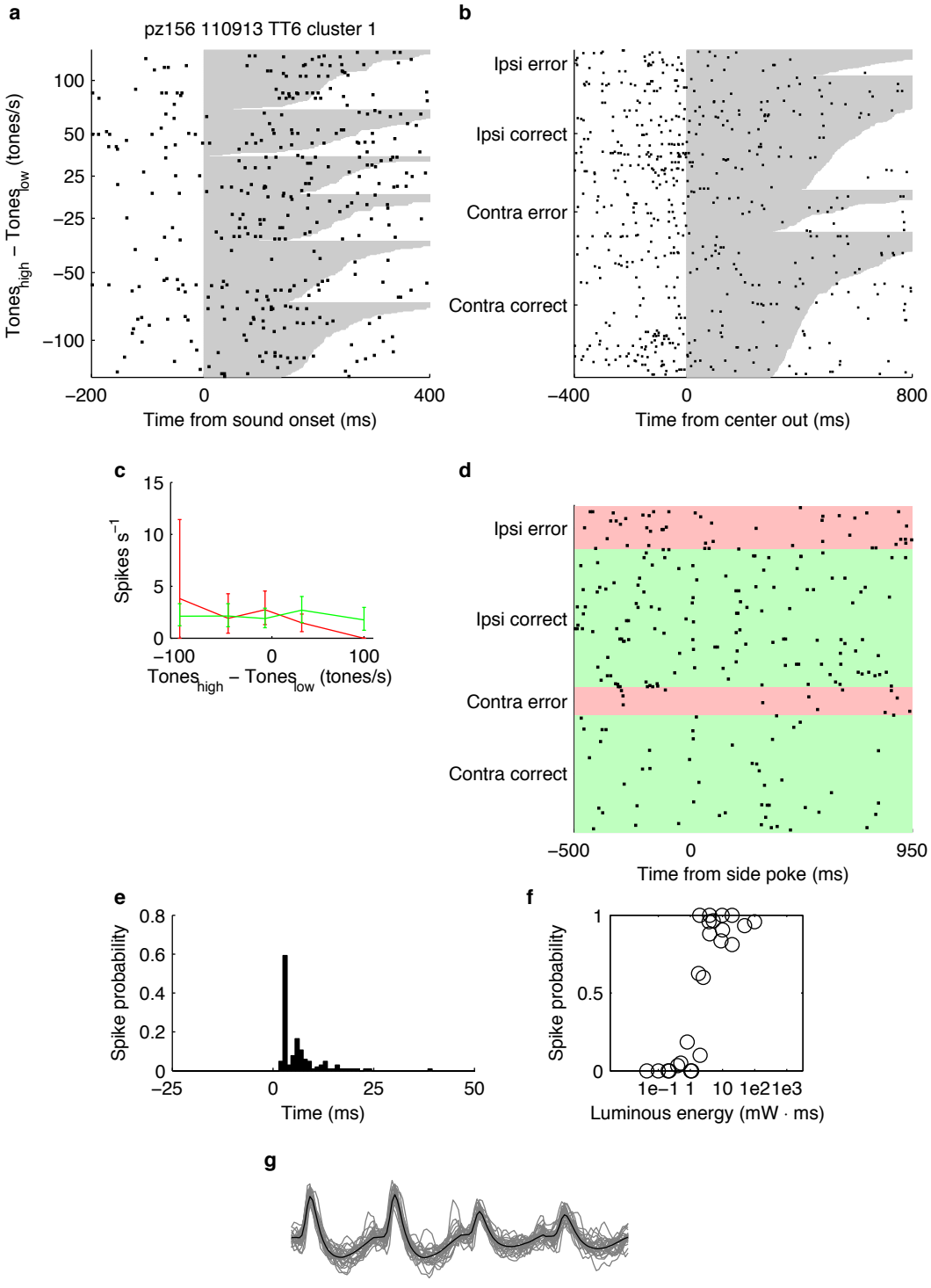

Figure A.2: pz156 110913 TT6 cluster 1

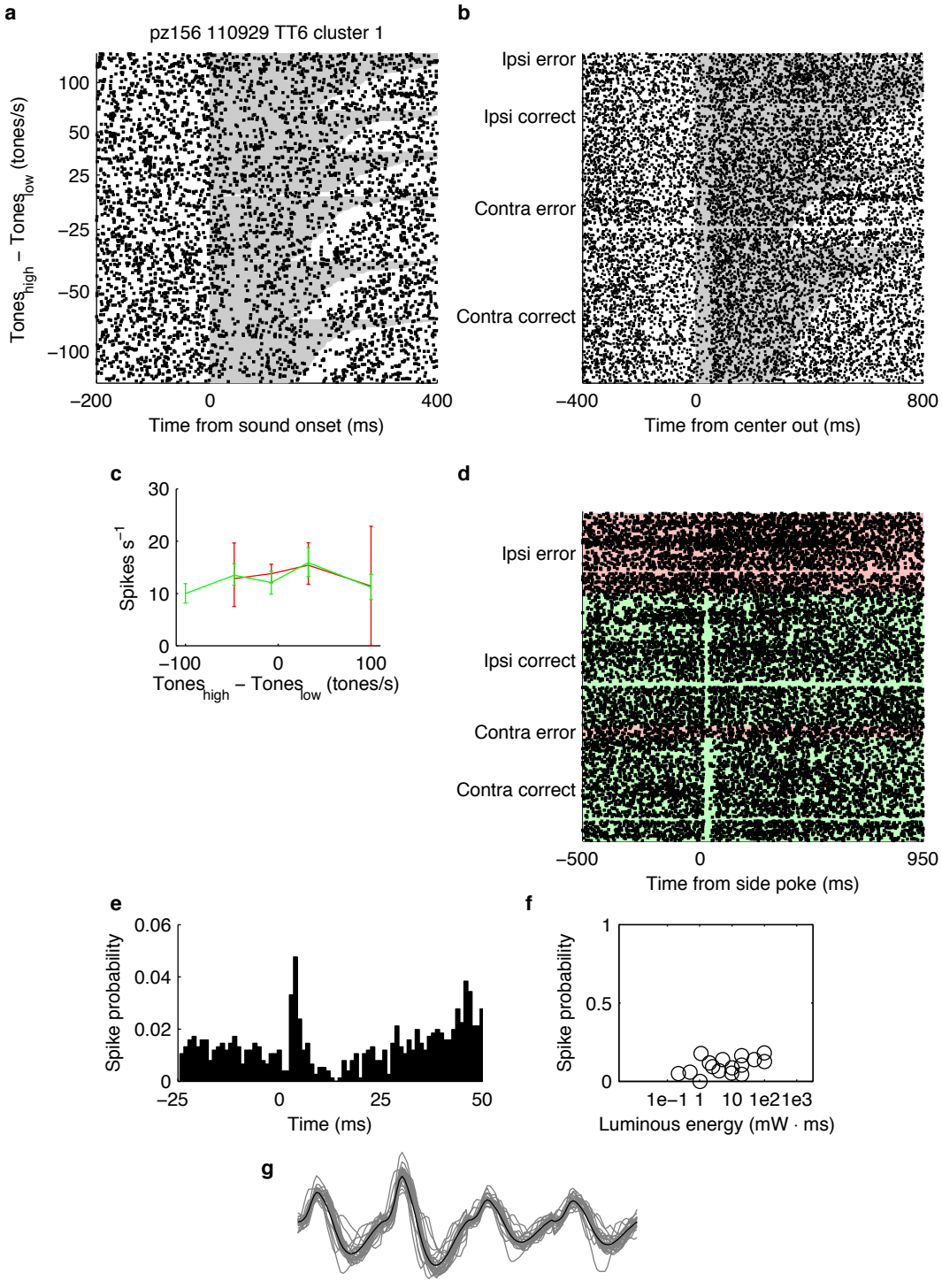

Figure A.3: pz156 110929 TT6 cluster 1

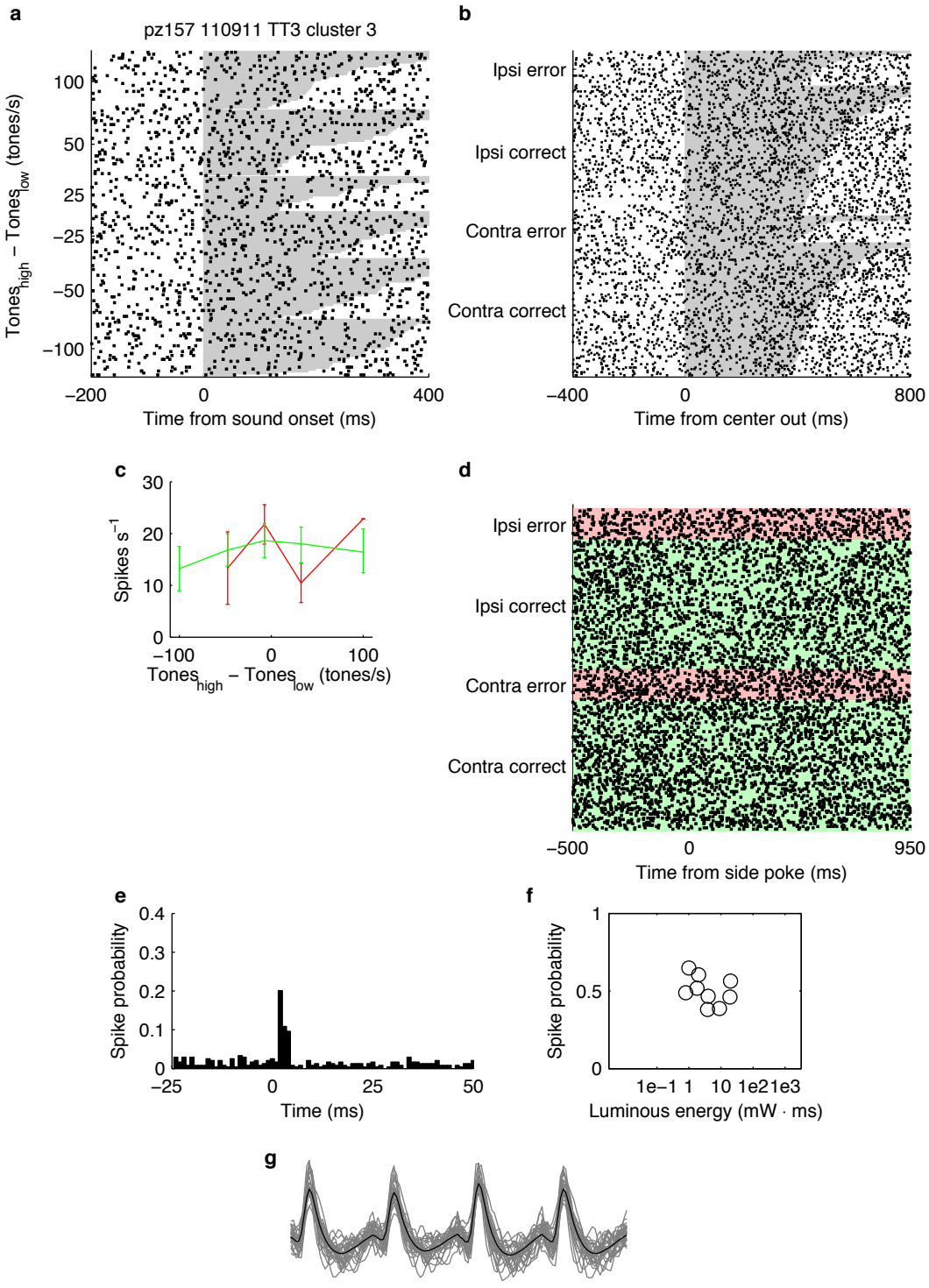

Figure A.4: pz157 110911 TT3 cluster 3

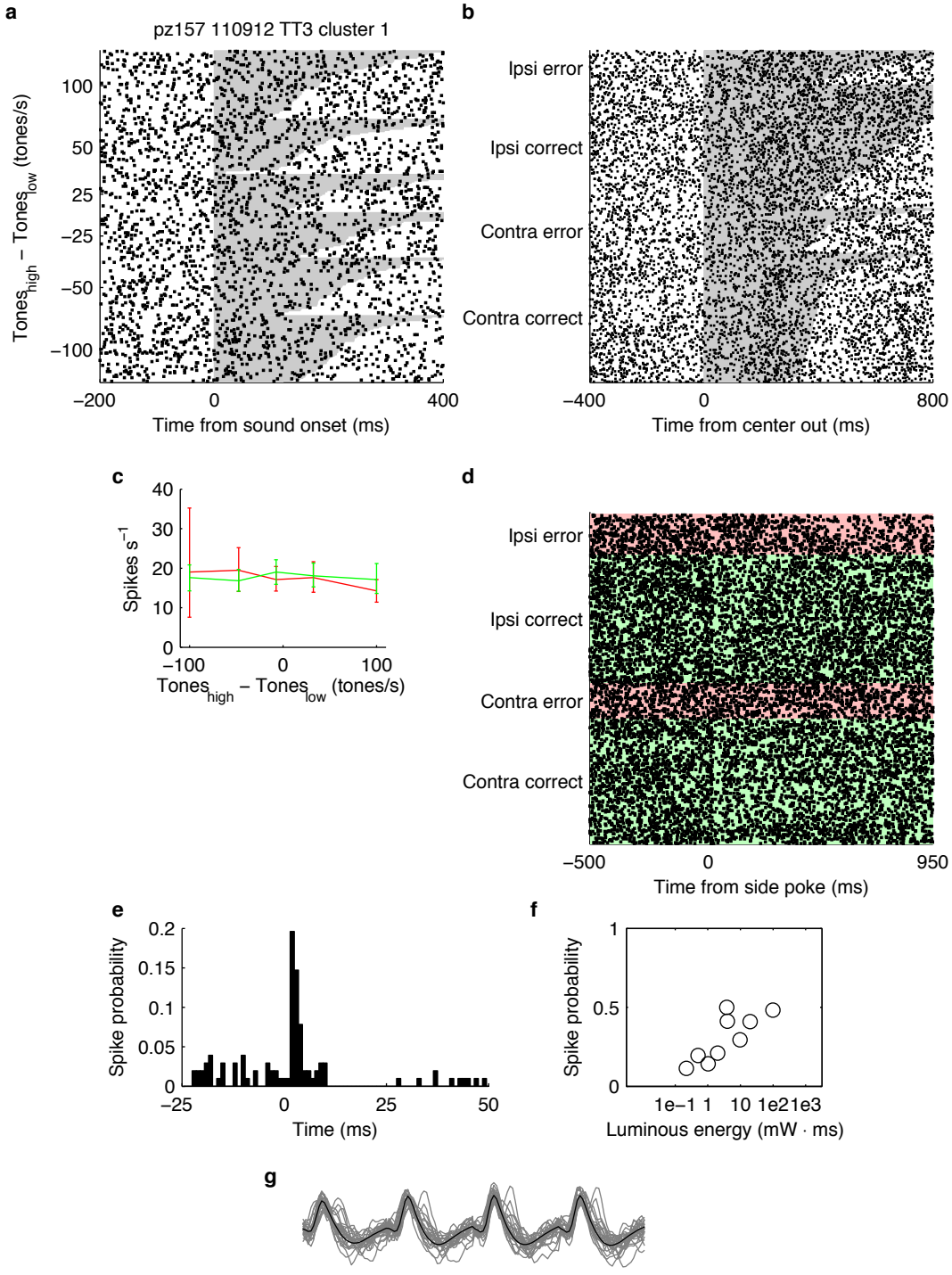

Figure A.5: pz157 110912 TT3 cluster 1

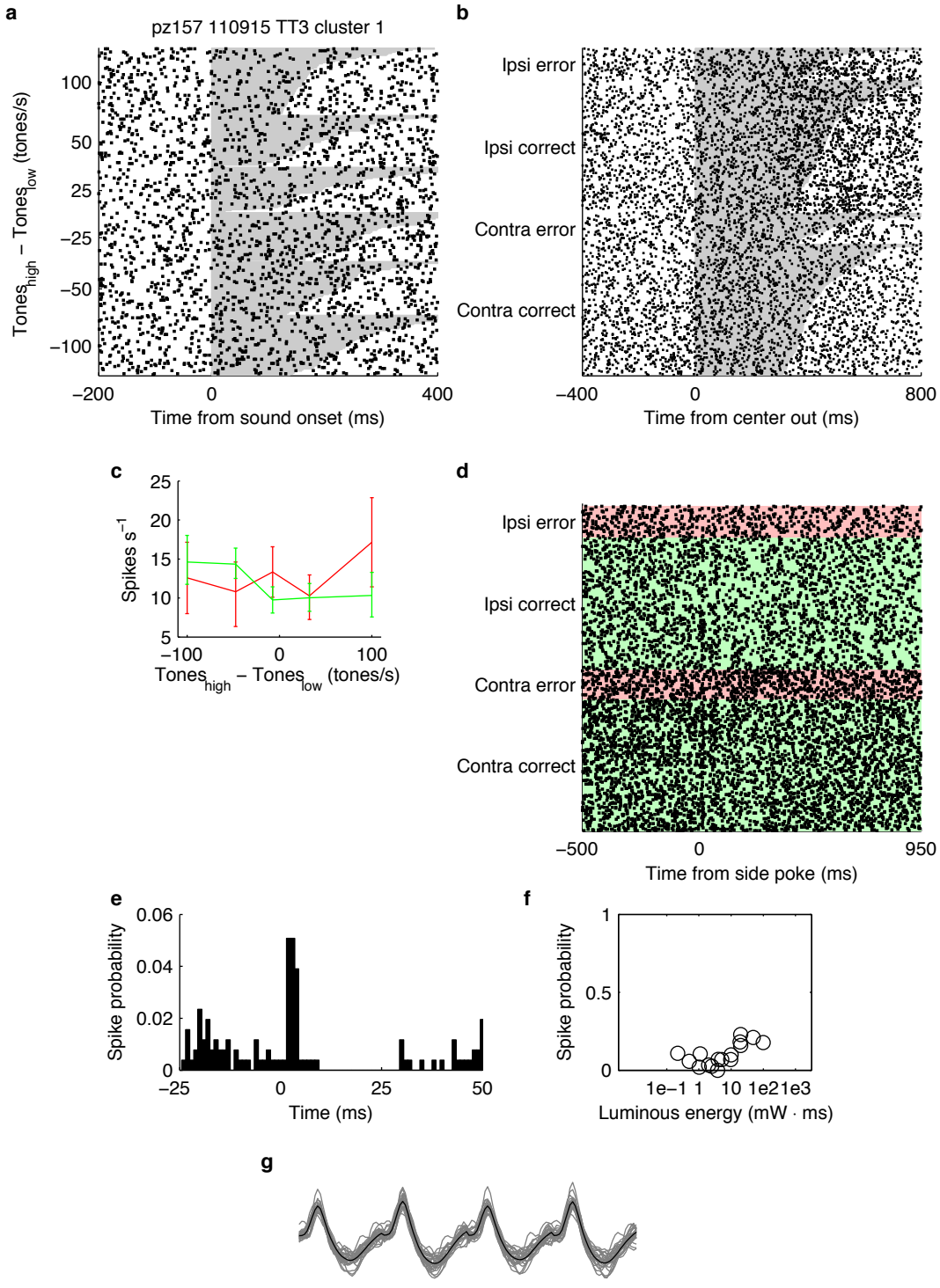

Figure A.6: pz157 110915 TT3 cluster 1

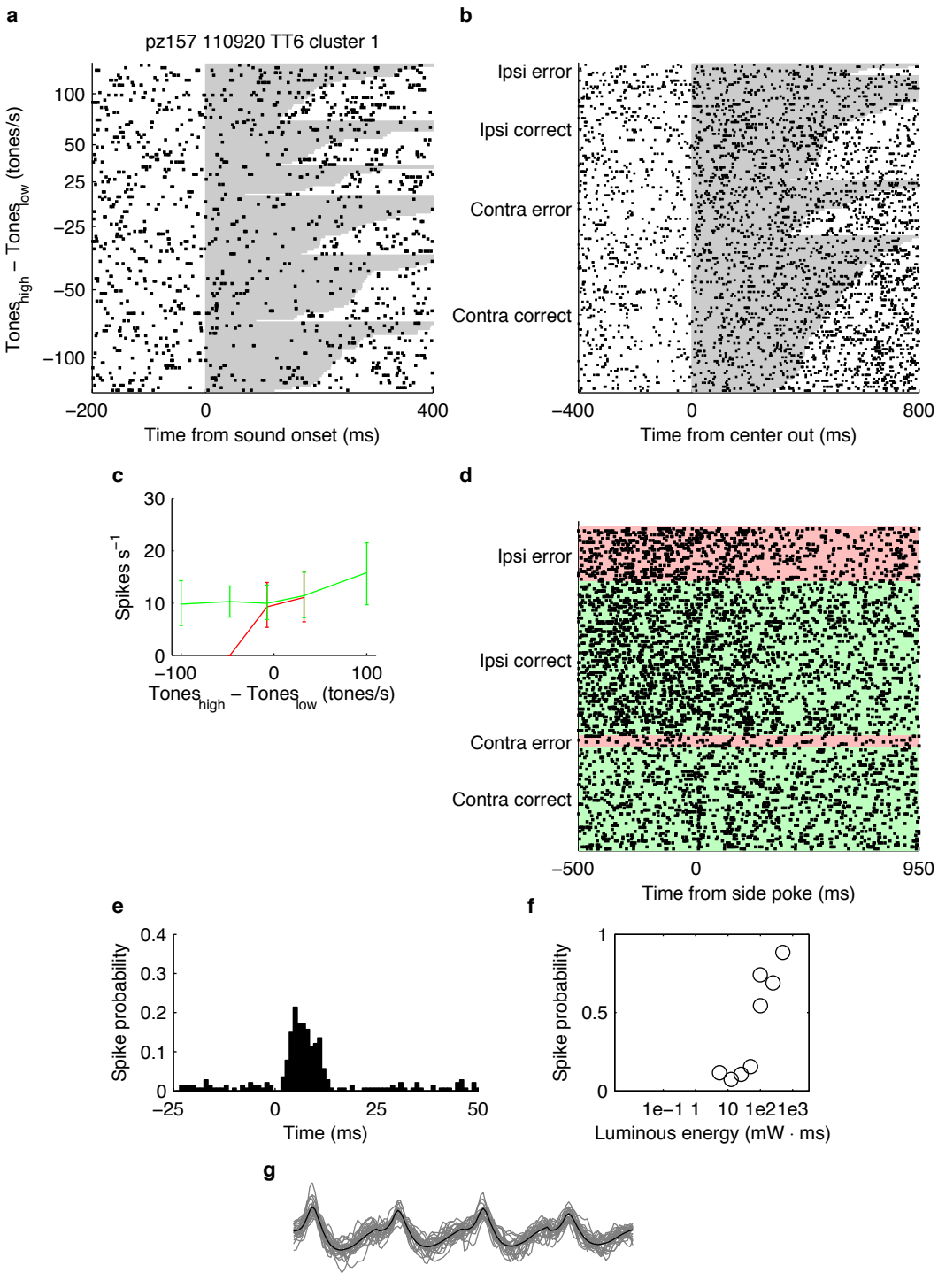

Figure A.7: pz157 110920 TT6 cluster 1

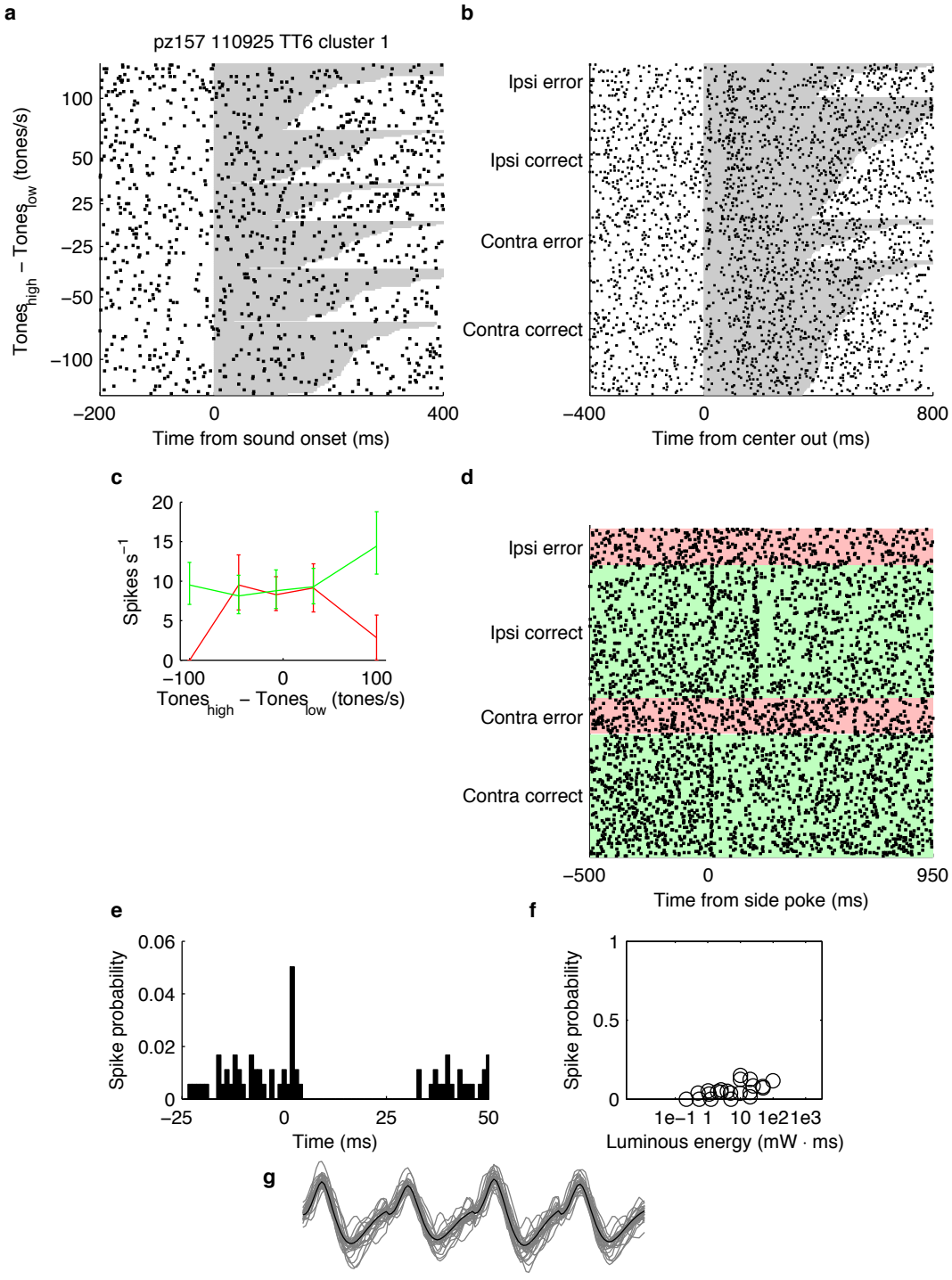

Figure A.8: pz157 110925 TT6 cluster 1

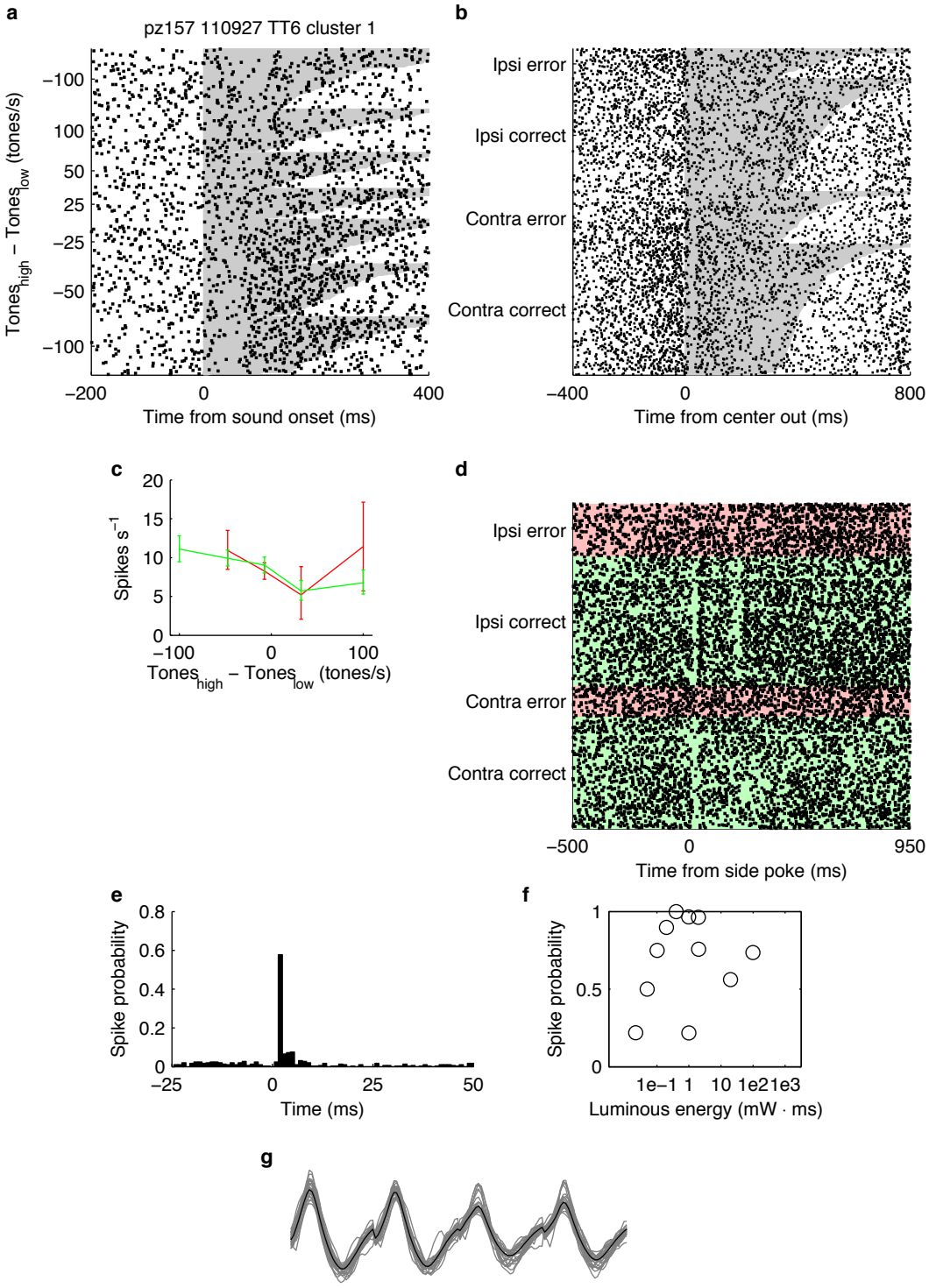

Figure A.9: pz157 110927 TT6 cluster 1

References

Adamantidis AR, Zhang F, Aravanis AM, Deisseroth K, de Lecea L. 2007. Neural substrates of awakening probed with optogenetic control of hypocretin neurons. *Nature* **450**: 420–4.

Aertsen AM, Gerstein GL, Habib MK, Palm G. 1989. Dynamics of neuronal firing correlation: modulation of "effective connectivity". *Journal of neurophysiology* **61**: 900–17.

Albright TD. 1984. Direction and orientation selectivity of neurons in visual area MT of the macaque. *J Neurophysiol* **52**: 1106–1130.

Albright TD, Desimone R, Gross CG. 1984. Columnar organization of directionally selective cells in visual area MT of the macaque. *Journal of neurophysiology* **51**: 16–31.

Allen Brain Institute. 2012. Allen Mouse Connectivity Atlas.

Alloway KD, Crist J, Mutic JJ, Roy SA. 1999. Corticostriatal Projections from Rat Barrel Cortex Have an Anisotropic Organization that Correlates with Vibrissal Whisking Behavior. *J Neurosci* **19**: 10908–10922.

Andersen RA, Asanuma C, Essick G, Siegel RM. 1990. Corticocortical connections of anatomically and physiologically defined subdivisions within the inferior parietal lobule. *The Journal of comparative neurology* **296**: 65–113.

Anselmi F, Ventalon C, Bègue A, Ogden D, Emiliani V. 2011. Three-dimensional imaging and photostimulation by remote-focusing and holographic light patterning. *Proceedings of the National Academy of Sciences of the United States of America* **108**: 19504–9.

Aravanis AM, Wang LP, Zhang F, Meltzer LA, Mogri MZ, Schneider MB, Deisseroth K. 2007. An optical neural interface: in vivo control of rodent motor cortex with integrated fiberoptic and optogenetic technology. *Journal of neural engineering* **4**: S143–56.

Armbruster BN, Li X, Pausch MH, Herlitze S, Roth BL. 2007. Evolving the lock to fit the key to create a family of G protein-coupled receptors potently activated by an inert ligand. *Proceedings of the National Academy of Sciences of the United States of America* **104**: 5163–8.

Atasoy D, Aponte Y, Su HH, Sternson SM. 2008. A FLEX switch targets Channelrhodopsin-2 to multiple cell types for imaging and long-range circuit mapping. *The Journal of neuroscience : the official journal of the Society for Neuroscience* **28**: 7025–30.

Bandyopadhyay S, Shamma SA, Kanold PO. 2010. Dichotomy of functional organization in the mouse auditory cortex. *Nature neuroscience* **13**: 361–8.

Barthó P, Hirase H, Monconduit L, Zugaro M, Harris KD, Buzsáki G. 2004a. Characterization of neocortical principal cells and interneurons by network interactions and extracellular features. *Journal of neurophysiology* **92**: 600–8.

Barthó P, Hirase H, Monconduit L, Zugaro M, Harris KD, Buzsáki G. 2004b. Characterization of neocortical principal cells and interneurons by network interactions and extracellular features. *Journal of neurophysiology* **92**: 600–8.

Barto A. 1995. Adaptive Critics and the Basal Ganglia. In Houk JC, Davis J, Beiser D, editors, *Models of Information Processing in the Basal Ganglia*, 215 – 232. Cambridge, MA: MIT Press.

Beckstead RM, Domesick VB, Nauta WJ. 1979. Efferent connections of the substantia nigra and ventral tegmental area in the rat. *Brain Research* **175**: 191–217.

Berke JD, Okatan M, Skurski J, Eichenbaum HB. 2004. Oscillatory entrainment of striatal neurons in freely moving rats. *Neuron* **43**: 883–96.

Bisley JW, Goldberg ME. 2010. Attention, intention, and priority in the parietal lobe. *Annual review of neuroscience* **33**: 1–21.

Bordi F, LeDoux J. 1992. Sensory tuning beyond the sensory system: an initial analysis of auditory response properties of neurons in the lateral amygdaloid nucleus and overlying areas of the striatum. *J Neurosci* **12**: 2493–2503.

Bordi F, LeDoux J, Clugnet MC, Pavlides C. 1993. Single-unit activity in the lateral nucleus of the amygdala and overlying areas of the striatum in freely behaving rats: rates, discharge patterns, and responses to acoustic stimuli. *Behavioral neuroscience* **107**: 757–69.

Boyden ES, Zhang F, Bamberg E, Nagel G, Deisseroth K. 2005. Millisecond-timescale, genetically targeted optical control of neural activity. *Nature neuroscience* **8**: 1263–8.

Britten KH, Newsome WT, Shadlen MN, Celebrini S, Movshon JA. 1996. A relationship between behavioral choice and the visual responses of neurons in macaque MT. *Visual neuroscience* **13**: 87–100.

Brody CD. 1999. Correlations Without Synchrony. *Neural Computation* **11**: 1537–1551.

Calabresi P, Maj R, Pisani A, Mercuri N, Bernardi G. 1992a. Long-term synaptic depression in the striatum: physiological and pharmacological characterization. *J Neurosci* **12**: 4224–4233.

Calabresi P, Pisani A, Mercuri NB, Bernardi G. 1992b. Long-term Potentiation in the Striatum is Unmasked by Removing the Voltage-dependent Magnesium Block of NMDA Receptor Channels. *The European journal of neuroscience* **4**: 929–935.

Cardin JA, Carlén M, Meletis K, Knoblich U, Zhang F, Deisseroth K, Tsai LH, Moore CI. 2009. Driving fast-spiking cells induces gamma rhythm and controls sensory responses. *Nature* **459**: 663–7.

Chevalier G, Deniau JM. 1990. Disinhibition as a basic process in the expression of striatal functions. *Trends in neurosciences* **13**: 277–80.

Chow BY, Han X, Dobry AS, Qian X, Chuong AS, Li M, Henninger MA, Belfort GM, Lin Y, Monahan PE, et al. 2010. High-performance genetically targetable optical neural silencing by light-driven proton pumps. *Nature* **463**: 98–102.

Ciocchi S, Herry C, Grenier F, Wolff SBE, Letzkus JJ, Vlachos I, Ehrlich I, Sprengel R, Deisseroth K, Stadler MB, et al. 2010. Encoding of conditioned fear in central amygdala inhibitory circuits. *Nature* **468**: 277–82.

Cui G, Jun SB, Jin X, Pham MD, Vogel SS, Lovinger DM, Costa RM. 2013. Concurrent activation of striatal direct and indirect pathways during action initiation. *Nature* **494**: 238–242.

Curanovic D, Enquist LW. 2009. Virion-incorporated glycoprotein B mediates transneuronal spread of pseudorabies virus. *Journal of virology* **83**: 7796–804.

DeLong MR. 1990. Primate models of movement disorders of basal ganglia origin. *Trends in neurosciences* **13**: 281–5.

Deniau J, Menetrey A, Charpier S. 1996. The lamellar organization of the rat substantia nigra pars reticulata: Segregated patterns of striatal afferents and relationship to the topography of corticostriatal projections. *Neuroscience* **73**: 761–781.

DeWeese MR, Zador AM. 2006. Non-Gaussian membrane potential dynamics imply sparse, synchronous activity in auditory cortex. *The Journal of neuroscience : the official journal of the Society for Neuroscience* **26**: 12206–18.

Ding L, Gold JI. 2012. Separate, causal roles of the caudate in saccadic choice and execution in a perceptual decision task. *Neuron* **75**: 865–74.

Dong JY, Fan PD, Frizzell RA. 1996. Quantitative analysis of the packaging capacity of recombinant adeno-associated virus. *Human gene therapy* **7**: 2101–12.

Doron NN, Ledoux JE, Semple MN. 2002. Redefining the tonotopic core of rat auditory cortex: physiological evidence for a posterior field. *The Journal of comparative neurology* **453**: 345–60.

Eblen F, Graybiel A. 1995. Highly restricted origin of prefrontal cortical inputs to striosomes in the macaque monkey. *J Neurosci* **15**: 5999–6013.

Feierbach B, Bisher M, Goodhouse J, Enquist LW. 2007. In vitro analysis of transneuronal spread of an alphaherpesvirus infection in peripheral nervous system neurons. *Journal of virology* **81**: 6846–57.

Felleman DJ, Van Essen DC. 1987. Receptive field properties of neurons in area V3 of macaque monkey extrastriate cortex. *Journal of neurophysiology* **57**: 889–920.

Felleman DJ, Van Essen DC. 1991. Distributed hierarchical processing in the primate cerebral cortex. *Cerebral cortex (New York, NY : 1991)* **1**: 1–47.

Felsen G, Mainen ZF. 2008. Neural substrates of sensory-guided locomotor decisions in the rat superior colliculus. *Neuron* **60**: 137–48.

Ferguson SM, Eskenazi D, Ishikawa M, Wanat MJ, Phillips PEM, Dong Y, Roth BL, Neumaier JF. 2011. Transient neuronal inhibition reveals opposing roles of indirect and direct pathways in sensitization. *Nature neuroscience* **14**: 22–4.

Ficalora A, Mize R. 1989. The neurons of the substantia nigra and zona incerta which project to the cat superior colliculus are GABA immunoreactive: A double-label study using GABA immunocytochemistry and lectin retrograde transport. *Neuroscience* **29**: 567–581.

Fife KH, Berns KI, Murray K. 1977. Structure and nucleotide sequence of the terminal regions of adeno-associated virus DNA. *Virology* **78**: 475–487.

Finke S, Conzelmann KK. 2005. Replication strategies of rabies virus. *Virus research* **111**: 120–31.

Fraefel C, Song S, Lim F, Lang P, Yu L, Wang Y, Wild P, Geller AI. 1996. Helper virus-free transfer of herpes simplex virus type 1 plasmid vectors into neural cells. *Journal of virology* **70**: 7190–7.

Fujiyama F, Sohn J, Nakano T, Furuta T, Nakamura KC, Matsuda W, Kaneko T. 2011. Exclusive and common targets of neostriatofugal projections of rat striosome neurons: a single neuron-tracing study using a viral vector. *The European journal of neuroscience* **33**: 668–77.

Geller AI, Breakefield XO. 1988. A defective HSV-1 vector expresses Escherichia coli beta-galactosidase in cultured peripheral neurons. *Science (New York, NY)* **241**: 1667–9.

Gerdeman GL, Ronesi J, Lovinger DM. 2002. Postsynaptic endocannabinoid release is critical to long-term depression in the striatum. *Nature neuroscience* **5**: 446–51.

Gerfen CR, Surmeier DJ. 2011. Modulation of striatal projection systems by dopamine. *Annual review of neuroscience* **34**: 441–66.

Gnadt JW, Andersen RA. 1988. Memory related motor planning activity in posterior parietal cortex of macaque. *Experimental brain research Experimentelle Hirnforschung Expérimentation cérébrale* **70**: 216–20.

Graybiel AM, Ragsdale CW. 1978. Histochemically distinct compartments in the striatum of human, monkeys, and cat demonstrated by acetylthiocholinesterase staining. *Proceedings of the National Academy of Sciences of the United States of America* **75**: 5723–6.

Han X, Boyden ES. 2007. Multiple-color optical activation, silencing, and desynchronization of neural activity, with single-spike temporal resolution. *PloS one* **2**: e299.

Hanks TD, Ditterich J, Shadlen MN. 2006. Microstimulation of macaque area LIP affects decision-making in a motion discrimination task. *Nature neuroscience* **9**: 682–9.

Heffner HE, Heffner RS. 1986. Hearing loss in Japanese macaques following bilateral auditory cortex lesions. *Journal of neurophysiology* **55**: 256–71.

Heffner HE, Heffner RS. 1990. Effect of bilateral auditory cortex lesions on absolute thresholds in Japanese macaques. *Journal of neurophysiology* **64**: 191–205.

Heffner HE, Heffner RS, Contos C, Ott T. 1994. Audiogram of the hooded Norway rat. *Hearing research* **73**: 244–7.

Hollis ER, Kadoya K, Hirsch M, Samulski RJ, Tuszynski MH. 2008. Efficient retrograde neuronal transduction utilizing self-complementary AAV1. *Molecular therapy : the journal of the American Society of Gene Therapy* **16**: 296–301.

Hopkins DA, Niessen LW. 1976. Substantia nigra projections to the reticular formation, superior colliculus and central gray in the rat, cat and monkey. *Neuroscience Letters* **2**: 253–259.

Houweling AR, Brecht M. 2008. Behavioural report of single neuron stimulation in somatosensory cortex. *Nature* **451**: 65–8.

Hromadka T. 2007. *Representation of sounds in the auditory cortex of awake rats*. Ph.D. thesis.

Hromádka T, Deweese MR, Zador AM. 2008. Sparse representation of sounds in the unanesthetized auditory cortex. *PLoS biology* **6**: e16.

Hromádka T, Deweese MR, Zador AM. 2010. Up-states are rare in awake auditory cortex. In *Computational and Systems Neuroscience*. Salt Lake City, UT.

Hubel DH, Wiesel TN. 1959. Receptive fields of single neurones in the cat's striate cortex. *The Journal of physiology* **148**: 574–91.

Huber D, Petreanu L, Ghitani N, Ranade S, Hromádka T, Mainen Z, Svoboda K. 2008. Sparse optical microstimulation in barrel cortex drives learned behaviour in freely moving mice. *Nature* **451**: 61–4.

Huk AC, Shadlen MN. 2005. Neural activity in macaque parietal cortex reflects temporal integration of visual motion signals during perceptual decision making. *The Journal of neuroscience : the official journal of the Society for Neuroscience* **25**: 10420–36.

Jiang H, Stein BE, McHaffie JG. 2011. Physiological evidence for a trans-basal ganglia pathway linking extrastriate visual cortex and the superior colliculus. *The Journal of physiology* **589**: 5785–99.

Jinno S, Kosaka T. 2004. Parvalbumin is expressed in glutamatergic and GABAergic corticostriatal pathway in mice. *The Journal of comparative neurology* **477**: 188–201.

Kawaguchi Y. 1993. Physiological, morphological, and histochemical characterization of three classes of interneurons in rat neostriatum. *The Journal of neuroscience : the official journal of the Society for Neuroscience* **13**: 4908–23.

Kawaguchi Y, Wilson CJ, Augood SJ, Emson PC. 1995. Striatal interneurones: chemical, physiological and morphological characterization. *Trends in neurosciences* **18**: 527–35.

Kelly JB. 1980. Effects of auditory cortical lesions on sound localization by the rat. *J Neurophysiol* **44**: 1161–1174.

Kelly JB, Masterton B. 1977. Auditory sensitivity of the albino rat. *Journal of comparative and physiological psychology* **91**: 930–6.

Kimura A, Donishi T, Okamoto K, Tamai Y. 2004. Efferent connections of "posterodorsal" auditory area in the rat cortex: implications for auditory spatial processing. *Neuroscience* **128**: 399–419.

Kravitz AV, Freeze BS, Parker PRL, Kay K, Thwin MT, Deisseroth K, Kreitzer AC. 2010. Regulation of parkinsonian motor behaviours by optogenetic control of basal ganglia circuitry. *Nature* **466**: 622–6.

Kreitzer AC, Malenka RC. 2008. Striatal plasticity and basal ganglia circuit function. *Neuron* **60**: 543–54.

Lee SH, Kwan AC, Zhang S, Phoumthipphavong V, Flannery JG, Masmanidis SC, Taniguchi H, Huang ZJ, Zhang F, Boyden ES, et al. 2012. Activation of specific interneurons improves V1 feature selectivity and visual perception. *Nature* **488**: 379–83.

Lewis TL, Mao T, Svoboda K, Arnold DB. 2009. Myosin-dependent targeting of transmembrane proteins to neuronal dendrites. *Nature neuroscience* **12**: 568–76.

Lilley CE, Groutsi F, Han Z, Palmer JA, Anderson PN, Latchman DS, Coffin RS. 2001. Multiple immediate-early gene-deficient herpes simplex virus vectors allowing efficient gene delivery to neurons in culture and widespread gene delivery to the central nervous system in vivo. *Journal of virology* **75**: 4343–56.

Lima SQ, Hromádka T, Znamenskiy P, Zador AM. 2009. PINP: a new method of tagging neuronal populations for identification during in vivo electrophysiological recording. *PloS one* **4**: e6099.

Madisen L, Zwingman TA, Sunkin SM, Oh SW, Zariwala HA, Gu H, Ng LL, Palmiter RD, Hawrylycz MJ, Jones AR, et al. 2010. A robust and high-throughput Cre reporting and characterization system for the whole mouse brain. *Nature neuroscience* **13**: 133–40.

Markram H. 1997. Regulation of Synaptic Efficacy by Coincidence of Postsynaptic APs and EPSPs. *Science* **275**: 213–215.

Mazarakis ND, Azzouz M, Rohll JB, Ellard FM, Wilkes FJ, Olsen AL, Carter EE, Barber RD, Baban DF, Kingsman SM, et al. 2001. Rabies virus glycoprotein pseudotyping of lentiviral vectors enables retrograde axonal transport and access to the nervous system after peripheral delivery. *Human molecular genetics* **10**: 2109–21.

McCarthy KM, Tank DW, Enquist LW. 2009. Pseudorabies virus infection alters neuronal activity and connectivity in vitro. *PLoS pathogens* **5**: e1000640.

McCarty DM, Fu H, Monahan PE, Toulson CE, Naik P, Samulski RJ. 2003. Adeno-associated virus terminal repeat (TR) mutant generates self-complementary vectors to overcome the rate-limiting step to transduction in vivo. *Gene therapy* **10**: 2112–8.

McCarty DM, Monahan PE, Samulski RJ. 2001. Self-complementary recombinant adeno-associated virus (scAAV) vectors promote efficient transduction independently of DNA synthesis. *Gene therapy* **8**: 1248–54.

McGeorge AJ, Faull RL. 1989. The organization of the projection from the cerebral cortex to the striatum in the rat. *Neuroscience* **29**: 503–37.

McVoy MA, Nixon DE, Adler SP, Mocarski ES. 1998. Sequences within the herpesvirus-conserved pac1 and pac2 motifs are required for cleavage and packaging of the murine cytomegalovirus genome. *Journal of virology* **72**: 48–56.

Mebatsion T, König M, Conzelmann KK. 1996. Budding of Rabies Virus Particles in the Absence of the Spike Glycoprotein. *Cell* **84**: 941–951.

Mendez MF, Geehan GR. 1988. Cortical auditory disorders: clinical and psychoacoustic features. *Journal of Neurology, Neurosurgery & Psychiatry* **51**: 1–9.

Merchant H, Zainos A, Hernandez A, Salinas E, Romo R. 1997. Functional Properties of Primate Putamen Neurons During the Categorization of Tactile Stimuli. *J Neurophysiol* **77**: 1132–1154.

Miao CH, Nakai H, Thompson AR, Storm TA, Chiu W, Snyder RO, Kay MA. 2000. Nonrandom transduction of recombinant adeno-associated virus vectors in mouse hepatocytes in vivo: cell cycling does not influence hepatocyte transduction. *Journal of virology* **74**: 3793–803.

Moriizumi T, Hattori T. 1991. Pyramidal cells in rat temporoauditory cortex project to both striatum and inferior colliculus. *Brain Research Bulletin* **27**: 141–144.

Moriizumi T, Hattori T. 1992. Separate neuronal populations of the rat globus pallidus projecting to the subthalamic nucleus, auditory cortex and pedunculopontine tegmental area. *Neuroscience* **46**: 701–10.

Nagel G, Szellas T, Huhn W, Kateriya S, Adeishvili N, Berthold P, Ollig D, Hegemann P, Bamberg E. 2003. Channelrhodopsin-2, a directly light-gated cation-selective membrane channel. *Proceedings of the National Academy of Sciences of the United States of America* **100**: 13940–5.

Newsome W, Pare E. 1988. A selective impairment of motion perception following lesions of the middle temporal visual area (MT). *J Neurosci* **8**: 2201–2211.

Nienborg H, Cumming BG. 2007. Psychophysically measured task strategy for disparity discrimination is reflected in V2 neurons. *Nature neuroscience* **10**: 1608–14.

Nienborg H, Cumming BG. 2009. Decision-related activity in sensory neurons reflects more than a neuron's causal effect. *Nature* **459**: 89–92.

Niwa H, Yamamura K, Miyazaki J. 1991. Efficient selection for high-expression transfectants with a novel eukaryotic vector. *Gene* **108**: 193–9.

Nomoto K, Schultz W, Watanabe T, Sakagami M. 2010. Temporally extended dopamine responses to perceptually demanding reward-predictive stimuli. *The Journal of neuroscience : the official journal of the Society for Neuroscience* **30**: 10692–702.

O'Connor DH, Huber D, Svoboda K. 2009. Reverse engineering the mouse brain. *Nature* **461**: 923–9.

Pai S, Erlich JC, Kopec C, Brody CD. 2011. Minimal impairment in a rat model of duration discrimination following excitotoxic lesions of primary auditory and prefrontal cortices. *Frontiers in systems neuroscience* **5**: 74.

Palmer J, Huk A, Shadlen M. 2005. The effect of stimulus strength on the speed and accuracy of a perceptual decision. *Journal of Vision* **5**: 376–404.

Papagiakoumou E, Anselmi F, Bègue A, de Sars V, Glückstad J, Isacoff EY, Emiliani V. 2010. Scanless two-photon excitation of channelrhodopsin-2. *Nature methods* **7**: 848–54.

Pienkowski M, Eggermont JJ. 2011. Sound frequency representation in primary auditory cortex is level tolerant for moderately loud, complex sounds. *Journal of neurophysiology* **106**: 1016–27.

Pomeranz LE, Reynolds AE, Hengartner CJ. 2005. Molecular biology of pseudorabies virus: impact on neurovirology and veterinary medicine. *Microbiology and molecular biology reviews : MMBR* **69**: 462–500.

Prieto J, Solera J, Tabarés E. 2002. Development of new expression vector based on Pseudorabies virus amplicons: application to human insulin expression. *Virus research* **89**: 123–9.

Rao RPN. 2010. Decision making under uncertainty: a neural model based on partially observable markov decision processes. *Frontiers in computational neuroscience* **4**: 146.

Reale RA, Imig TJ. 1983. Auditory cortical field projections to the basal ganglia of the cat. *Neuroscience* **8**: 67–86.

Reiner A, Jiao Y, Del Mar N, Laverghetta AV, Lei WL. 2003. Differential morphology of pyramidal tract-type and intratelencephalically projecting-type corticostriatal neurons and their intrastriatal terminals in rats. *The Journal of comparative neurology* **457**: 420–40.

Reynolds JN, Hyland BI, Wickens JR. 2001. A cellular mechanism of reward-related learning. *Nature* **413**: 67–70.

Rizzolatti G, Riggio L, Dascola I, Umiltá C. 1987. Reorienting attention across the horizontal and vertical meridians: evidence in favor of a premotor theory of attention. *Neuropsychologia* **25**: 31–40.

Roger M, Arnault P. 1989. Anatomical study of the connections of the primary auditory area in the rat. *The Journal of comparative neurology* **287**: 339–56.

Rothschild G, Nelken I, Mizrahi A. 2010. Functional organization and population dynamics in the mouse primary auditory cortex. *Nature neuroscience* **13**: 353–60.

Saint-Cyr JA, Ungerleider LG, Desimone R. 1990. Organization of visual cortical inputs to the striatum and subsequent outputs to the pallido-nigral complex in the monkey. *The Journal of comparative neurology* **298**: 129–56.

Salzman CD, Britten KH, Newsome WT. 1990. Cortical microstimulation influences perceptual judgements of motion direction. *Nature* **346**: 174–7.

Salzman CD, Murasugi CM, Britten KH, Newsome WT. 1992. Microstimulation in visual area MT: effects on direction discrimination performance. *The Journal of neuroscience : the official journal of the Society for Neuroscience* **12**: 2331–55.

Schultz W. 1997. A Neural Substrate of Prediction and Reward. *Science* **275**: 1593–1599.

Schultz W, Apicella P, Ljungberg T. 1993. Responses of monkey dopamine neurons to reward and conditioned stimuli during successive steps of learning a delayed response task. *J Neurosci* **13**: 900–913.

Shadlen MN. 1996. Motion perception: Seeing and deciding. *Proceedings of the National Academy of Sciences* **93**: 628–633.

Shadlen MN, Britten KH, Newsome WT, Movshon JA. 1996. A computational analysis of the relationship between neuronal and behavioral responses to visual motion. *The Journal of neuroscience : the official journal of the Society for Neuroscience* **16**: 1486–510.

Shadlen MN, Newsome WT. 2001. Neural Basis of a Perceptual Decision in the Parietal Cortex (Area LIP) of the Rhesus Monkey. *J Neurophysiol* **86**: 1916–1936.

Shen W, Flajolet M, Greengard P, Surmeier DJ. 2008. Dichotomous dopaminergic control of striatal synaptic plasticity. *Science (New York, NY)* **321**: 848–51.

Sineshchekov OA, Jung KH, Spudich JL. 2002. Two rhodopsins mediate phototaxis to low- and high-intensity light in Chlamydomonas reinhardtii. *Proceedings of the National Academy of Sciences of the United States of America* **99**: 8689–94.

Smith GA, Enquist LW. 2000. A self-recombining bacterial artificial chromosome and its application for analysis of herpesvirus pathogenesis. *Proceedings of the National Academy of Sciences of the United States of America* **97**: 4873–8.

Snyder RO, Samulski RJ, Muzyczka N. 1990. In vitro resolution of covalently joined AAV chromosome ends. *Cell* **60**: 105–13.

Sohal VS, Zhang F, Yizhar O, Deisseroth K. 2009. Parvalbumin neurons and gamma rhythms enhance cortical circuit performance. *Nature* **459**: 698–702.

Straus SE, Sebring ED, Rose JA. 1976. Concatemers of alternating plus and minus strands are intermediates in adenovirus-associated virus DNA synthesis. *Proceedings of the National Academy of Sciences of the United States of America* **73**: 742–6.

Sutton RS. 1988. Learning to predict by the methods of temporal differences. *Machine Learning* **3**: 9–44.

Taharaguchi S, Kon Y, Yoshino S, Ono E. 2003. Impaired development of the cerebellum in transgenic mice expressing the immediate-early protein IE180 of pseudorabies virus. *Virology* **307**: 243–254.

Tai LH. 2008. *Neural Mechanisms of Selective Auditory Attention in Rats*. Ph.D. thesis.

Tai LH, Lee AM, Benavidez N, Bonci A, Wilbrecht L. 2012. Transient stimulation of distinct subpopulations of striatal neurons mimics changes in action value. *Nature neuroscience* **15**: 1281–9.

Talwar SK, Musial PG, Gerstein GL. 2001. Role of Mammalian Auditory Cortex in the Perception of Elementary Sound Properties. *J Neurophysiol* **85**: 2350–2358.

Ts'o D, Gilbert C, Wiesel T. 1986. Relationships between horizontal interactions and functional architecture in cat striate cortex as revealed by cross-correlation analysis. *J Neurosci* **6**: 1160–1170.

Wang X, Lu T, Snider RK, Liang L. 2005. Sustained firing in auditory cortex evoked by preferred stimuli. *Nature* **435**: 341–6.

Warden MR, Selimbeyoglu A, Mirzabekov JJ, Lo M, Thompson KR, Kim SY, Adhikari A, Tye KM, Frank LM, Deisseroth K. 2012. A prefrontal cortexbrainstem neuronal projection that controls response to behavioural challenge. *Nature* **advance on**.

Yamada S, Shimizu M. 1994. Isolation and characterization of mutants of pseudorabies virus with deletion in the immediate-early regulatory gene. *Virology* **199**: 366–75.

Yeterian EH, Pandya DN. 1998. Corticostriatal connections of the superior temporal region in rhesus monkeys. *The Journal of comparative neurology* **399**: 384–402.

Yin HH, Mulcare SP, Hilário MRF, Clouse E, Holloway T, Davis MI, Hansson AC, Lovinger DM, Costa RM. 2009. Dynamic reorganization of striatal circuits during the acquisition and consolidation of a skill. *Nature neuroscience* **12**: 333–41.

Znamenskiy P, Zador AM. 2013. Corticostriatal neurons in auditory cortex drive decisions during auditory discrimination. *Nature* **in press**.

Zohary E, Shadlen MN, Newsome WT. 1994. Correlated neuronal discharge rate and its implications for psychophysical performance. *Nature* **370**: 140–3.